Supporting Information

Acylhydrazone-based reversibly photoswitchable ion pair transporter with OFF–ON transport activity

Sandip Chattopadhayay,[a,c] Paras Wanjari[a,b,c] and Pinaki Talukdar[*a]

[a] Department of Chemistry, Indian Institute of Science Education and Research Pune, Dr. Homi Bhabha Road, Pashan, Pune 411008, Maharashtra, India.

[b] Present Address: Institut Europeen des Membranes, University of Montpellier, ENSCM-CNRS, UMR 5635 Place E. Bataillon CC047, 34095 Montpellier, France.

[c] Authors contributed equally.

Table of Content

I. General methods:

Reagents and compounds used for the synthesis were purchased from Sigma-Aldrich, Avra Chemicals, and Spectrochem, and used without further purification. For dry reaction, MeOH was purchased from commercial suppliers and used without further purification. All the reactions were performed under a nitrogen atmospheric environment using an N_2 gas balloon and monitored by checking TLC, performed on pre-coated aluminum plates of Silica gel 60 F_{254} (0.25 mm, E. Merck). Column chromatographies were performed on Merck silica gel (100–200 mesh). Egg yolk phosphatidylcholine (EYPC) was obtained from Avanti Polar Lipids as a solution in $CHCl_3$ (25 mg/mL). HEPES buffer, HPTS, Lucigenin, Triton X–100, NaOH, and inorganic salts were purchased of molecular biology grade from Sigma. Large unilamellar vesicles (LUVs) were prepared by using a mini extruder, equipped with a polycarbonate membrane of 100 nm or 200 nm pore size, purchased from Avanti Polar Lipids.

II. Physical measurements:

The ^1H NMR spectra were recorded at 400 MHz and ^{13}C spectra at 101 MHz either in Jeol or Bruker NMR instruments. The residual (deuterium) solvent signals were considered as an internal reference (δH = 2.50 ppm for DMSO-d_6) to calibrate spectra. All the chemical shifts were reported in ppm. The following abbreviations were used to indicate multiplicity patterns s: singlet, d: doublet, t: triplet, m: multiplet. Coupling constants were measured in Hz. High-resolution mass spectra (HRMS) were recorded on electrospray ionization time-of-flight (ESI–TOF) with +ve mode. Adjustment of pH of buffer solutions was made using Hanna HI98108 PHep+ pH meter. ChemBio Draw 22.2.0 software was used for drawing structures and processing Figures. All buffer solutions were prepared from the autoclaved water. Fluorescence experiments were recorded on Fluoromax-4 from Jobin Yvon Edison, equipped with an injector port and magnetic stirrer in a microfluorescence cuvette. The extravesicular dye was removed by performing gel chromatography using Sephadex G-50. The fluorescence studies were processed using Origin 8.5 software. All theoretical calculations were performed using CONFLEX 8 and Gaussian 09 software programs. Data were analyzed and visualized using GaussView 6.0 and Discovery Studio 2021 software. 'PARAM Brahma Facility' under the National Supercomputing Mission, Government of India at IISER, Pune, was used to perform the geometry optimization.

III. Synthesis:
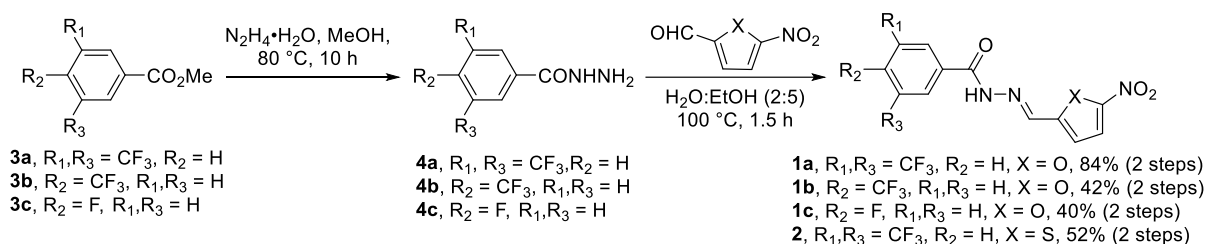
Scheme S1. Synthetic scheme for the compounds **1a–1c** and **2**.

The synthetic procedure of compound 3a–3c: Compound **3a–3c** were synthesized by using the reported literature procedure.[S1]

The general synthetic procedure of 4a–4c: In a 25 mL round bottom flask, compound **3a–3c** (1 equiv) was dissolved in dry MeOH (5 mL). To the clear solution, $NHNH_2 \cdot H_2O$ (1.5 equiv) was added, and the solution was kept at 80 °C for 10 h. After completion of the reaction, MeOH was evaporated, and EtOH was added to the reaction mixture.

A white precipitate was formed, which was filtered and directly used for the next step of the reaction without any further purification.

The general synthetic procedure of 1a–1c and 2: In a clean and dried 25 mL round bottom flask, compound **4a–4c** (1 equiv) was taken and dissolved in 10 mL water:ethanol (2:5) mixture. 5-nitrofuran-2-carbaldehyde or 5-nitrothiophene-2-carbaldehyde (1 equiv) was added to the reaction mixture, and it was kept at 100 °C for 1.5 h. After completion of the reaction, the solution was transferred to the separating funnel with $CHCl_3$ (25 mL) and washed with water (25 mL). The aqueous layer was extracted with $CHCl_3$ (3 × 25 mL), and then the combined organic layer was washed with brine solution (25 mL). Finally, the organic layer was dried over Na_2SO_4, and the solvent was evaporated under reduced pressure. Further purification of the compound was done by column chromatography to get the pure product of **1a–1c** and **2**.

Synthesis of (*E*)-*N*'-((5-nitrofuran-2-yl)methylene)-3,5-bis(trifluoromethyl)benzohydrazide (1a):
By taking 200 mg of compound **3a**, compound **4a** was synthesized. It was utilized directly for the next
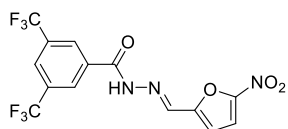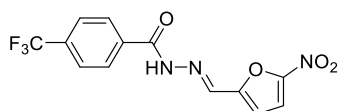

step reaction without any purification. The crude product was purified by silica gel column chromatography (Eluent: 15% ethyl acetate in petroleum ether) to obtain **1a** [244 mg, Yield = 84 % (2 steps)]. **^{1}H NMR (400 MHz, DMSO-d_6):** δ 12.56 (s, 1H), 8.56 (s, 2H), 8.42 (s, 1H), 8.41 (s, 1H), 7.82 (d, J = 3.9 Hz, 1H), 7.35 (d, J = 3.9 Hz, 1H). **^{19}F NMR (377 MHz, DMSO-d_6):** δ -61.26. **^{13}C NMR (101 MHz, DMSO-d_6):** δ 160.61, 152.09, 151.20, 136.83, 135.14, 131.13, 130.81, 130.48, 130.14, 128.61, 127.10, 125.72, 124.39, 121.68, 118.96, 116.17, 114.51. **HRMS (ESI) m/z:** [M+H]$^+$ Calcd. for $C_{14}H_7F_6N_3O_4H^+$ 396.0414;

Found 396.0416. **IR (Neat, v/cm^{-1}):** 3004.79, 1736.97, 1667.95, 1560.80, 1481.37, 1348.19, 1279.29, 1180.26, 1161.29, 1139.34, 1083.15, 1017.10, 912.12, 814.66, 705.15, 681.51.
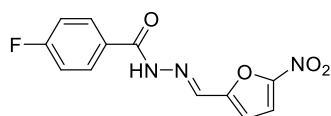
Synthesis of (*E*)-*N'*-((5-nitrofuran-2-yl)methylene)-4-(trifluoromethyl)benzohydrazide (1b): By taking 200 mg of compound **3b**, compound **4b** was synthesized. It was utilized directly for the next step reaction without any purification. The crude product was purified by silica gel column chromatography (Eluent: 20% ethyl acetate in petroleum ether) to obtain **1b** [135 mg, Yield = 42 % (2 steps)]. **^{1}H NMR (400 MHz, DMSO-*d$_6$*):** δ 12.42 (s, 1H), 8.42 (s, 1H), 8.13 (d, J = 8.0 Hz, 2H), 7.95 (d, J = 8.0 Hz, 2H), 7.81 (d, J = 4.0 Hz, 1H), 7.32 (d, J = 4.0 Hz, 1H). **^{19}F NMR: (377 MHz, DMSO-*d$_6$*):** δ -61.42. **^{13}C NMR (101 MHz, DMSO-*d$_6$*):** δ 162.32, 152.04, 151.48, 144.75, 136.60, 136.34, 131.75, 128.75, 127.92, 125.63, 125.21, 122.49, 115.84, 114.61. **HRMS (ESI) m/z:** [M+H]$^+$ Calcd. for C$_{13}$H$_8$F$_3$N$_3$O$_4$H$^+$ 328.0540; Found 328.0544. **IR (Neat, v/cm^{-1}):** 3207.55, 1738.67, 1656.22, 1561.41, 1519.44, 1476.26, 1350.29, 1327.03, 1305.66, 1283.96, 1247.11, 1151.05, 1133.09, 1107.32, 1063.30, 1025.56, 966.58, 946.62, 859.24, 823.46, 813.91, 769.39, 738.41, 710.88.
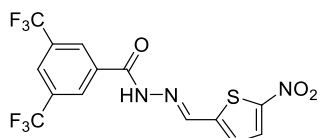
Synthesis of (*E*)-4-fluoro-*N'*-((5-nitrofuran-2-yl)methylene)benzohydrazide (1c): By taking 200 mg of compound **3c**, compound **4c** was synthesized. It was utilized directly for the next step reaction without any purification. The crude product was purified by silica gel column chromatography (Eluent: 35% ethyl acetate in petroleum ether) to obtain **1c** [144 mg, Yield = 40 % (2 steps)]. **^{1}H NMR (400 MHz, DMSO-*d$_6$*):** δ 12.26 (s, 1H), 8.40 (s, 1H), 8.03 – 7.98 (m, 2H), 7.81 (d, J = 4.0 Hz, 1H), 7.40 (t, J = 8.7 Hz, 2H), 7.29 (d, J = 3.2 Hz, 1H). **^{19}F NMR (377 MHz, DMSO-*d$_6$*):** δ -107.43. **^{13}C NMR (101 MHz, DMSO-*d$_6$*):** δ 165.63, 163.15, 162.36, 151.95, 151.68, 135.61, 130.63, 129.26, 115.77, 115.53, 114.66. **HRMS (ESI) m/z:** [M+H]$^+$ Calcd. for C$_{12}$H$_8$FN$_3$O$_4$H$^+$ 278.0572; Found 278.0571. **IR (Neat, v/cm^{-1}):** 2970.15, 1738.65, 1653.32, 1601.14, 1559.63, 1508.44, 1471.23, 1351.67, 1306.86, 1279.62, 1230.87, 1174.68, 1160.76, 1144.32, 1096.69, 1069.69, 1020.66, 963.67, 936.15, 902.97, 851.67, 816.32, 760.00, 736.95, 673.45, 612.26.

Synthesis of (*E*)-*N'*-((5-nitrothiophen-2-yl)methylene)-3,5-bis(trifluoromethyl)benzohydrazide (2): By taking 200 mg of compound **3a**, compound **4a** was synthesized. It was utilized directly for the next step reaction without any purification. The crude product was purified by silica gel column chromatography (Eluent: 25% ethyl acetate in petroleum ether) to obtain **2** [156 mg, Yield = 52 % (2 steps)]. **^{1}H NMR (400 MHz, DMSO-*d$_6$*):** δ 12.56 (s, 1H), 8.68 (s, 1H), 8.55 (s, 2H), 8.42 (s, 1H), 8.16 (d, J = 4.1 Hz, 1H), 7.66 (d, J = 4.4 Hz, 1H). **^{19}F NMR (377 MHz, DMSO-*d$_6$*):** δ -61.27. **^{13}C NMR (101 MHz, DMSO-*d$_6$*):** δ 160.56, 151.23, 145.98, 142.45, 138.04, 135.23, 131.11, 130.77, 130.60, 130.45, 130.35, 130.11, 128.61, 128.58, 125.67, 124.39, 121.68. **HRMS (ESI) m/z:** [M+H]$^+$ Calcd. for C$_{14}$H$_7$F$_6$N$_3$O$_3$SH$^+$ 412.0185; Found 412.0188 **IR (Neat, v/cm^{-1}):** 2970.20, 1738.76, 1653.34, 1561.43, 1533.84, 1500.68,

1439.02, 1361.68, 1439.02, 1361.68, 1337.35, 1263.84, 1229.84, 1216.73, 1173.19, 1122.36, 1074.22, 1036.54, 949.83, 906.32, 846.03, 814.34, 786.20, 758.60, 729.96, 710.99, 697.39, 681.00.

IV. UV-Vis studies:

A. Photo-switching Studies

During all of the photo-switching experiments, 3 LEDs (with 3.8-watt power) were used. LEDs were kept approximately 3-5 cm away from the samples during photo-irradiation.

Photo-isomerization studies of the transporters were carried out through UV-Vis spectroscopy. A fresh solution of compound **1a** was prepared in MeOH and 64 μM of compound **1a** was used during the experiment. *E*-conformer of compound **1a** showed an instance peak at 365 nm, which diminished upon 365 nm photo-irradiation for 330 s. Irradiation with 365 nm of light emerged a new peak at 450 nm, confirming the rapid *E*→*Z* photo-isomerization of compound **1a** in MeOH solvent. To scrutinize the photo-reversibility nature of compound **1a**, the photo-isomerized *Z*-conformer was again irradiated with 450 nm of LED light. Even after 20 min of photo-irradiation with 450 nm of LED light, no re-emergence of the initial UV-Vis spectrum was observed, indicating reverse isomerization from *Z*→*E* isomer was not occurring with compound **1a**.

We speculate this irreversible photo-isomerization was due to the presence of strong intramolecular hydrogen bonding present in the *Z*-conformer between the oxygen atom of chromophoric moiety and the hydrogen atom of CONH$_a$ group. To reduce the intramolecular H-bonding strength in **1a$_z$**, the oxygen atom was replaced with the comparatively larger-sized sulfur atom in the chromophoric moiety of compound **2**.
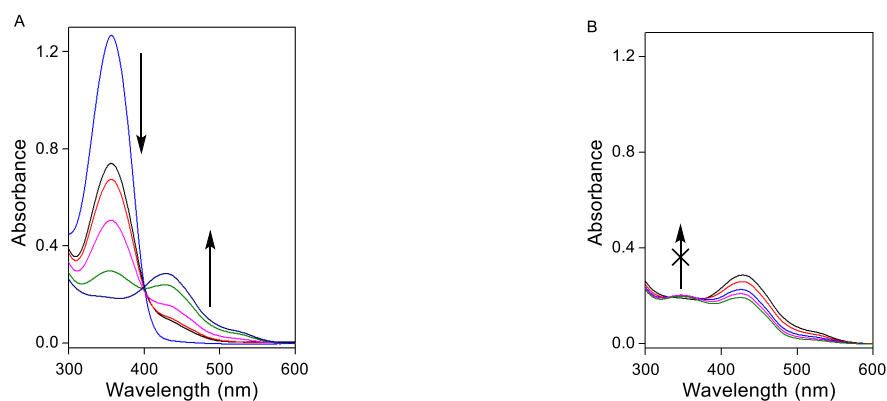

Fig. S1 Photo-irradiation of compound **1a** (64 μM) in MeOH with 365 nm UV light for 0-5.5 min (A). Reverse photo-isomerization of compound **1a** (64 μM) in MeOH with 450 nm LED light for 0-19 min (B).
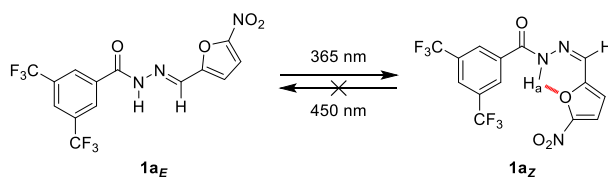

Fig. S2 Representation of irreversibility in photo-switching for compound **1a**.

A rapid *E→Z* photo-isomerization of compound **2** (64 μM) in MeOH was observed within 5 s of 365 nm of photo-irradiation. Further, to elucidate the reversibility of the isomerization process, 450 nm of LED light was used. Interestingly, the isomerized *Z*-conformer of compound **2** reverts to its initial *E*-conformer within 9 min of photo-irradiation, indicating the photo-reversibility nature of compound **2**.
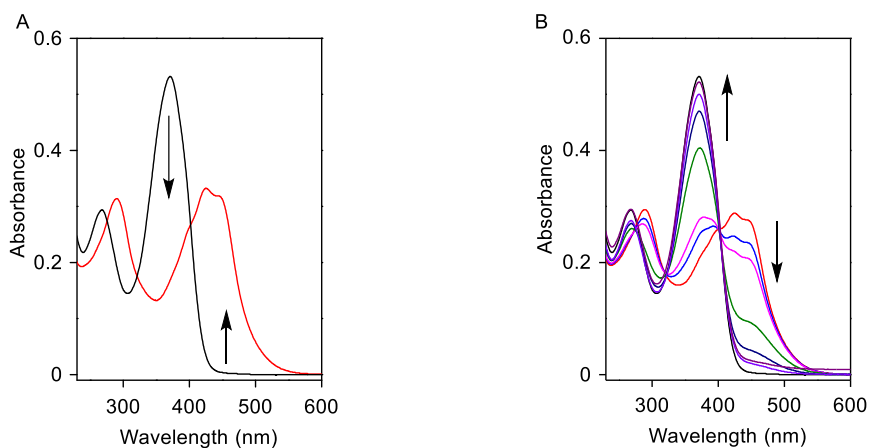

Fig. S3 Photo-irradiation of **2** (64 μM) in MeOH with 365 nm UV light for 5 s (A). Reverse photo-isomerization of compound **2** (64 μM) with 450 nm LED light for 9 min (B).
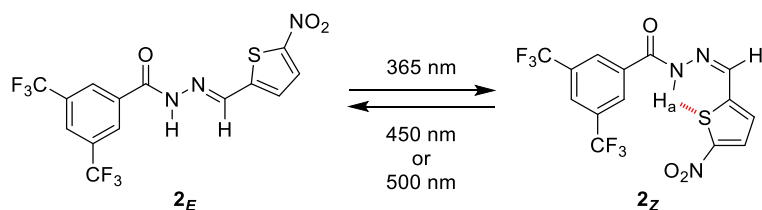

Fig. S4 Representation of reversibility in photo-switching for **2**.

Further, a photo-reversible cycle was carried out to scrutinize its photo-reversible efficiency and the stability of the compound during the photo-switching process. Investigation revealed that after the initial drop in the absorbance intensity of the active conformer for the first cycle, and the intensity remained
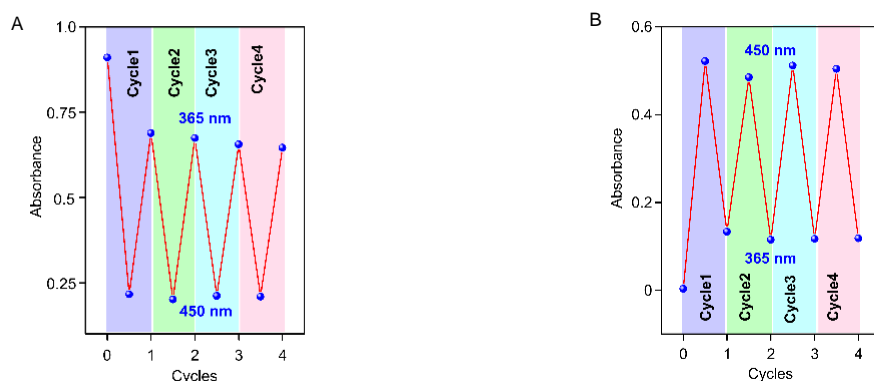

Fig. S5 Change in the UV absorbance of compound **2** (64 μM) at 365 nm wavelength (A) and 450 nm wavelength (B) during the photo-reversible cycle.

constant during the remaining cycles. This data indicated that compound **2** can be utilized as an efficient molecular switch system even after 4 cycles of photo-switching process.

Hence, this rapid reversible photo-switching between the *E* and *Z*-conformers can be useful for utilizing it as a photo-controllable ion transport process.
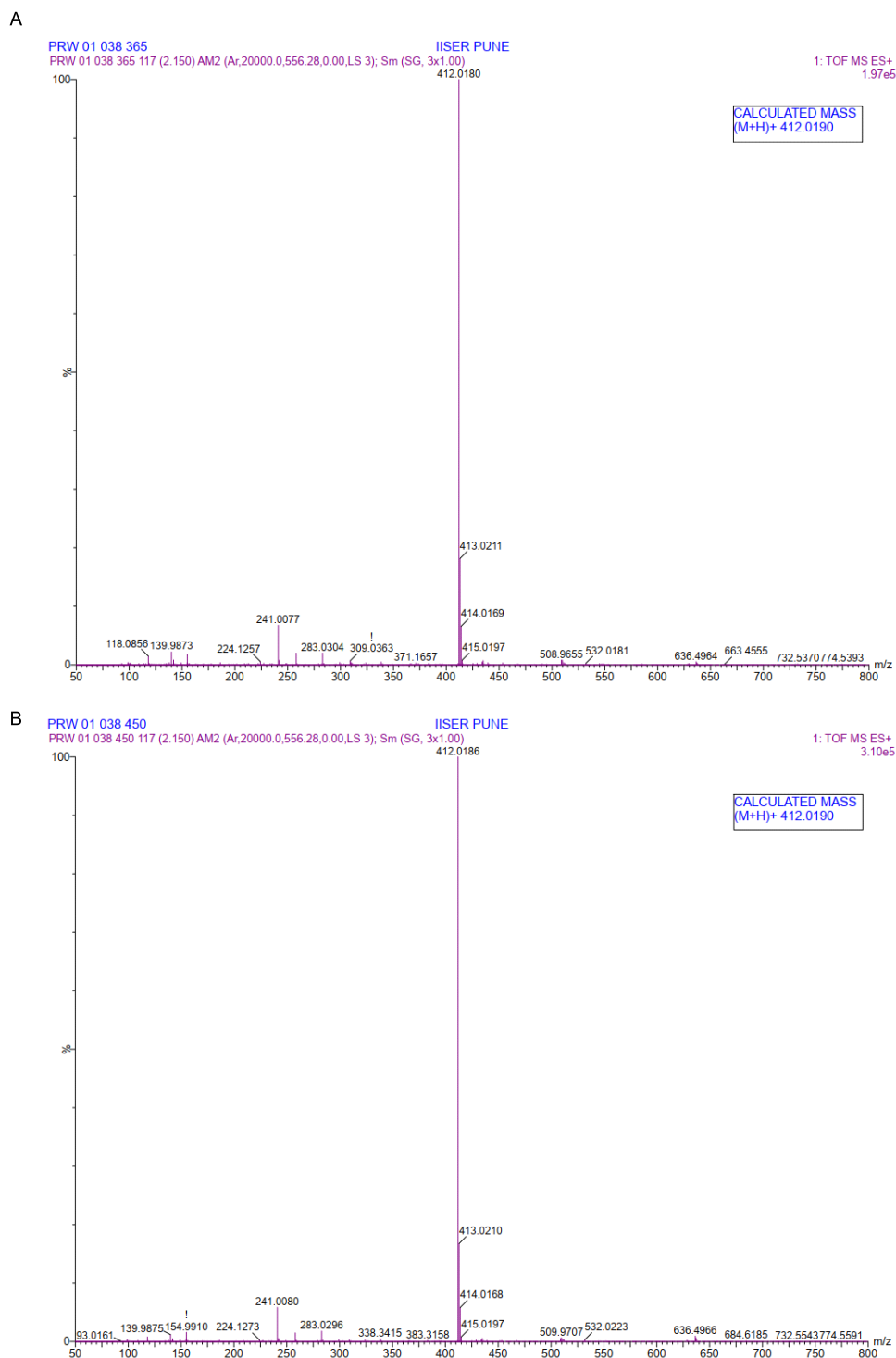

Fig. S6 Change in the HRMS spectra of compound **2** after irradiation with 365 nm UV light (A) and 450 nm LED light (B).

Since the photoisomerized 2_Z isomer also has a small UV absorbance at 500 nm, we irradiated the 2_Z conformer with 500 nm of light to reconvert it to its initial 2_E conformer. Interestingly, we noticed that irradiation of 500 nm of LED light significantly reconverts the $2_E \rightarrow 2_Z$ within 14 min. Further, a photoswitching cycle was conducted with sequential photoirradiation with 365 nm and 500 nm of light up to 4 cycles. The investigation revealed that the initial drop in the absorbance intensity was negligible for the first cycle as compared to the 365 nm-450 nm photo-reversible cycle, and the intensity remained consistent even up to 4 cycles. This data divulges that compound **2** can be utilized as a stable photoswitcher even with sequential photoirradiation with 365 nm and 500 nm LED light.
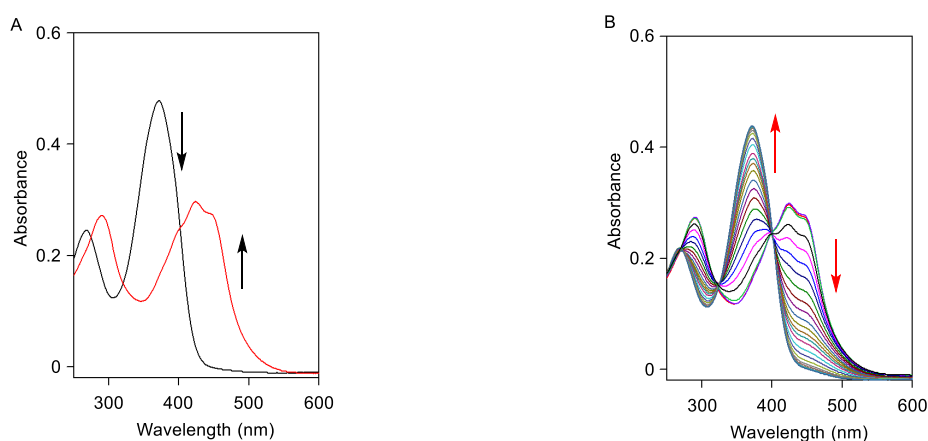

Fig. S7 Photo-irradiation of **2** (64 μM) in MeOH with 365 nm UV light for 5 s (A). Reverse photo-isomerization of compound **2** (64 μM) with 500 nm LED light for 14 min (B).

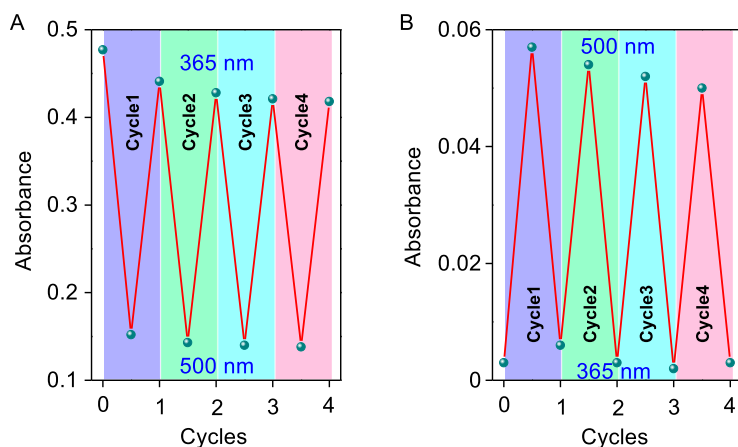**Fig. S8** Change in the UV absorbance of compound 2 (64 μM) at 365 nm wavelength (A) and 500 nm wavelength (B) during the photo-reversible cycle.

B. Thermal stability studies:[S2]

Slow thermal relaxation influenced us to investigate the photostationary state composition during $2_Z \rightarrow 2_E$ thermal relaxation by ^{1}H NMR in MeOH-d_4 solvent at 25 °C. 2 mM concentration was used

during the experiment. The spectrum was recorded for compound **2** before and after 365 nm irradiation at different time interval. The estimated the photostationary state (PSS) of $2_Z \rightarrow 2_E$ thermal relaxation is around 80 %.
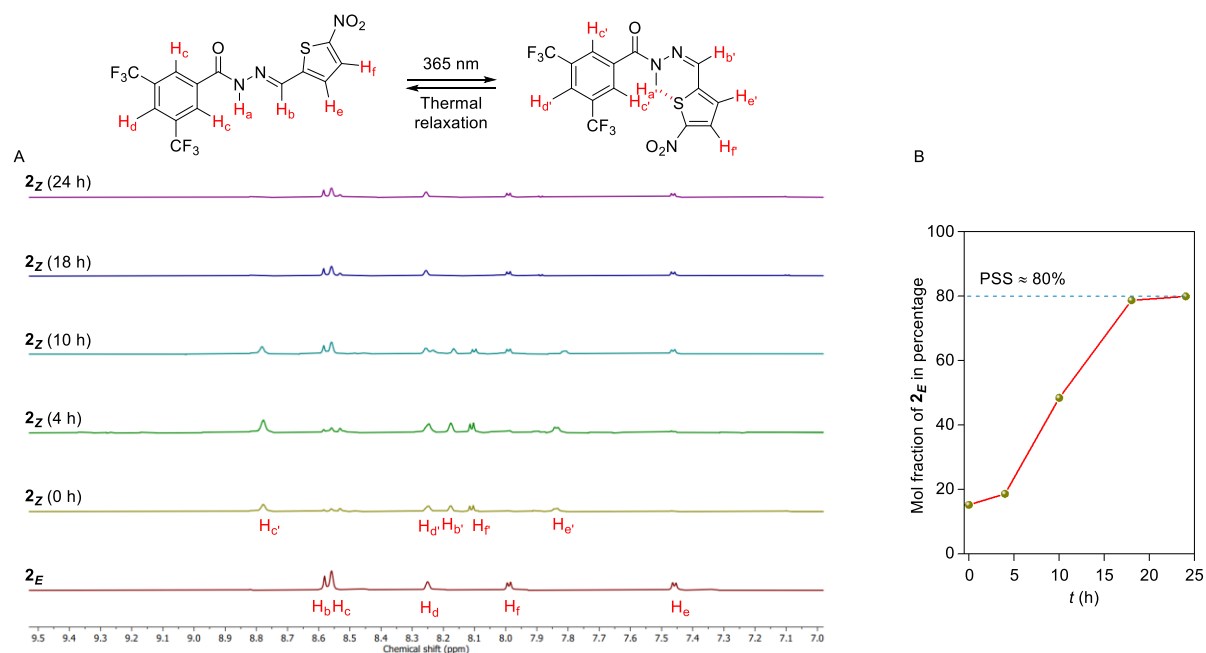

Fig. S9 Time-dependent ^{1}H NMR spectrum of thermal relaxation of $2_Z \rightarrow 2_E$ (2 mM) in MeOH-d_4 solvent at 25 °C (A), Changes in the mole fraction of 2_E during thermal relaxation of $2_Z \rightarrow 2_E$ after photoirradiation with 365 nm light on 2_E conformer (B).

Since all the OFF-ON transport experiments were carried out in a buffer medium, we additionally investigated the stability of photoisomerized 2_Z conformer in MeOH-d_4:D$_2$O (2:1 v/v) system by using ^{1}H NMR at 25 °C. Interestingly, we noticed the stability of photoisomerized 2_Z conformer increases MeOH-d_4:D$_2$O systems as compared to the pure MeOH-d_4 solvent system. The calculated photostationary state (PSS) of $2_Z \rightarrow 2_E$ thermal relaxation is approximately 85%. This data gives additional evidence that the stability of the photoisomerized 2_Z conformer is solvent-dependent phenomenon.
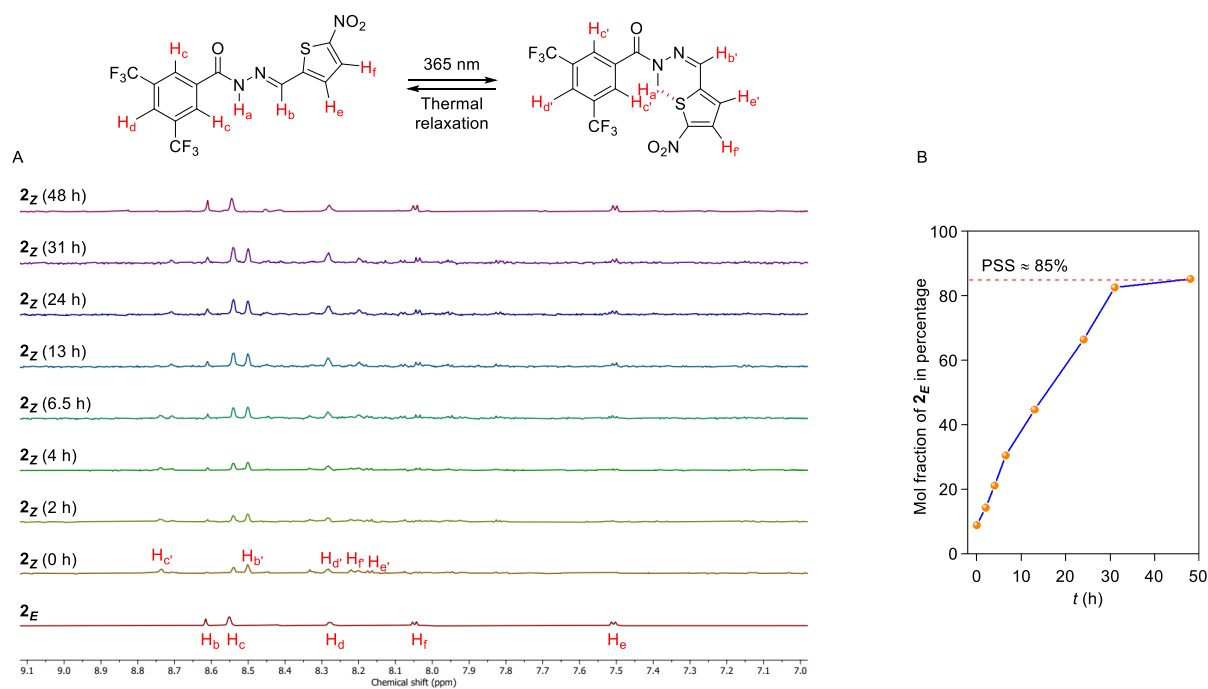
Fig. S10 Time-dependent ^{1}H NMR spectrum of thermal relaxation of $\mathbf{2_Z} \rightarrow \mathbf{2_E}$ (2 mM) in MeOH-d_4: D$_2$O solvent (2:1 v/v) at 25 °C (A), Changes in the mole fraction of $\mathbf{2_E}$ during thermal relaxation of $\mathbf{2_Z}$ $\rightarrow \mathbf{2_E}$ after photoirradiation with 365 nm light on $\mathbf{2_E}$ conformer (B).
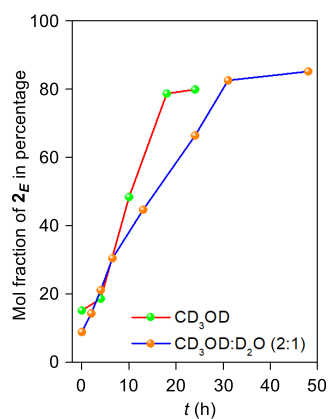
Fig. S11 Changes in the mole fraction of $\mathbf{2_E}$ during thermal relaxation of $\mathbf{2_Z} \rightarrow \mathbf{2_E}$ in different solvent systems.
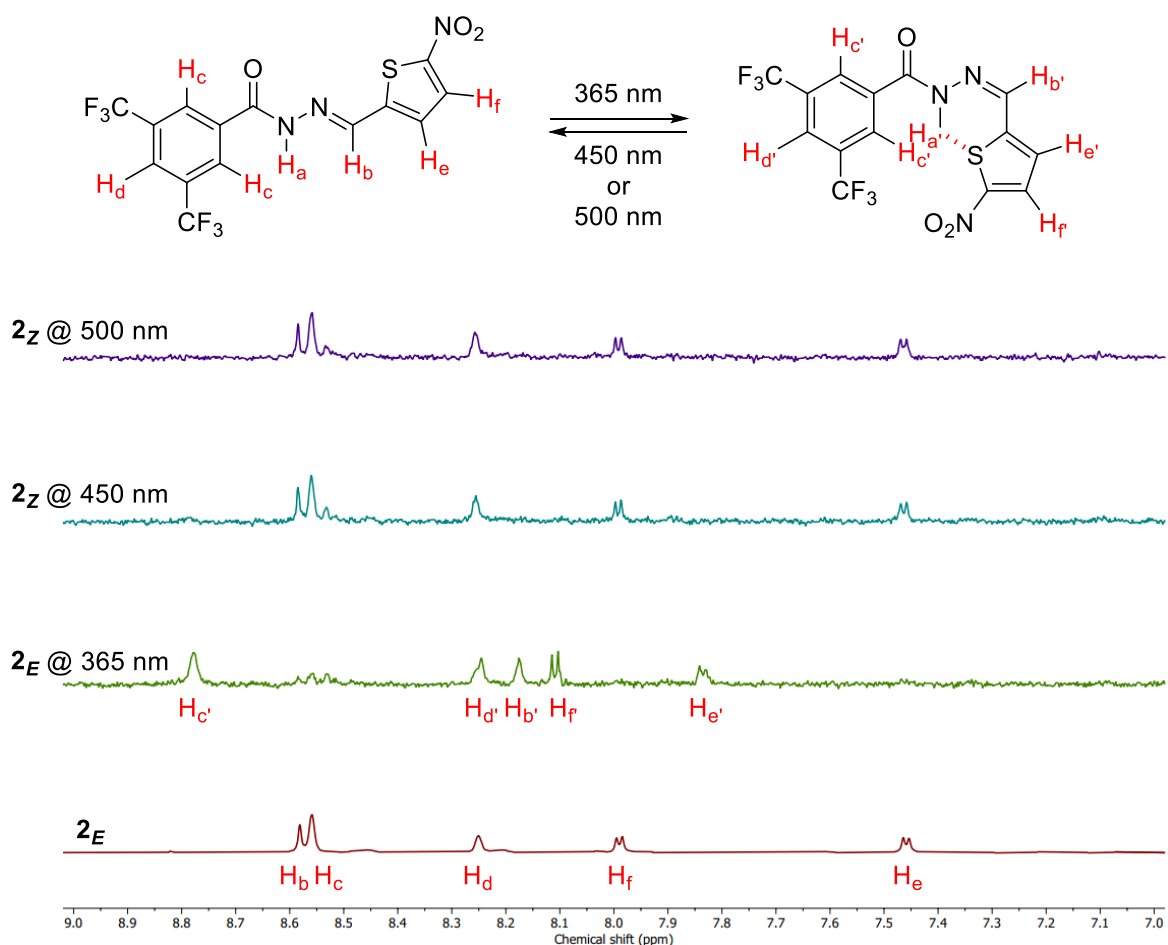
Fig. S12 ^{1}H NMR after sequential irradiation with 365 nm, 450 nm or 500 nm LED light.

IV. Ion Binding Studies:[S3]

For evaluating the ion binding efficiency of compound **2** towards anions, ^{1}H NMR titration was carried out with different TBAX salts ($X^- = Cl^-$, Br^-, and I^-). The guest (salts) concentration was increased gradually, and the ^{1}H NMR was recorded after each addition. A significant downfield shift of N-H_a, C-H_b, and C-H_c protons implied that protons H_a, H_b, and H_c are involved in the overall binding of the anions. The BindFit v0.5 software was used to analyze the binding constant with different ions with a 1:1 binding model.

Fig. S13 ^{1}H NMR titration of compound **1a** (2 mM) with TBACl salt in CD$_3$CN at 25 °C.

Fig. S14 Screenshot of the fitted data plot from supramolecular.org in BindFit v0.5. The calculated binding constant was found to be 995 M^{-1} ± 5% in 1:1 receptor-to-anion binding model (left side). The changing pattern of chemical shift and chemical shift residuals with the increasing equivalent of TBACl (right side). The Bindfit URL for this experiment is: http://app.supramolecular.org/bindfit/view/dff8777c-bc5f-4a97-b185-7c9e42929078.

Fig. S15 ^{1}H NMR titration of compound **1b** (2 mM) with TBACl salt in CD$_3$CN at 25 °C.

Fig. S16 Screenshot of the fitted data plot from supramolecular.org in BindFit v0.5. The calculated binding constant was found to be 662 M^{-1} ± 6% in 1:1 receptor-to-anion binding model (left side). The changing pattern of chemical shift and chemical shift residuals with the increasing equivalent of TBACl (right side). The Bindfit URL for this experiment is: http://app.supramolecular.org/bindfit/view/08ab0ac7-1c6a-4a4f-84fb-5b0676c70170.
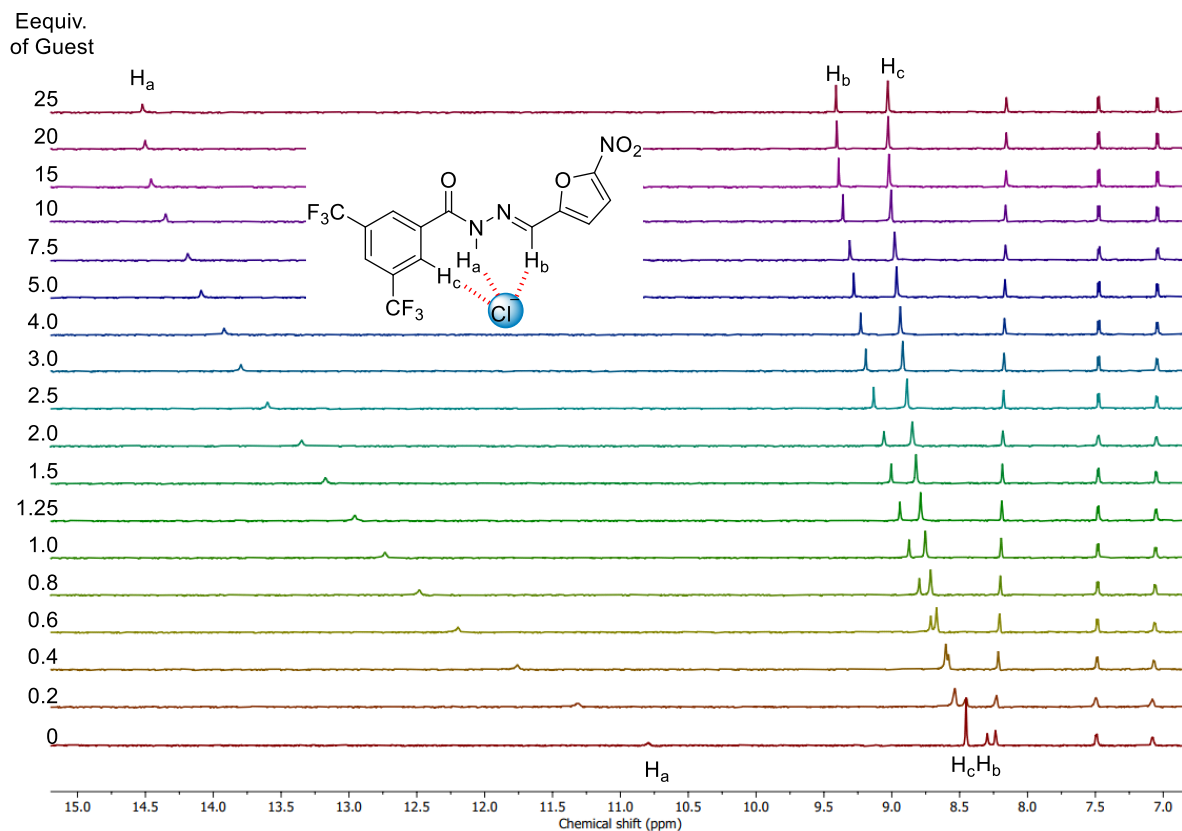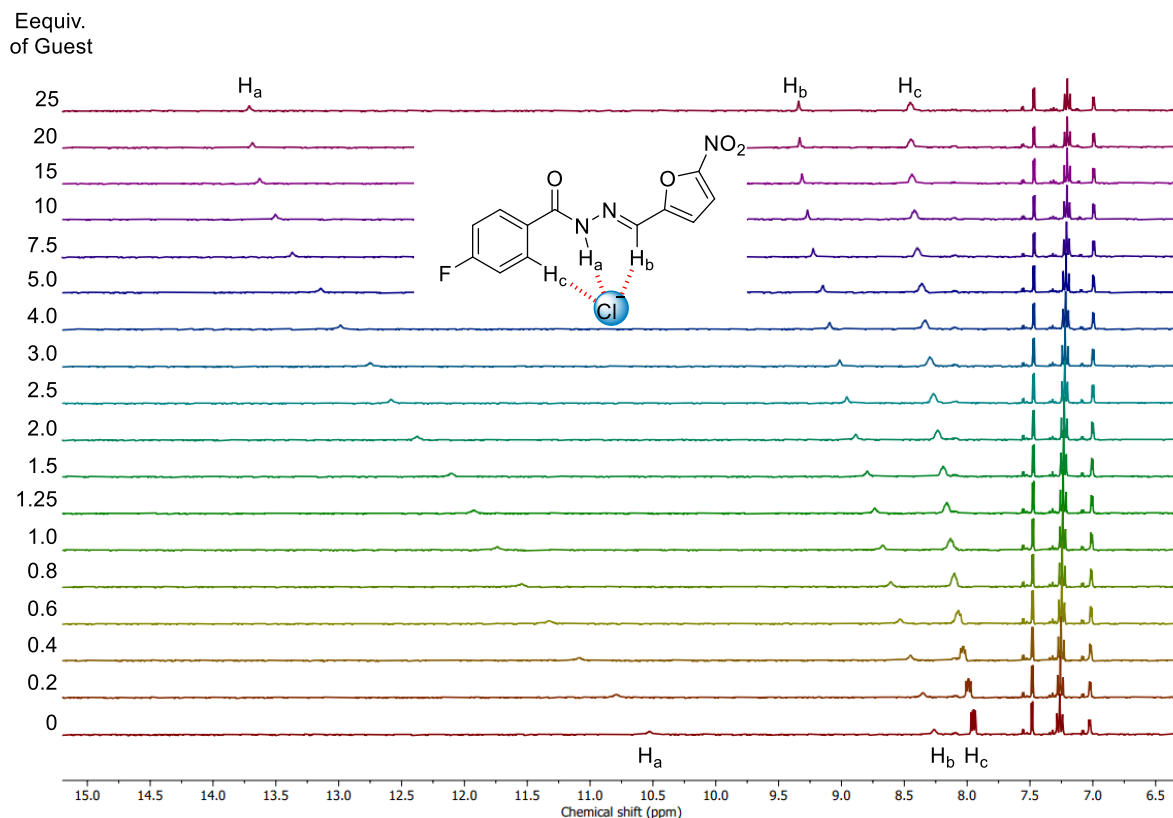
Fig. S17 ^{1}H NMR titration of compound **1c** (2 mM) with TBACl salt in CD$_3$CN at 25 °C.
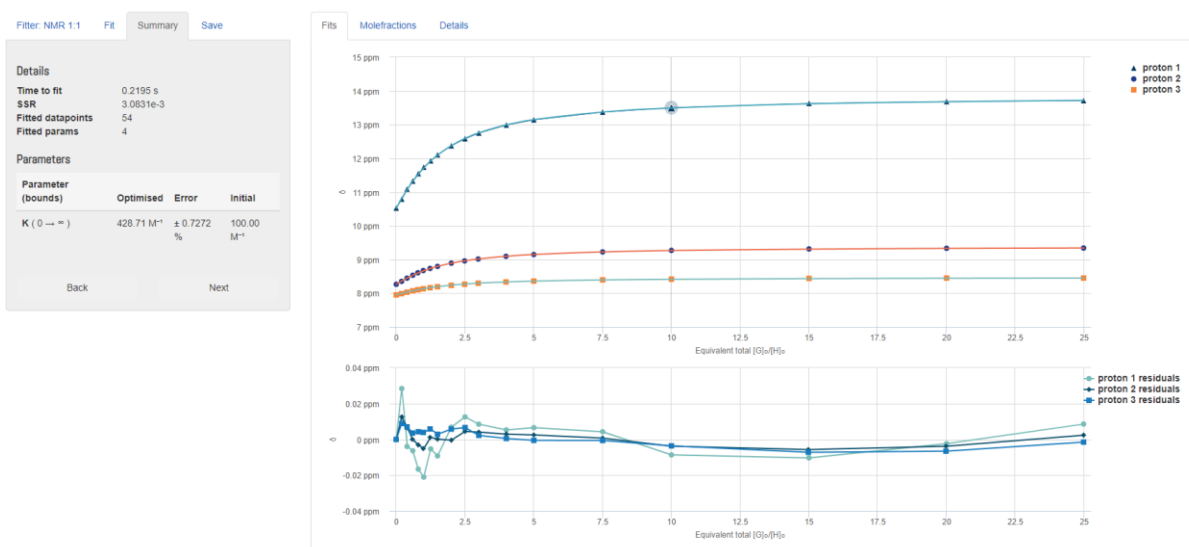
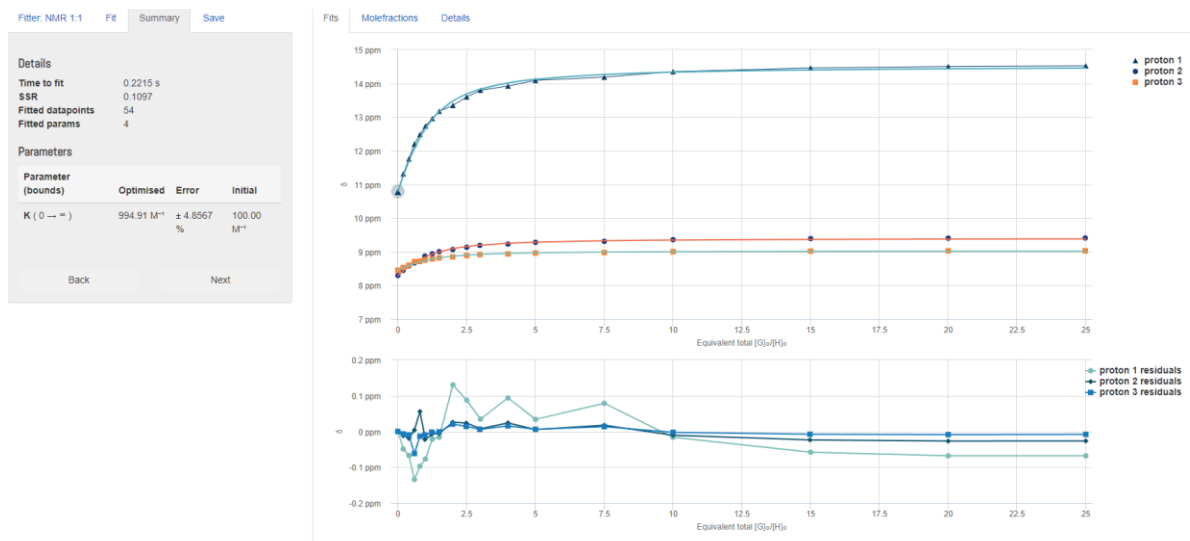**Fig. S18** Screenshot of the fitted data plot from supramolecular.org in BindFit v0.5. The calculated binding constant was found to be 429 M^{-1} ± 0.7% in 1:1 receptor-to-anion binding model (left side). The changing pattern of chemical shift and chemical shift residuals with the increasing equivalent of TBACl (right side). The Bindfit URL for this experiment is: http://app.supramolecular.org/bindfit/view/fe941510-fa2e-411f-8597-c48087b008e9.
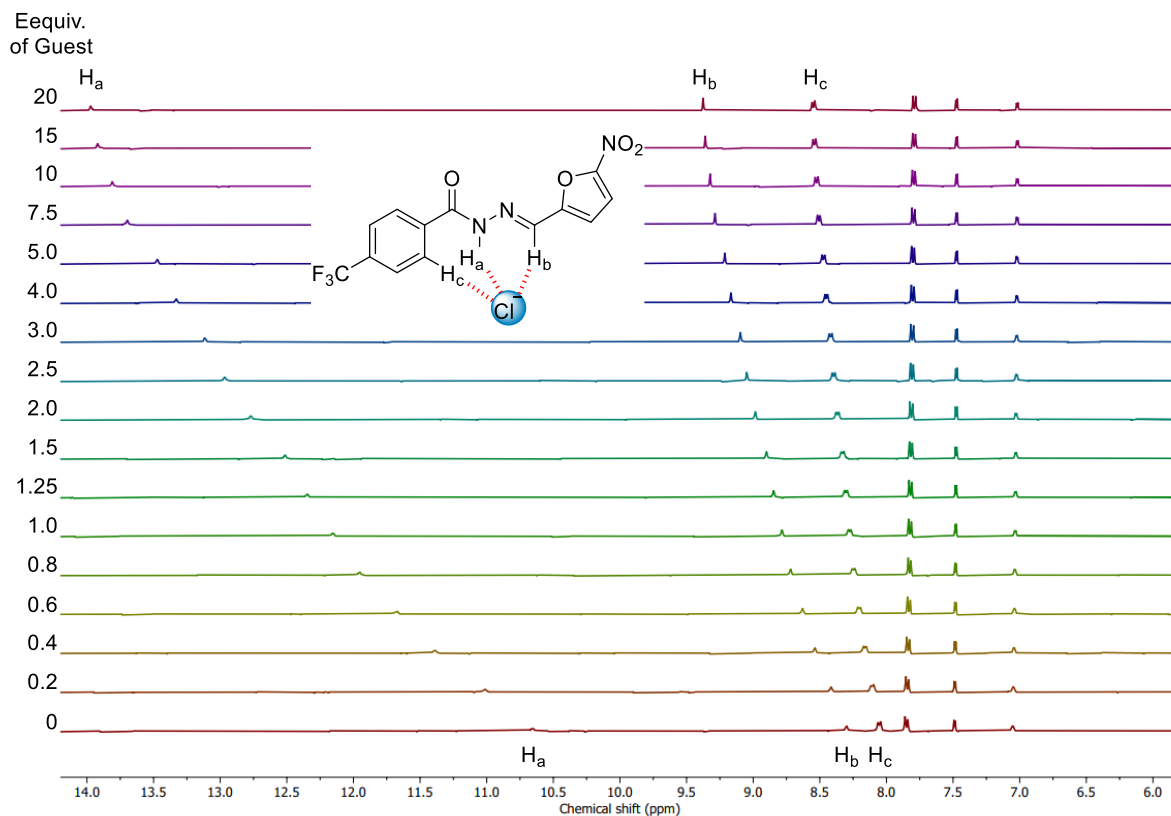
Fig. S19 ^{1}H NMR titration of compound **2** (2 mM) with TBACl salt in CD$_3$CN at 25 °C.

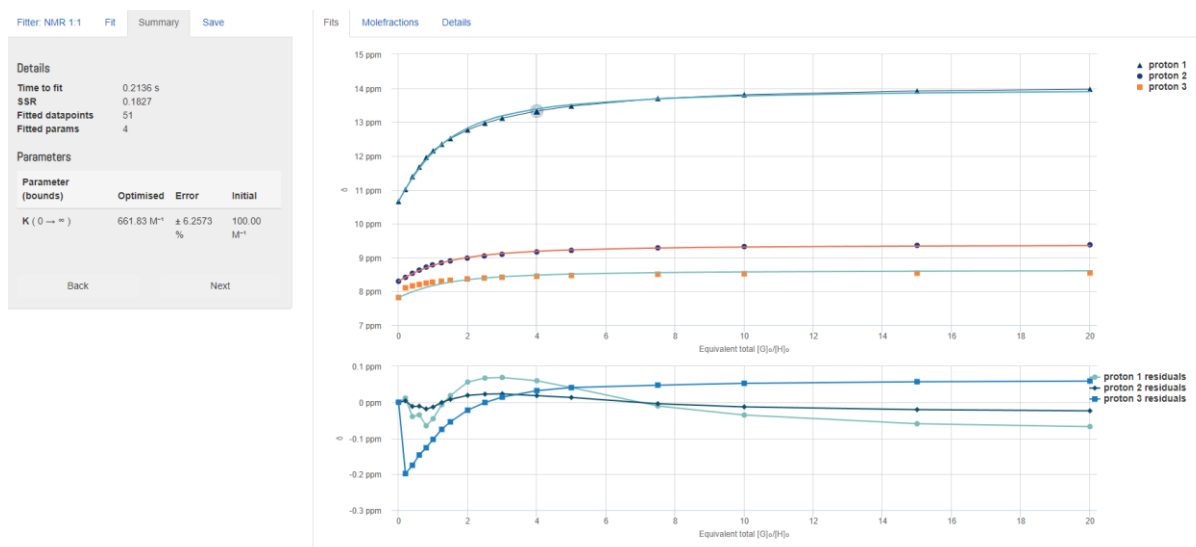**Fig. S20** Screenshot of the fitted data plot from supramolecular.org in BindFit v0.5. The calculated binding constant was found to be 935 M^{-1} ± 3% in 1:1 receptor-to-anion binding model (left side). The changing pattern of chemical shift and chemical shift residuals with the increasing equivalent of TBACl (right side). The Bindfit URL for this experiment is: http://app.supramolecular.org/bindfit/view/75eb208e-0b5d-4c66-b8a1-8a4508a15e6d.
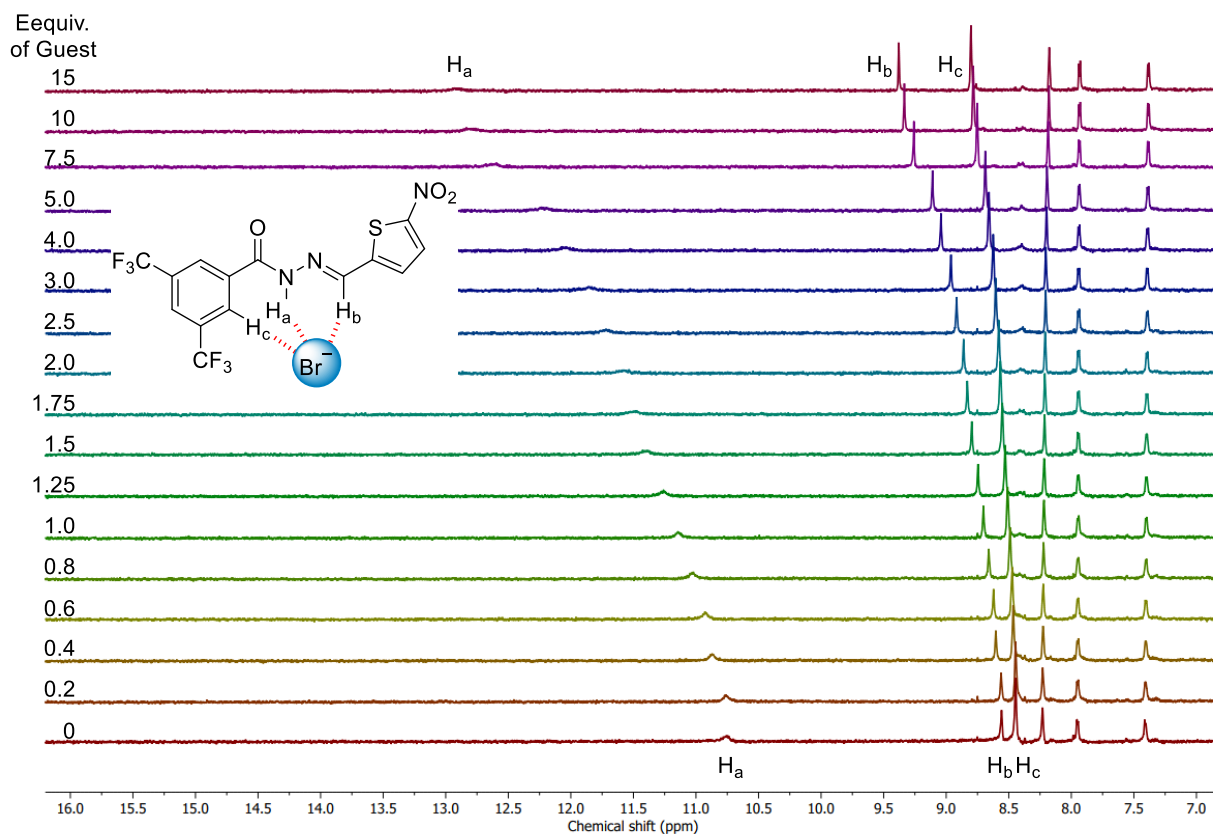
Fig. S21 ^{1}H NMR titration of compound **2** (2 mM) with TBABr salt in CD$_3$CN at 25 °C.
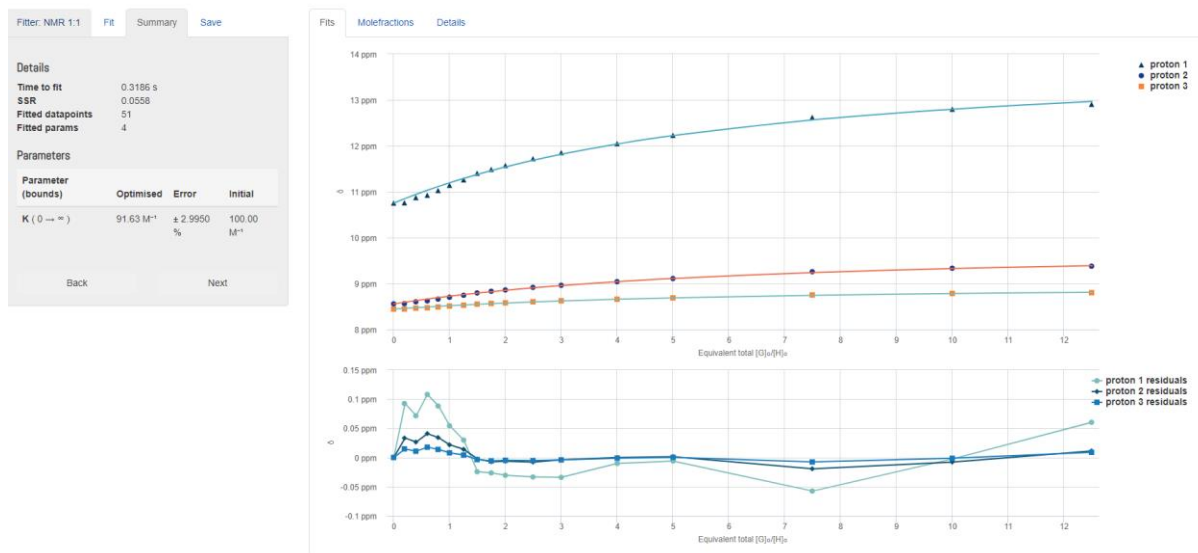
Fig. S22 Screenshot of the fitted data plot from supramolecular.org in BindFit v0.5. The calculated binding constant was found to be 91 M^{-1} ± 3% in 1:1 receptor-to-anion binding model (left side). The changing pattern of chemical shift and chemical shift residuals with the increasing equivalent of TBAI (right side). The Bindfit URL for this experiment is: http://app.supramolecular.org/bindfit/view/a717e4bb-3fd7-4887-9e33-019a29f055d1.
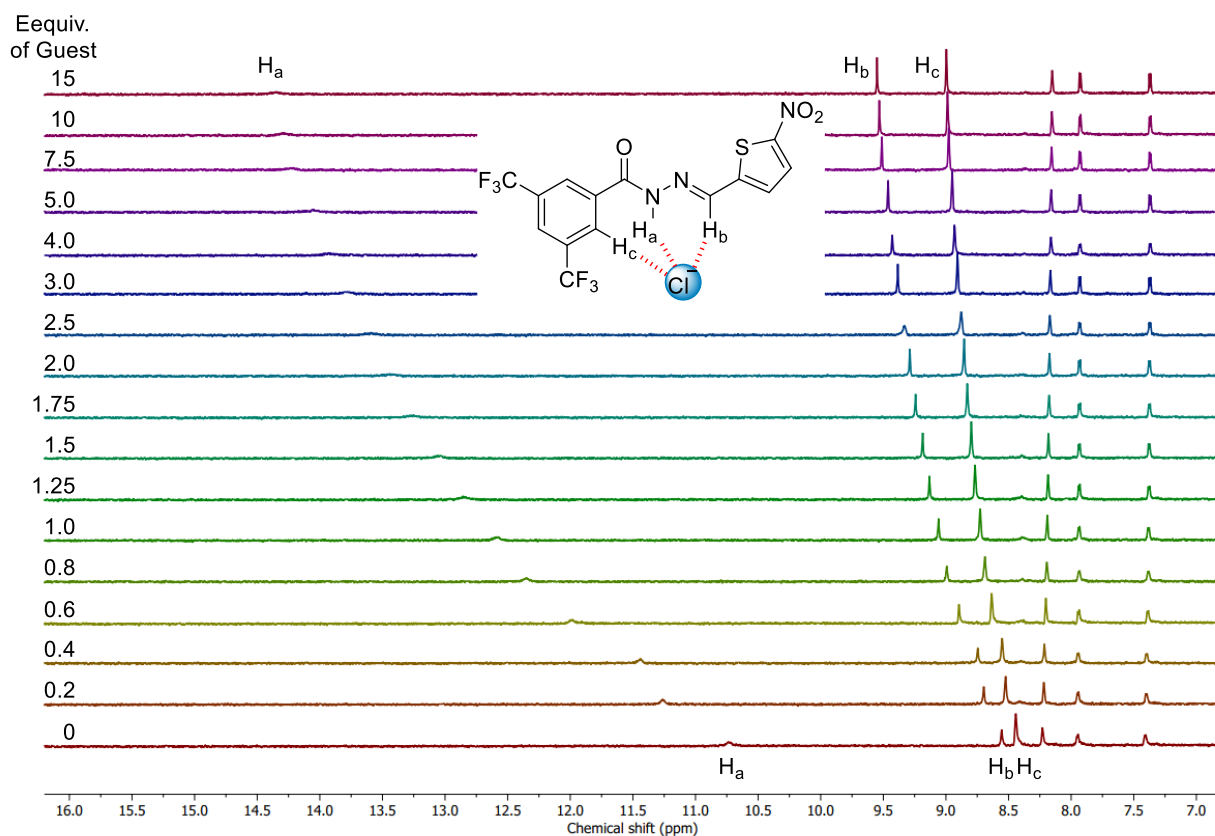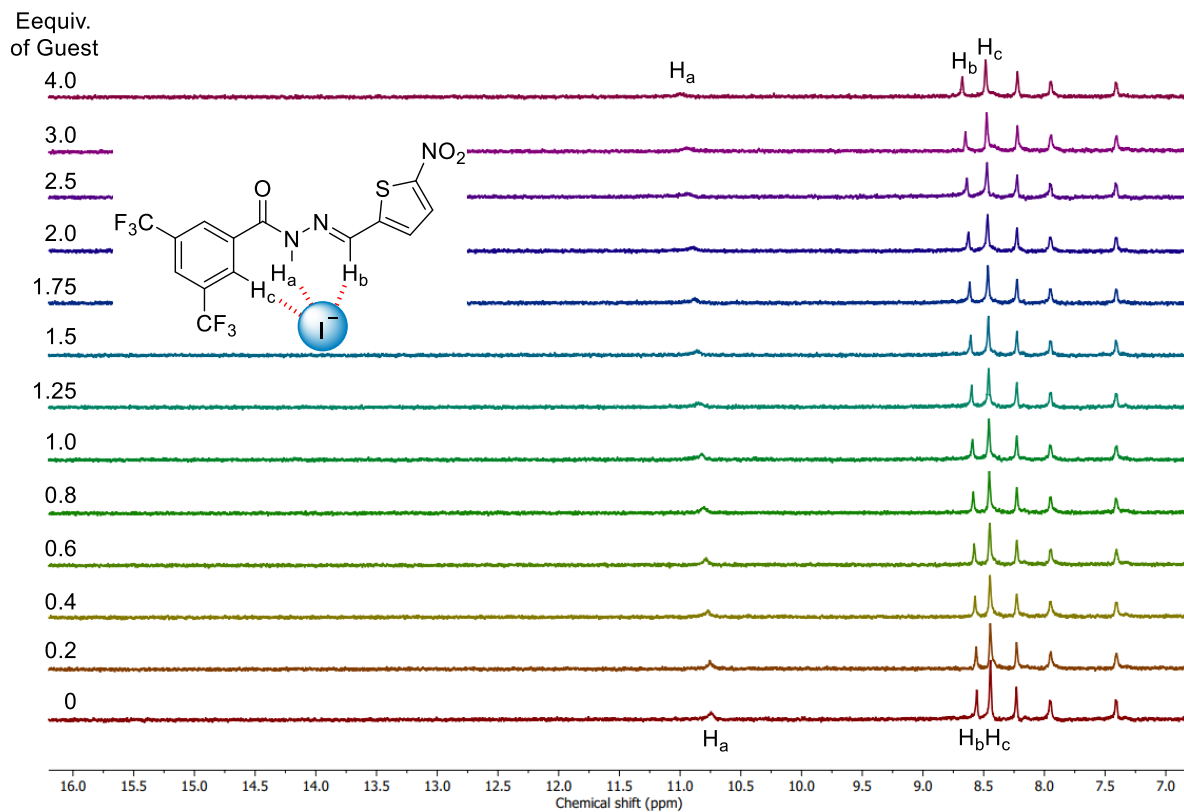
Fig. S23 ^{1}H NMR titration of compound **2** (2 mM) with TBAI salt in CD$_3$CN at 25 °C.
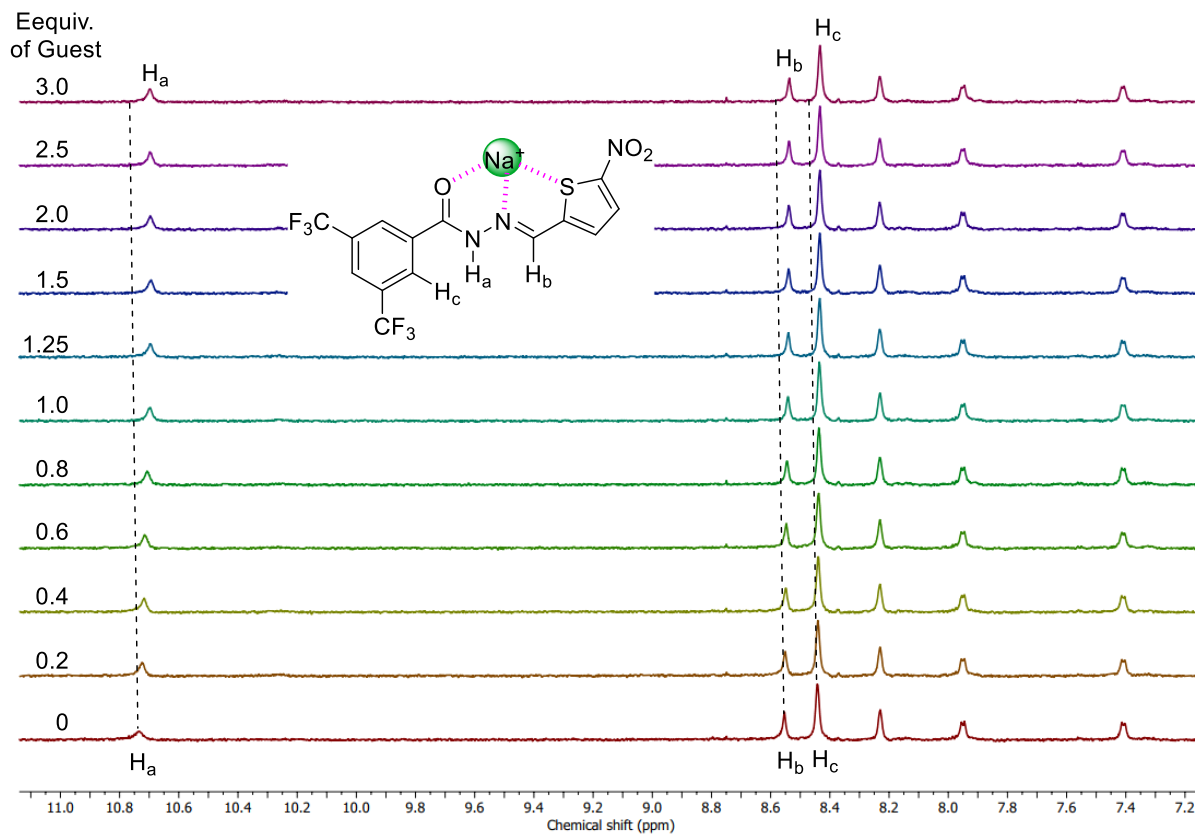
Fig. S24 ^{1}H NMR titration of compound **2** (2 mM) with NaPF$_6$ salt in CD$_3$CN at 25 °C.
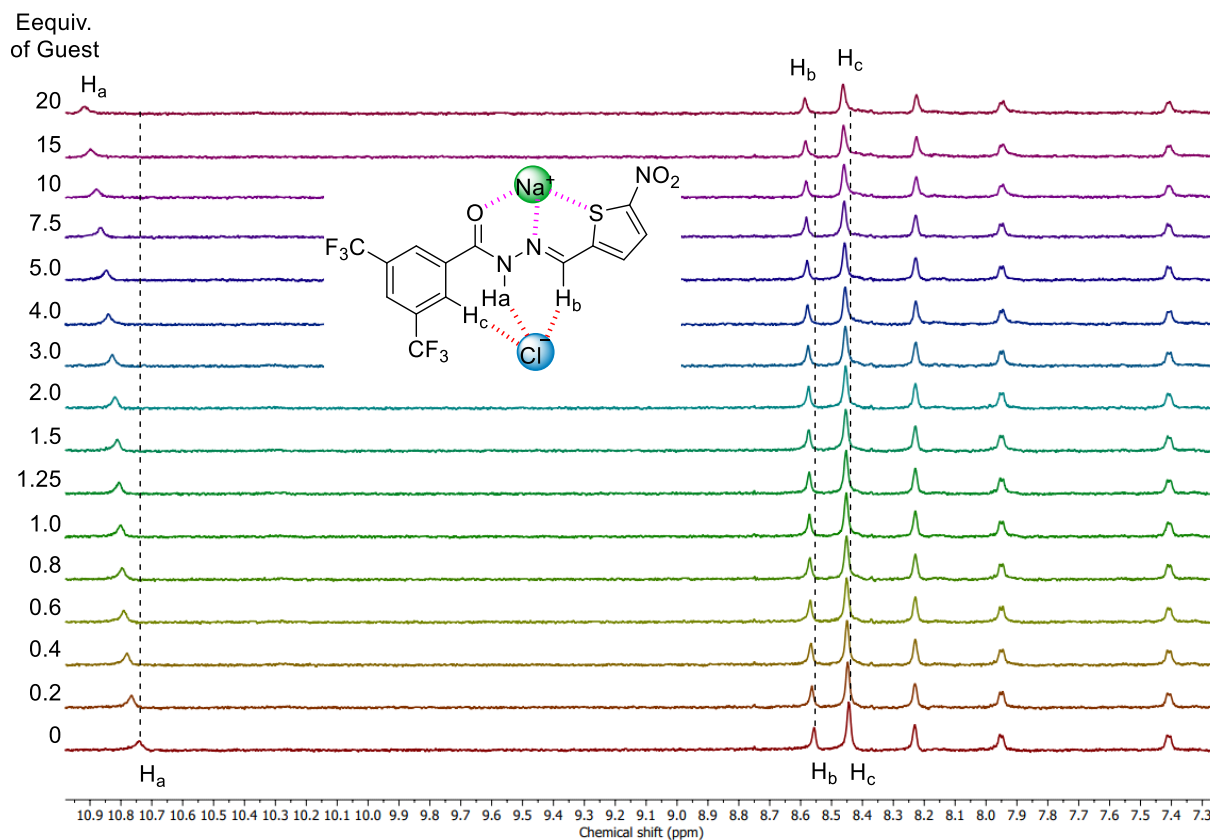
Fig. S25 ¹H NMR titration of compound **2** (2 mM) with Na⁺Cl⁻ ion pairs (mixture of 1:1 NaPF₆ and TBACl) salt in CD₃CN at 25 °C.

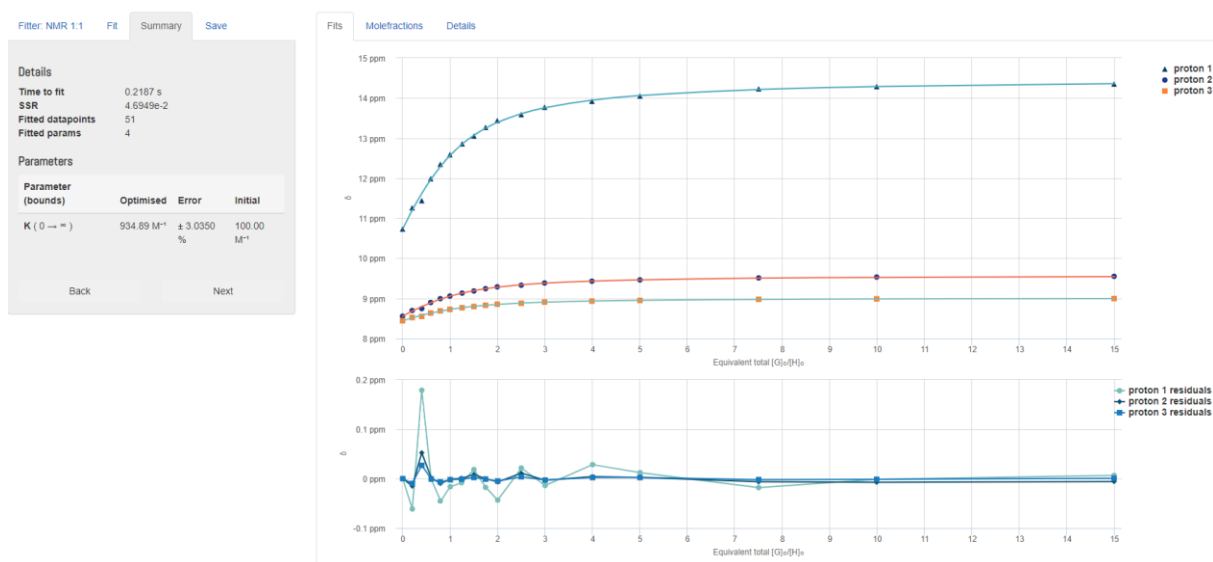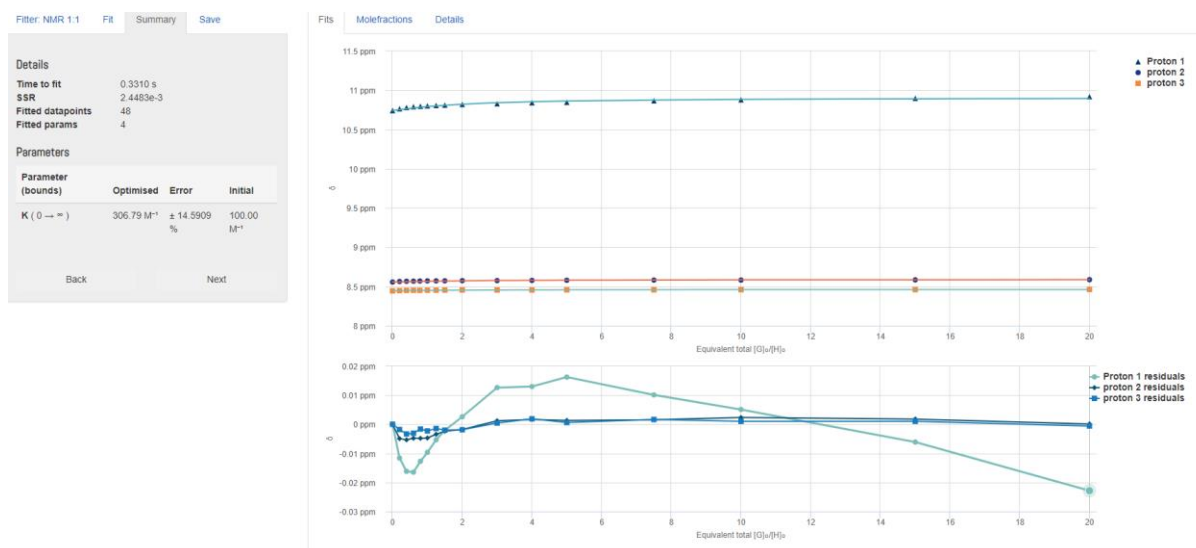**Fig. S26** Screenshot of the fitted data plot from supramolecular.org in BindFit v0.5. The calculated binding constant was found to be 307 M⁻¹ ± 14% in 1:1 receptor-to-anion binding model (left side). The changing pattern of chemical shift and chemical shift residuals with the increasing NaCl (1:1 mixture of NaPF₆ and TBACl) equivalent (right side). The Bindfit URL for this experiment is: http://app.supramolecular.org/bindfit/view/75c9d81b-2291-4518-9fa4-5f0d5a612780.

IV. Ion Transport Studies:[S4–S7]

A. Ion transporting activity studies across EYPC–LUVs⊃HPTS:

Preparation of HEPES buffer and stock solutions: The HEPES buffer (pH = 7.0) was prepared by dissolving an appropriate amount of solid HEPES (10 mM) and NaCl (100 mM) in autoclaved water. The pH was adjusted to 7.0 by the addition of aliquots from the NaOH solution (0.5 M). HPLC grade DMSO was used for the stock solution preparation of all the derivatives.

Preparation of EYPC–LUVs⊃HPTS with NaCl: In a clean and dried round bottom flux (10 mL), 1 mL of egg yolk phosphatidylcholine (EYPC, 25 mg/mL in CHCl$_3$) was dried by purging nitrogen gas with continuous rotation to make a thin transparent film of EYPC. Then, to remove a trace amount of CHCl$_3$, it was kept under a high vacuum for 4 h. Further, the dried thin film was hydrated with 1 mL HEPES buffer (1 mM HPTS, 10 mM HEPES, 100 mM NaCl, pH = 7.0), and the resulting suspension was vortexed for 1 h at 10 min intervals. This hydrated suspension was subjected to 21 cycles of freeze–thaw (liquid N$_2$ and 55 °C hot water bath) followed by extrusion through 100 nm pore size containing polycarbonate membrane 21 times (must be an odd number), in order to achieve uniform distribution of LUVs of an average 100 nm diameter. Finally, size exclusion chromatography using gel filtration (Sephadex G-50) was carried out to remove the unentrapped extravesicular HPTS dyes with HEPES buffer (10 mM HEPES, 100 mM NaCl, pH = 7.0). Collected vesicles were diluted to 6 mL to get EYPC–LUVs⊃HPTS. Final conditions: ~ 5.0 mM EYPC, Inside: 1 mM HPTS, 10 mM HEPES, 100 mM NaCl, pH = 7.0, Outside: 10 mM HEPES, 100 mM NaCl, pH = 7.0.

Ion transport activity by HPTS assay: In clean and well-dry fluorescence cuvette, 1975 μL of HEPES buffer (10 mM HEPES, 100 mM NaCl, pH =7.0) and 25 μL of EYPC–LUVs⊃HPTS vesicle was added. The cuvette was placed in a slowly stirring condition using a magnetic stirrer equipped with the fluorescence instrument (t = 0 s). The time-dependent HPTS emission intensity was monitored at λ_{em} = 510 nm (λ_{ex} = 450 nm) by creating a pH gradient (~ 0.8) between the intra- and extra-vesicular system by the addition of 20 μL NaOH (0.5 M) at t = 20 s. Then, different concentrations of transporter molecules in DMSO were added at t = 100 s. Finally, the vesicles were lysed by the addition of 10% Triton X−100 solutions (25 μL) at t = 300 s (for longer kinetics, Triton X−100 solutions was added at t = 600 s) for destruction pH gradient (Fig. S1).
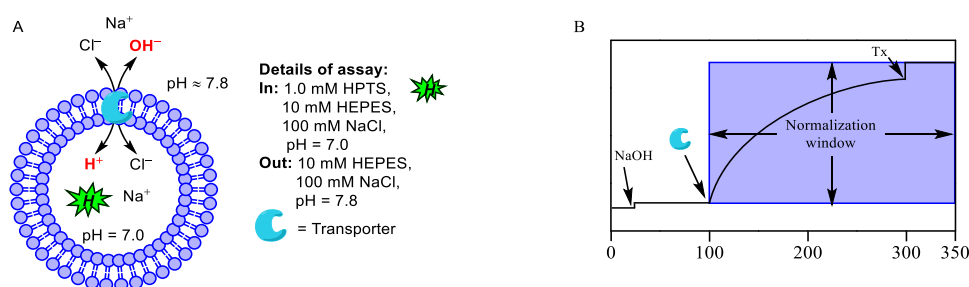
Fig. S27 Schematic representation of ion transport activity across EYPC–LUVs⊃HPTS vesicle **(A)**, and normalization window for same fluorescence kinetics experiment of ion transport **(B)**.

The time axis was normalized according to Equation S3:

$$t = t - 100 \qquad \qquad \text{Equation S3}$$

where, in normalized data $t = 0$ s was the timing of compound addition during the experiment, and $t = 200$ s was the timing of Triton X–100 addition.

The time-dependent data were normalized to fractional fluorescence intensity (in percentage) using Equation S4

$$I_F = [(I_t - I_0) / (I_\infty - I_0)] \times 100 \qquad \qquad \text{Equation S4}$$

where, I_0 = Fluorescence intensity just before the transporter molecule addition (at 0 s), I_∞ = Final fluorescence intensity after addition of Triton X–100, I_t = Fluorescence intensity at time t.

Comparison of ion transport activity in EYPC–LUVs⊃HPTS: To investigate the relative transport activity of transporter molecules **1a–1c** and **2**, an ion transport experiment was done across EYPC–LUVs⊃HPTS. A Comparison study with 300 nM concentration revealed the activity sequence of **1a** > **2** > **1b** > **1c** (Fig. S28).
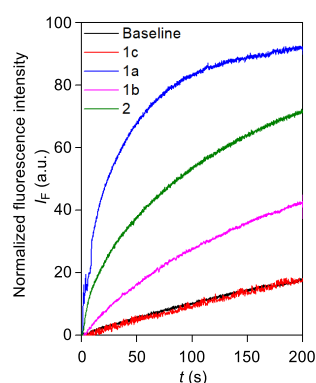
Fig. S28 Comparison of ion transport activity of compounds **1a–1c** and **2** in EYPC–LUVs⊃HPTS at 300 nM.

Dose-response activity in EYPC–LUVs⊃HPTS: The fluorescence kinetics of each transporter molecule at different concentrations was studied over the course of time. The concentration profile data were evaluated at $t = 290$ s to get effective concentration, EC_{50} (i.e. the concentration of transporter needed to achieve 50% ion efflux activity)[S8] using Hill equation (Equation S5):

$$Y = Y_\infty + (Y_0 - Y_\infty) / [1 + (c/EC_{50})^n]$$ Equation S5

where, Y_0 = Fluorescence intensity just before the addition of transporter molecule (at $t = 0$ s), Y_∞ = Fluorescence intensity with excess compound concentration, c = concentration of transporter molecule, and n = Hill coefficient (i.e. indicative for the number of monomers needed to form an active supramolecule).

Dose-response activity of compounds 1a–1c with NaCl salt:
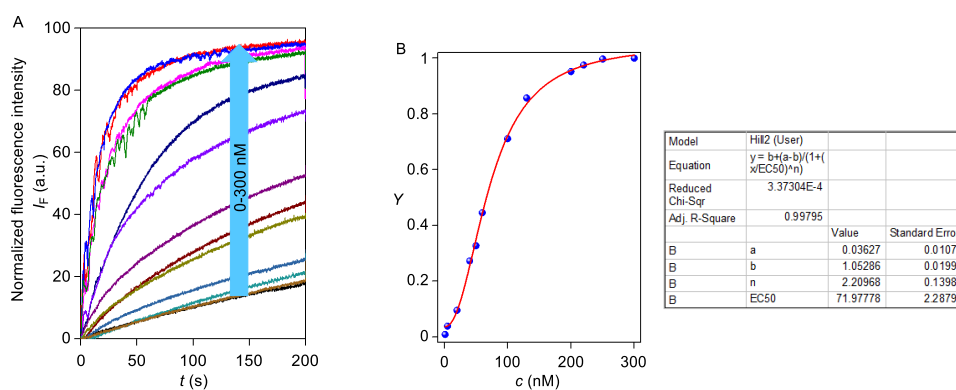
Fig. S29 Concentration dependent ion transport activity of compound **1a** (0–300 nM) with NaCl salt across EYPC–LUVs⊃HPTS (**A**), and corresponding Hill plot of compound **1a** at $t = 190$ s (**B**).
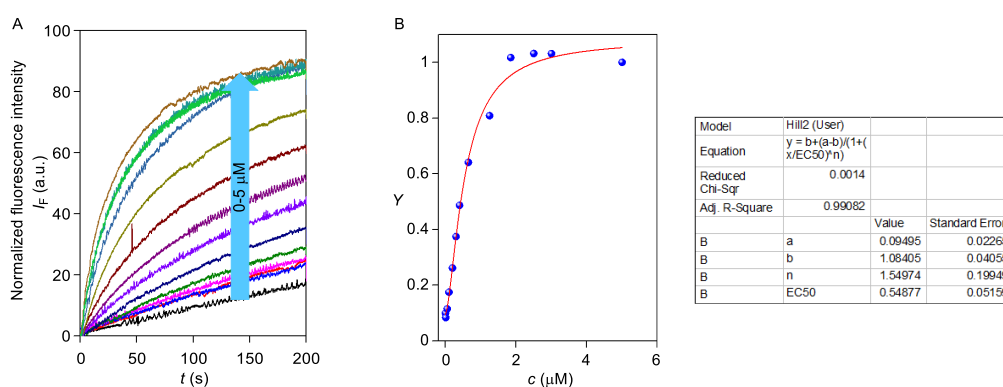
Fig. S30 Concentration dependent ion transport activity of compound **1b** (0–5 μM) with NaCl salt across EYPC–LUVs⊃HPTS (**A**), and corresponding Hill plot of compound **1b** at $t = 190$ s (**B**).
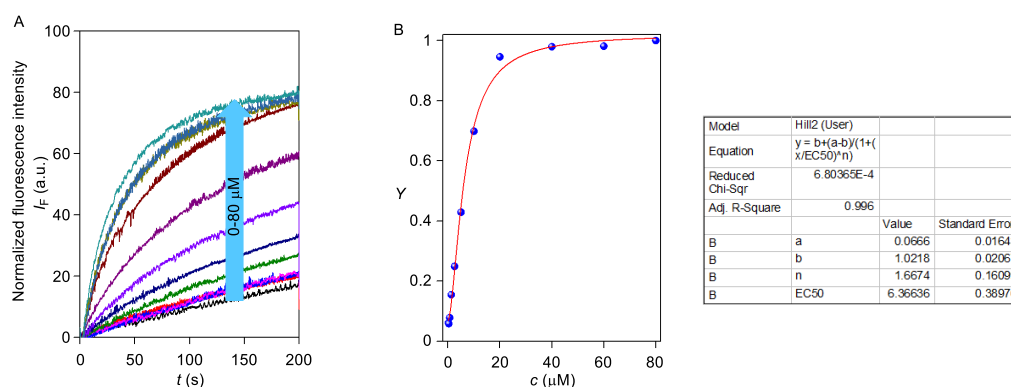
Fig. S31 Concentration dependent ion transport activity of compound **1c** (0–80 μM) with NaCl salt across EYPC–LUVs⊃HPTS (**A**), and corresponding Hill plot of compound **1c** at t = 190 s (**B**).
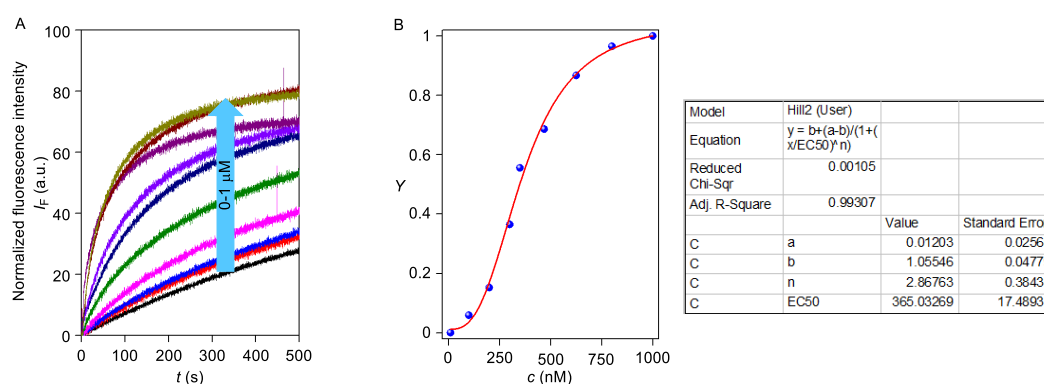
Fig. S32 Concentration dependent ion transport activity of compound **2** (0–1 μM) with NaCl salt across EYPC–LUVs⊃HPTS (**A**), and corresponding Hill plot of compound **2** at t = 190 s (**B**).

B. Ion selectivity studies across EYPC–LUVs⊃HPTS:[S5,S7]

Buffer and stock solution preparation: HEPES buffer was prepared by dissolving an appropriate amount of solid HEPES and a salt (either of NaF, NaCl, NaBr, NaI, NaNO₃, NaSCN, LiCl, KCl, RbCl, and CsCl) in autoclaved water to get 10 mM HEPES and 100 mM salt respectively. Subsequently, the pH was adjusted to 7.0 by the addition of 0.5 M NaOH solution. The stock solution of compound **2** was prepared in HPLC grade DMSO solution for the studies.

Preparation of EYPC–LUVs⊃HPTS for anion selectivity: The vesicles were prepared by the same protocol described above. Final Condition: EYPC–LUVs⊃HPTS (~ 5.0 mM EYPC), Inside: 1 mM HPTS, 10 mM HEPES, 100 mM NaCl, pH = 7.0 and Outside: 10 mM HEPES, 100 mM NaX, pH = 7.0 (where, X^- = F^-, Cl^-, Br^-, I^-, SCN^-, and NO_3^-).

Anion selectivity assay: In a clean fluorescence cuvette, 1975 μL of HEPES buffer (10 mM HEPES, 100 mM NaX, at pH = 7.0; where, X^- = F^-, Cl^-, Br^-, I^-, SCN^-, and NO_3^-) was added, followed by addition of 25 μL of EYPC–LUVs⊃HPTS vesicle in slowly stirring condition by a magnetic stirrer equipped with the fluorescence instrument (at t = 0 s). The time-dependent HPTS emission intensity

was monitored at λ_{em} = 510 nm (λ_{ex} = 450 nm) by creating a pH gradient (~0.8) between intra- and extra-vesicular system by the addition of 20 μL NaOH (0.5 M) at t = 20 s. The transporter **2** was added at t = 100 s and at t = 300 s, 25 μL of 10% Triton X–100 was added to lyze all vesicles for the complete destruction of the pH gradient. For data analysis and comparison, time (X-axis) was normalized between the point of addition of transporter molecule (i.e. t = 100 s was normalized to t = 0 s) and the endpoint of the experiment (i.e. t = 300 s was normalized to t = 200 s) using Equation S3. Fluorescence intensities (I_t) were normalized to fractional emission intensity I_F using Equation S4.

Preparation of EYPC–LUVs⊃HPTS for cation selectivity: Similarly, the cation selectivity of the highest active compound **2** was explored by changing extravesicular solution (10 mM HEPES, 100 mM MCl, pH = 7.0) of MCl salts (M^+ = Li^+, Na^+, K^+, Rb^+, and Cs^+). For data analysis and comparison, time (X-axis) was normalized between the point of addition of transporter molecule (i.e. t = 100 s was normalized to t = 0 s) and the endpoint of the experiment (i.e. t = 300 s was normalized to t = 200 s) using Equation S3. Fluorescence intensities (I_t) were normalized to fractional emission intensity I_F using Equation S4.

Cation selectivity assay: In a clean fluorescence cuvette, 1975 μL of HEPES buffer (10 mM HEPES, 100 mM MCl, at pH = 7.0; where, M^+ = Li^+, Na^+, K^+, Rb^+, and Cs^+) was added, followed by the addition of 25 μL of EYPC–LUVs⊃HPTS vesicle in slowly stirring condition by a magnetic stirrer equipped with the fluorescence instrument (at t = 0 s). The time-dependent HPTS emission intensity was monitored at λ_{em} = 510 nm (λ_{ex} = 450 nm) by creating a pH gradient (~0.8) between intra- and extra-vesicular system by the addition of 20 μL NaOH (0.5 M) at t = 20 s. The transporter **2** was added at t = 100 s and at t = 300 s, 25 μL of 10% Triton X–100 was added to lyze all vesicles for the destruction of pH gradient. For data analysis and comparison, time (X-axis) was normalized between the point of addition of the transporter molecule (i.e. t = 100 s was normalized to t = 0 s) and the endpoint of the experiment (i.e. t = 300 s was normalized to t = 200 s) using Equation S3. Fluorescence intensities (I_t) were normalized to fractional emission intensity I_F using Equation S4.

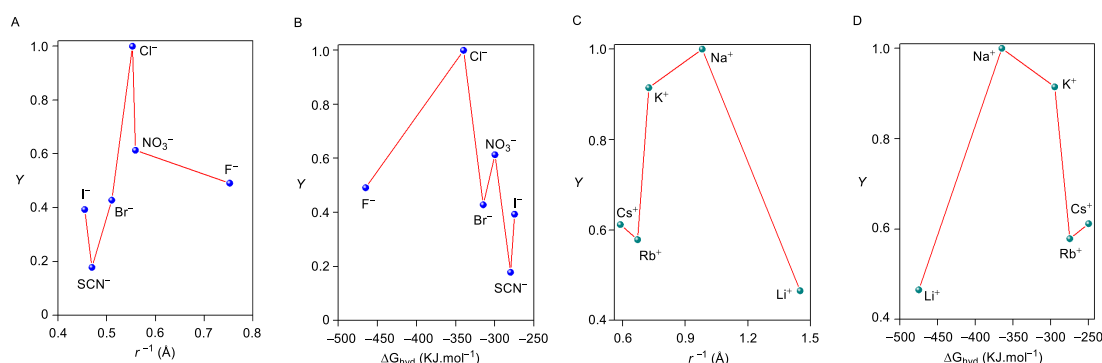**Fig. S33** Fractional activity Y (relative to Cl^-) as a function of the reciprocal anion radius (**A**); fractional activity Y (relative to Cl^-) as a function of the anion hydration energy (**B**); fractional activity Y (relative to Na^+) as a function of the reciprocal cation radius (**C**); and fractional activity Y (relative to Na^+) as a function of the cation hydration energy (**D**).

C. Chloride transport activity across EYPC–LUVs⊃lucigenin vesicles:[S9]

Buffer and stock solution preparation: HEPES buffer was prepared by dissolving an appropriate amount of solid HEPES and a $NaNO_3$ salt in autoclaved water to get 10 mM HEPES and 200 mM $NaNO_3$ salt, respectively. Subsequently, the pH was adjusted to 7.0 by the addition of 0.5 M NaOH solution. The stock solution of compound **2** was prepared in HPLC grade ACN solution for the studies.

Preparation of EYPC–LUVs⊃lucigenin: In a clean and dried small (10 mL) round bottom flask, 1 mL egg yolk phosphatidylcholine (EYPC, 25 mg/mL stock in $CHCl_3$) was added. The solution was dried by purging nitrogen with continuous rotation to form a thin transparent film of EYPC. The transparent film was kept in a high vacuum for 4 h to remove all traces of $CHCl_3$ at room temperature. The resulting film was hydrated with 1 mL buffer solution (1 mM lucigenin, 10 mM HEPES, and 200 mM $NaNO_3$, pH = 7.0), and the resulting suspension was vortexed at 10 min intervals for 1 h. This hydrated suspension was subjected to 21 cycles of freeze-thaw (liquid N_2, 55 °C) followed by extrusion through 200 nm pore size containing polycarbonate membrane 21 times (must be an odd number), in order to achieve the vesicles of an average 200 nm diameter. Extravesicular dyes were removed by gel filtration (using Sephadex G-50) with buffer solution (10 mM HEPES and 200 mM $NaNO_3$, pH = 7.0), and diluted to 4 mL to get EYPC–LUVs⊃lucigenin. Final conditions: ~ 5 mM EYPC; Inside: 1 mM lucigenin, 10 mM HEPES, 200 mM $NaNO_3$, pH = 7.0; Outside: 10 mM HEPES, 200 mM $NaNO_3$, pH = 7.0.

Dose dependent Cl⁻ transport by lucigenin assay: In clean and dried fluorescence cuvette, 1975 μL of buffer solution (10 mM HEPES, 200 mM $NaNO_3$ and pH = 7.0) and 25 μL EYPC–LUVs⊃lucigenin were taken. This suspension was placed in a slow stirring condition in a fluorescence instrument equipped with a magnetic stirrer (at $t = 0$ s). The fluorescence intensity of lucigenin was monitored at $\lambda_{em} = 535$ nm ($\lambda_{ex} = 455$ nm) over the course of time. The chloride gradient was created by the addition of 2.0 M NaCl (33.3 μL) at $t = 20$ s between intra and extravesicular systems, followed by the addition of transporter molecule **2** at $t = 100$ s. Finally, vesicles were lysed by the addition of 10% Triton X–100 (25 μL) at $t = 300$ s for the complete destruction of the chloride gradient.
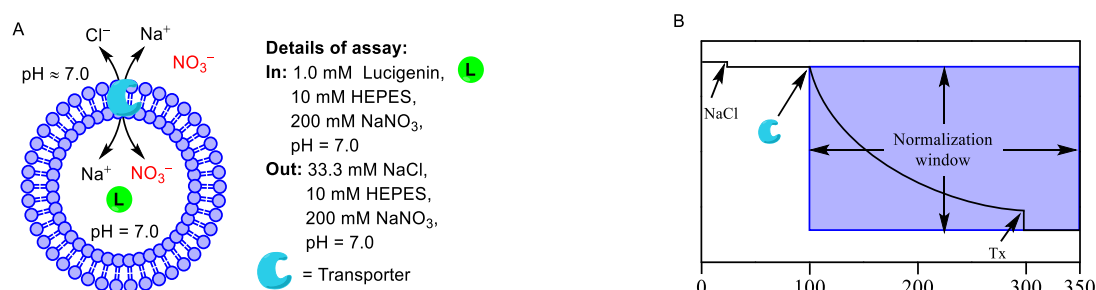

Fig. S34 Schematic representation of ion transport activity across EYPC–LUVs⊃lucigenin vesicle (**A**), and normalization window for same fluorescence kinetics experiment of ion transport (**B**).

The time-dependent data were normalized to fractional (in percentage) fluorescence intensity using Equation S6:

$$I_F = [(I_t - I_0) / (I_\infty - I_0)] \times (-100) \qquad \text{Equation S6}$$

where, I_0 = Fluorescence intensity just before the transporter molecule addition (at 0 s). I_∞ = Final fluorescence intensity after the addition of Triton X−100. I_t = Fluorescence intensity at time t.

For data analysis and comparison, time (X−axis) was normalized between the point of compound addition (i.e. t = 100 s was normalized to t = 0 s) and the endpoint of the experiment (i.e. t = 300 s was normalized to t = 200 s) according to the Equation S3.

Model	Hill2 (User)		
Equation	y = b+(a-b)/(1+(x/EC50)^n)		
Reduced Chi-Sqr	0.00124		
Adj. R-Square	0.99283		
		Value	Standard Error
D	a	0.00186	0.02728
D	b	1.00323	0.03133
D	n	1.94894	0.26259
D	EC50	2.47323	0.18462
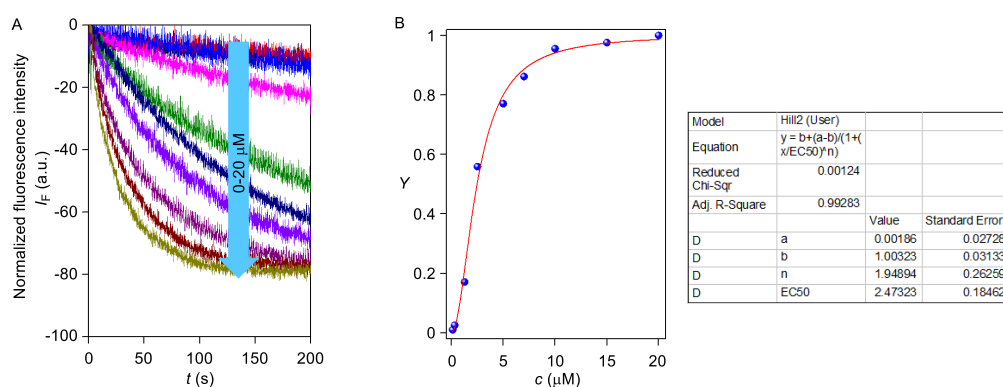
Fig. S35 Chloride influx study across EYPC–LUVs⊃lucigenin with transporter molecule **2** (**A**), and corresponding Hill plot of compound **2** at t = 190 s (**B**).

Cation selectivity assay across EYPC–LUVs⊃lucigenin vesicles: The vesicles were prepared by same procedure as discussed above.

Details of the assay: In clean and dried fluorescence cuvette, 1975 μL of buffer solution (10 mM HEPES, 200 mM $NaNO_3$ and pH = 7.0) and 25 μL EYPC–LUVs⊃lucigenin were taken. The suspension was kept in a slowly stirring condition in a fluorescence instrument equipped with a magnetic stirrer at t = 0 s. The quenching of fluorescence intensity of lucigenin was monitored as a course of time at λ_{em} = 535 nm (λ_{ex} = 455 nm). At t = 20 s, the chloride gradient was created by the addition of 2 M chloride salts (33.3 μL) of different cations MCl (M^+ = Li^+, Na^+, K^+, Rb^+ and Cs^+), followed by the addition of transporter molecule **2** at t = 100 s. Finally, vesicles were lysed by the addition of 10% Triton X−100 (25 μL) at t = 300 s to destroy the applied chloride gradient completely. The time-dependent data were normalized to fractional (in percentage) fluorescence intensity using Equation S4.

Fig. S36 Schematic representation of cation selectivity assay across EYPC–LUVs⊃lucigenin (**A**), Cation selectivity of transporter compound **2** (7 μM) by varying extravesicular cations (**B**).

Evidence of Na⁺ ion transport by using ²³Na NMR experiment:[S10–S12]

Preparation of vesicles and shift reagent: vesicles and shift reagent were prepared by following the reported literature.[S13]

Experimental procedure: 180 μl EYPC-LUVs suspension, 120 mL conductivity water, 100 μl D$_2$O, 100 μl shift reagent, and the required amount of compound **2** (dissolved in HPLC MeOH) were mixed in an NMR tube and kept at 25 °C for 30 min. ²³Na NMR spectrum was recorded for each concentration of samples after 30 min. The rate constant values for Na⁺ transport were calculated by using Equation S7.

$$K_{obs} = {}^1\!/_\tau = (v - v_0)$$
$\hspace{6cm}$ Equation S7

where, v = half line widths in the presence of compound **2**, v_0 = half line widths in the absence of compound **2**.

All half line widths were calculated by using the TopSpin 4.1.4 software programme.
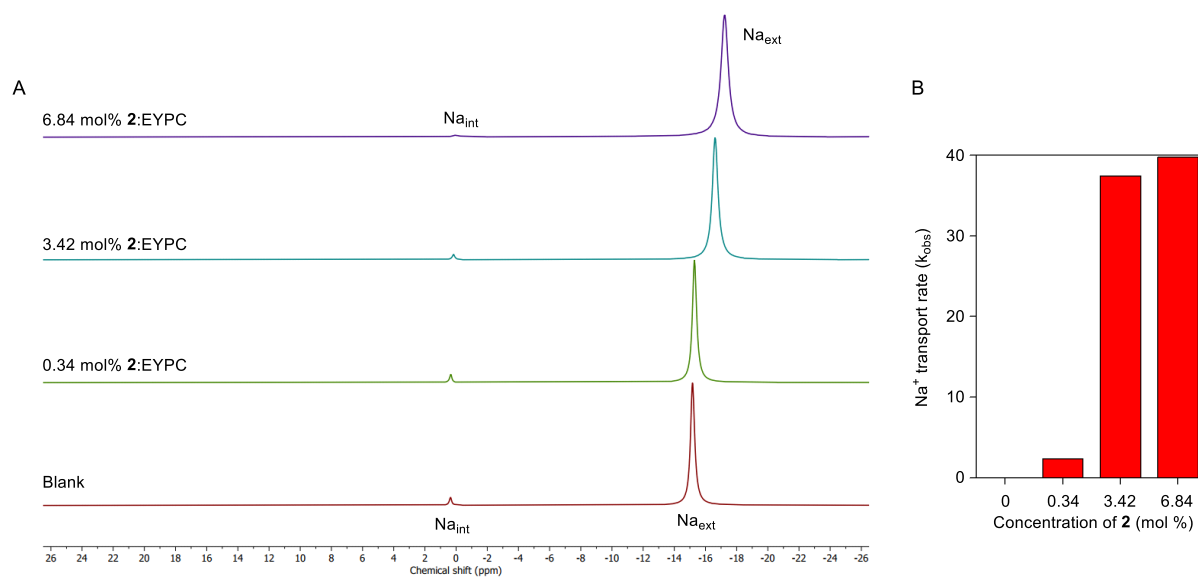
Fig. S37 Change in intravesicular and extravesicular ^{23}Na signal with increase in the concentration of compound **2** (**A**), calculated Na$^+$ ion transport rate at different concentrations of compound **2** (**B**).

D. Mechanistic study of ion transport across EYPC–LUVs⊃Lucigenin:

Cl$^-$ transport by Lucigenin assay in the presence of Valinomycin:[S14] In clean and dried fluorescence cuvette 1975 µL of buffer solution (10 mM HEPES, 200 mM NaNO$_3$ and pH = 7.0) and 25 µL EYPC–LUVs⊃lucigenin were taken and slowly stirred in fluorescence instrument equipped with a magnetic stirrer (at t = 0 s). The time-dependent fluorescence intensity of lucigenin was monitored at λ_{em} = 535 nm (λ_{ex} = 455 nm). A solution of 2 M KCl (33.3 µL) was added at t = 20 s to create a chloride gradient between intra- and extra-vesicular system, followed by the addition of valinomycin (0.5 µM) at t = 50 s and transporter molecule **2** (5 µM) at t = 100 s. Finally, the destruction of the chloride gradient was done by the addition of 10 % Triton X−100 (25 µL) at t = 300 s. The time-dependent data were normalized to fractional (in percentage) fluorescence intensity using Equation S4.

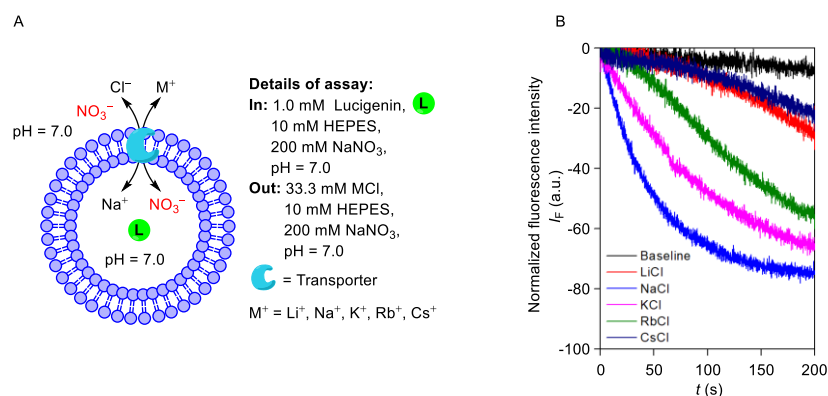**Fig. S38** Schematic representation of valinomycin assay across EYPC–LUVs⊃lucigenin (**A**), and normalization window for same fluorescence kinetics experiment of ion transport (**B**), evaluated chloride influx by compound **2** (5 μM) in presence and absence of valinomycin (0.5 μM) (**C**).

NO_3^-/SO_4^{2-} assay:[S14]

Buffer and stock solution preparation: HEPES buffer was prepared by dissolving an appropriate amount of solid HEPES and NaCl salt in autoclaved water to get 10 mM HEPES and 200 mM NaCl salt, respectively. Subsequently, the pH was adjusted to 7.0 by the addition of 0.5 M NaOH solution. Similarly, iso-osmolar $NaNO_3$ buffer (10 mM HEPES and 200 mM $NaNO_3$, pH = 7.0) and Na_2SO_4 (10 mM HEPES and 66.6 mM Na_2SO_4, pH = 7.0) buffer solution were prepared. A stock solution of compound **2** was prepared in HPLC grade ACN solution for the studies.

Preparation of EYPC–LUVs⊃lucigenin: Lucigenin vesicles were prepared by following the same protocol as mentioned above. Final conditions: ~ 5 mM EYPC; Inside: 1 mM lucigenin, 10 mM HEPES, 200 mM NaCl, pH = 7.0; Outside: 10 mM HEPES, 200 mM NaCl, pH = 7.0.

Fig. S39 Schematic representation of NO_3^-/SO_4^{2-} assay across EYPC–LUVs⊃lucigenin (**A**), and normalization window for same fluorescence kinetics experiment of ion transport (**B**).

Details of the assay: In clean and dried fluorescence cuvette 1950 μL of buffer solution (either 10 mM HEPES, 200 mM $NaNO_3$ and pH = 7.0 or 10 mM HEPES, 66.6 mM Na_2SO_4 and pH = 7.0) and 50 μL

EYPC–LUVs⊃lucigenin were taken and slowly stirred in fluorescence instrument equipped with a magnetic stirrer (at $t = 0$ s). Transporter molecule **2** (30 µM) was added at $t = 100$ s. The time-dependent fluorescence intensity of lucigenin was monitored at $\lambda_{em} = 535$ nm ($\lambda_{ex} = 455$ nm). Finally, the destruction of the chloride gradient was done by the addition of 10 % Triton X−100 (25 µL) at $t = 300$ s. The time-dependent data were normalized to fractional (in percentage) fluorescence intensity using Equation S4.
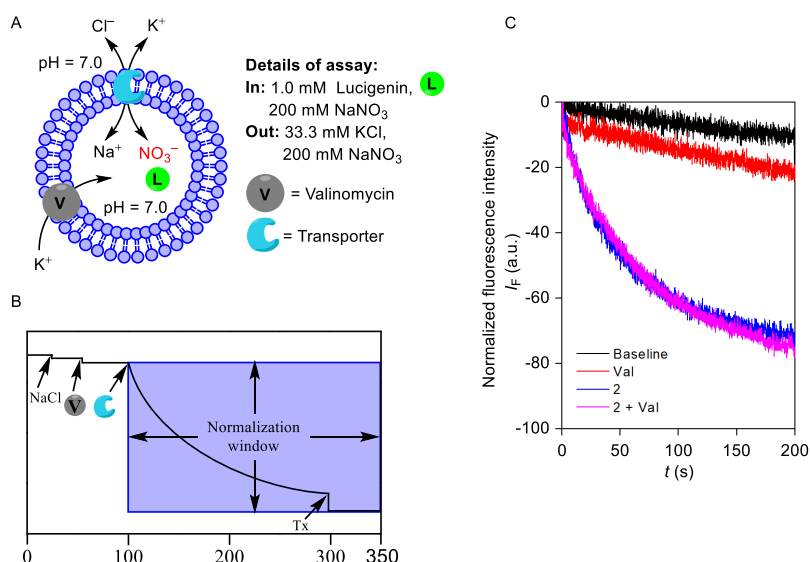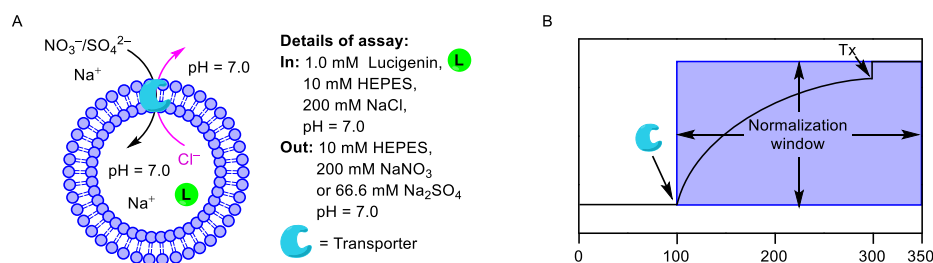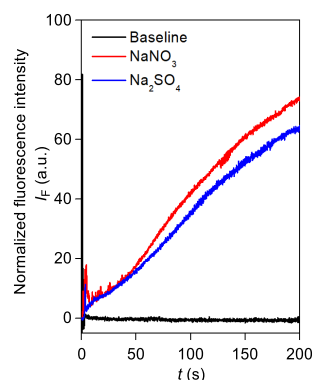

Fig. S40 Fluorescence kinetics experiment of Cl⁻ efflux by **2** (30 µM) across EYPC–LUVs⊃lucigenin in the presence of intravesicular Cl⁻ and either SO_4^{2-} or NO_3^- as an iso-osmolar extravesicular anion.

Cl⁻ influx in the presence of intravesicular NaNO₃ and Na₂SO₄ salts:

Buffer and stock solution preparation: HEPES buffer was prepared by dissolving an appropriate amount of solid HEPES and NaNO₃ salt in autoclaved water to get 10 mM HEPES and 200 mM NaNO₃ salt, respectively. Subsequently, the pH was adjusted to 7.0 by the addition of 0.5 M NaOH solution. Similarly, iso-osmolar Na₂SO₄ (10 mM HEPES and 66.6 mM Na₂SO₄, pH = 7.0) buffer solution was prepared. A stock solution of compound **2** was prepared in HPLC grade ACN solution for the studies.

Preparation of EYPC–LUVs⊃lucigenin: Lucigenin vesicles were prepared by following the same protocol as mentioned above. Final conditions: ~ 5 mM EYPC; Inside: 1 mM lucigenin, 10 mM HEPES, 200 mM NaNO₃ or 66.6 mM Na₂SO₄, pH = 7.0; Outside: 10 mM HEPES, 200 mM NaNO₃ or 66.6 mM Na₂SO₄, pH = 7.0.
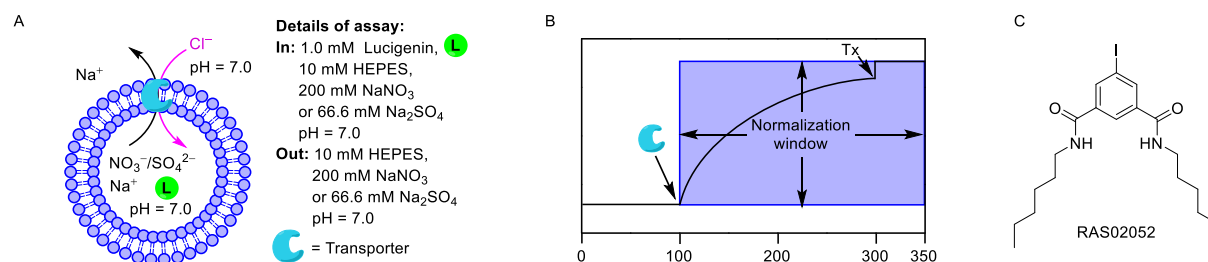
Fig. S41 Schematic representation of Cl⁻ influx assay by compound 2 in presence of intravesicular NaNO₃ or Na₂SO₄ salt across EYPC–LUVs⊃lucigenin (**A**), and normalization window for same

fluorescence kinetics experiment of ion transport (**B**). Compound RAS02052 was used as a control compound which is known to transport the Cl⁻ ion via antipot mechanism (**C**).

Details of the assay: In clean and dried fluorescence cuvette, 1975 µL of buffer solution (10 mM HEPES, 200 mM $NaNO_3$ or 66.6 mM Na_2SO_4 and pH = 7.0) and 25 µL EYPC–LUVs⊃lucigenin were taken. This suspension was placed in a slow stirring condition in a fluorescence instrument equipped with a magnetic stirrer (at $t = 0$ s). The fluorescence intensity of lucigenin was monitored at $\lambda_{em} = 535$ nm ($\lambda_{ex} = 455$ nm) over the course of time. The chloride gradient was created by the addition of 2.0 M NaCl (33.3 µL) at $t = 20$ s between intra and extravesicular systems, followed by the addition of transporter molecule **2** at $t = 100$ s. Finally, vesicles were lysed by the addition of 10% Triton X–100 (25 µL) at $t = 300$ s for the complete destruction of the chloride gradient. The time-dependent data were normalized to fractional (in percentage) fluorescence intensity using Equation S4.

**E. Evaluation of membrane stability by ANTS−DPX assay:** EYPC–LUVs were loaded with anionic fluorophore ANTS (8-aminonaphthalene-1,3,6-trisulfonic acid disodium salt) and cationic quencher DPX (1,1-[1,4-phenylenebis(methylene)]bis[pyridinium]bromide). Efflux of either ANTS or DPX through pores formed by compound **2** was followed by an increase in ANTS fluorescence emission intensity. All buffer solutions were prepared by a known method.[S15] Buffer A: 12.5 mM ANTS, 45.0 mM DPX, 5 mM TES, 20 mM KCl, pH = 7.0 Buffer B: 5 mM TES, 100 mM KCl, pH = 7.0.

Preparation of EYPC–LUVs⊃ANTS/DPX vesicles:[S16,S17] A thin film of EYPC lipid was prepared by evaporating 0.5 ml of EYPC lipid solution (25 mg/mL) in $CHCl_3$ by the flow of nitrogen and then it was kept in vacuo (4 h) to remove trace amount of $CHCl_3$. After 4 h, it was hydrated with 0.5 mL buffer A, followed by vortex treatment at 10 min intervals for 1 h. This hydrated suspension was subjected to 21 cycles of freeze-thaw (liquid N_2, 55 °C) followed by extrusion through 100 nm pore size containing polycarbonate membrane 21 times (must be an odd number), in order to achieve the vesicles of an average 100 nm diameter. Extravehicular ANTS/DPX dyes were removed by gel filtration (using Sephadex G-50) with buffer B solution (5 mM TES, 100 mM KCl, pH = 7.0), and diluted with the same buffer to 3 mL to get EYPC–LUVs⊃ANTS/DPX.

ANTS/DPX assay: In clean and dried fluorescence cuvette, 1950 µL of buffer B solution (5 mM TES, 100 mM KCl, pH = 7.0) and 50 µL EYPC–LUVs⊃ANTS/DPX were taken. The suspension was kept in a slow stirring condition in the fluorescence instrument equipped with a magnetic stirrer at $t = 0$ s. The fluorescence intensity was monitored as a course of time at $\lambda_{em} = 520$ nm ($\lambda_{ex} = 353$ nm). At $t = 100$ s, transporter **2** was added to it at different concentrations. Finally, vesicles were lysed by the addition of 10% Triton X−100 (25 µL) at $t = 300$ s for 100% efflux of ANTS/DPX dyes. The time-dependent data were normalized to fractional (in percentage) fluorescence intensity using Equation S4, and the time axis (X−axis) was normalized using Equation S3.
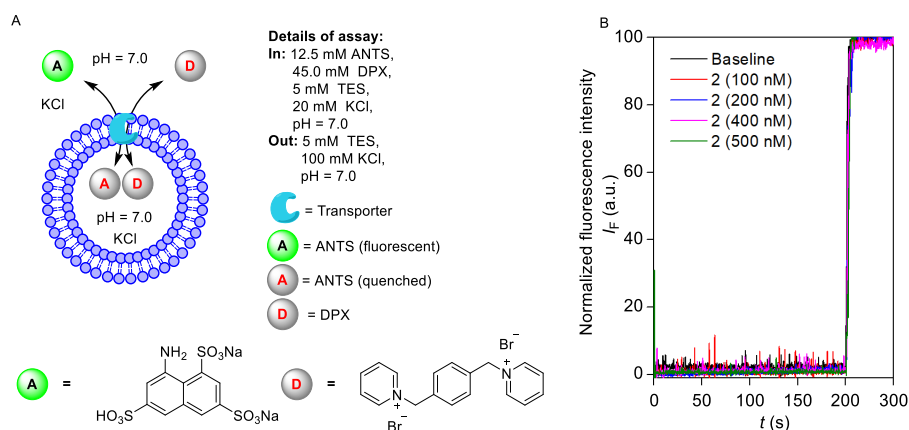
Fig. S42 Schematic representation of ANTS/DPX assay across EYPC–LUVs⊃ANTS/DPX (**A**), and fluorescence kinetics experiment of transporter **2** at different concentrations (**B**).

F. Evaluation of mode of ion transport

U-tube assay:[S18]

Buffer and stock solution preparation: Phosphate buffer was prepared by dissolving an appropriate amount of solid sodium phosphate dibasic heptahydrate, sodium phosphate monobasic monohydrate, and a NaCl salt in autoclaved water to get 5 mM phosphate buffer and 500 mM NaCl, pH = 7.0. A stock solution of compound **2** was prepared in HPLC grade CHCl$_3$ solution for the studies.

Details of the assay: In a clean and well-dried fluorescence U-shaped tube, 15 mL of CHCl$_3$ solution of compound **2** (1 mM) was added with a magnetic bid. A 7.5 mL of phosphate buffer containing NaCl salt (5 mM phosphate buffer, 500 mM NaCl, pH =7.0) was added in the source arm and 7.5 mL of phosphate buffer (5 mM phosphate buffer, pH =7.0) was added in the receiver arm. Changes in the chloride concentration in the receiver arm were checked over time using a chloride-selective electrode and change in the sodium concentration in the receiver was checked by using the inductively coupled plasma mass spectrometry (ICP-MS).

Fig. S43 Schematic representation of U-tube assay across with compound **2** (**A**), and change in the Na$^+$ and Cl$^-$ ions concentration in the receiver arm in the presence and absence of compound **2** (**B**).

S31

Effect of Photo-switching on Ion Transport:
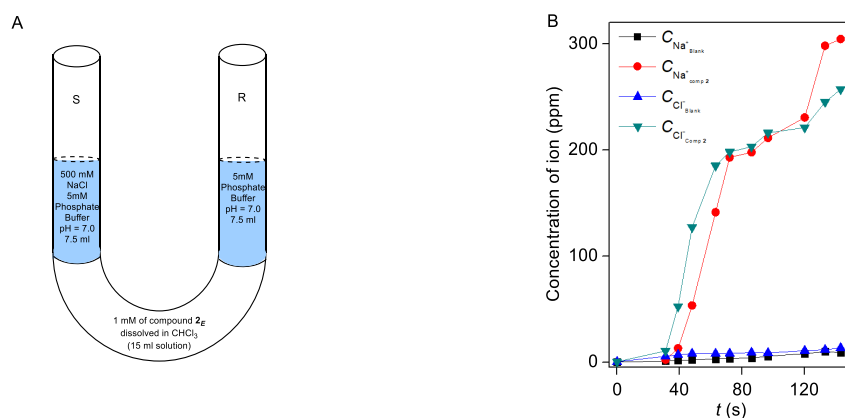
Effect of ion transport across EYPC-LUVs⊃HPTS:

Preparation of EYPC-LUVs⊃HPTS: Vesicles were prepared by using the above mention ptotocols.

Assay details: In clean and well-dry fluorescence cuvette, 1975 µL of HEPES buffer (10 mM HEPES, 100 mM NaCl, pH =7.0), compound **2** (stock solution in MeOH), and 25 µL of EYPC–LUVs⊃HPTS vesicle was added. The cuvette was photoirradiated with 365 nm of light to understand the effect of photoirradiation in the transport process. Then, the cuvette was placed in a slowly stirring condition using a magnetic stirrer equipped with the fluorescence instrument ($t = 0$ s). The time-dependent HPTS emission intensity was monitored at $\lambda_{em} = 510$ nm ($\lambda_{ex} = 450$ nm) by creating a pH gradient (~ 0.8) between the intra- and extra-vesicular system by the addition of 20 µL NaOH (0.5 M) at $t = 100$ s. Finally, the vesicles were lysed by the addition of 10% Triton X−100 solutions (25 µL) at $t = 300$ s for destruction pH gradient.

A concentration dependent transport study of **2$_Z$** was conducted by photoirradiating the membrane embedded **2$_E$** conformer. An insignificant increment of the HPTS fluorescence activity change was observed with time, even after going to the higher concentrations. We noticed the precipitation of the compound beyond 50 µM concentration. Hence we are unable to perform the concentration dependent study of the photoisomerized **2$_Z$** conformer.
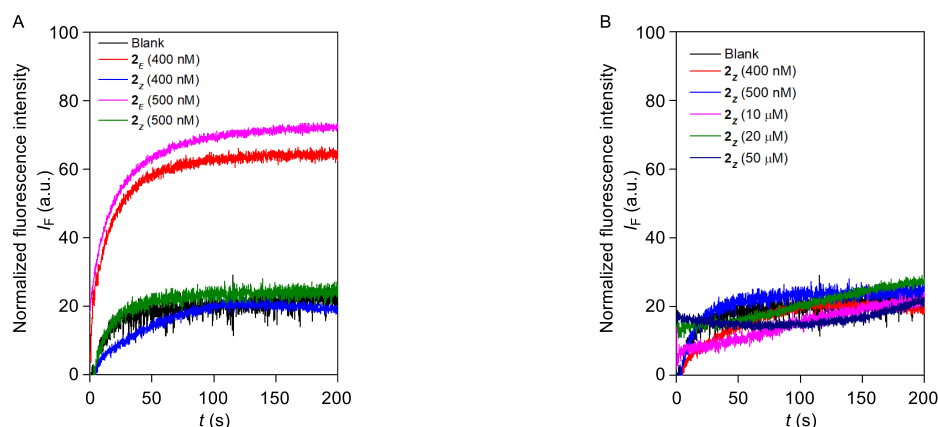
Fig. S44 Effect of photoirradiation in ion transport process on compound **2$_E$** at different concentrations with 365 nm photoirradiation (**A**), and concentration-dependent transport activity of photoisomerioced **2$_Z$** (**B**) across EYPC-LUVs⊃HPTS.

Effect in chloride ion transport upon photoirradiation by ISE experiments:

Preparation of EYPC-LUVs for ISE studies: A solution (1 mL) of EYPC lipid (25 mg/mL) lipid dissolved in CHCl$_3$ was taken in a clean and dry small round bottom flask. The solvent was evaporated slowly by purging nitrogen and dried in high vacuum condition for at least 5 h. Then 1 mL of 500 mM

NaCl (dissolved in 10 mM Phosphate buffer with pH = 7.0) was added. The suspension was then hydrated for 1 h with periodic vortexing at intervals of 10 min for 4-5 times and then subjected to a freeze-thaw cycle (21 times). The vesicle solution was extruded through a polycarbonate membrane with 200 nm pores for a minimum 21 times, which resulted in vesicles with a mean diameter of ~200 nm. Non-encapsulated NaCl salt was removed by dialyzing the vesicle solution three times in sodium nitrate solution (500 mM $NaNO_3$ dissolved in 10 mM Phosphate buffer with pH=7.0).

Assay details: 1925 µL of 500 mM $NaNO_3$ and 10 mM phosphate buffer solution, pH = 7.0 was taken and 75 µL of vesicle solution was added to a three-necked glass tube with a magnetic bead. The setup was kept over a magnetic stirrer and a chloride selective electrode was dipped inside the tube to measure the concentration of chloride outside the vesicle solution periodically after 10 s. At $t = 50$ s, 20 µL of compound **2** from 5 mM stock solution (50 µM inside the tube) was added to the glass tube and the chloride concentration was monitored for 250 s. Finally, 25 µL of 10% Triton X$-$100 was added into the solution to achieve maximum chloride concentration.

After analyzing the ion transport efficiency of the *E*-conformer of compound **2** (**2$_E$**), compound **2** was irradiated in MeOH solvent with 365 nm of light for 5 s to achieve the *Z*-conformer (**2$_Z$**), whose ion transport activity was further checked with the chloride selective electrode. The ion transport activity of **2** was greatly reduced upon photo-irradiation at 365 nm of light, likely due to the photo-isomerization of the **2$_E$** conformer to the **2$_Z$** conformer. Further, the isomerized *Z*-conformer was irradiated with 450 nm of LED light for 9 min to reconvert to its initial transport active *E*-conformer, whose transport activity was again checked with the chloride selective electrode. The activity was significantly regained back upon the 450 nm of photo-irradiation. This process of alternative photo-irradiation with 365 nm and 450 nm wavelengths of light was repeated for three cycles (Fig. 5B in the manuscript) and the effect of the photo-switching process in the ion transport was checked through the chloride selective electrode. The value at 50 s was considered 0% chloride efflux, and the final chloride reading at 250 s was set as 100% chloride efflux during the normalization.
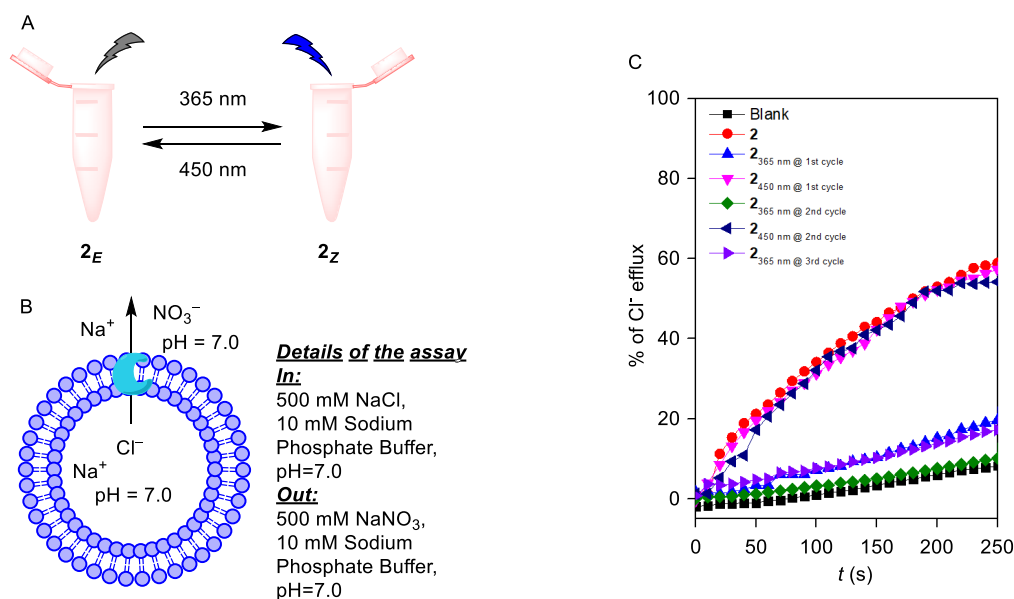
Fig. S45 Schematic representation of photoirradiation process (**A**), Cl⁻ efflux assay across EYPC–LUVs by using ISE experiment (**B**), and Cl⁻ transport activity curves during photoswitching cycle of compound **2** with sequential photoirradiation with 365 nm and 450 nm (**C**).

Effect in sodium ion transport upon photoirradiation by ^{23}Na experiments:

Preparation of vesicles and shift reagent: Vesicles and shift reagent were prepared by following the reported literature procedure.[S13]

Experimental procedure: 180 µl EYPC-LUVs suspension, 120 µL conductivity water, 100 µl D₂O, 100 µL shift reagent, and 3.42 mol% of compound **2** (dissolved in HPLC MeOH) relatives to phospholipids, were mixed in NMR tube and kept at 25 °C for 30 min. Initially, ^{23}Na NMR spectrum was recorded without any photo-irradiation. For one of the samples, ^{23}Na NMR was recorded after photoirradiation with 365 nm of UV light. To understand the regaining of the Na⁺ ion transport efficiency upon reverse photo isomerization, in one of the experimental setups, the sample was irradiated with 365 nm followed by 450 nm of light, and finally ^{23}Na NMR was recorded. The change in the line widths of the external Na⁺ ion signal was monitored during the experiment. The rate constant values for Na⁺ transport were calculated by using Equation S7.
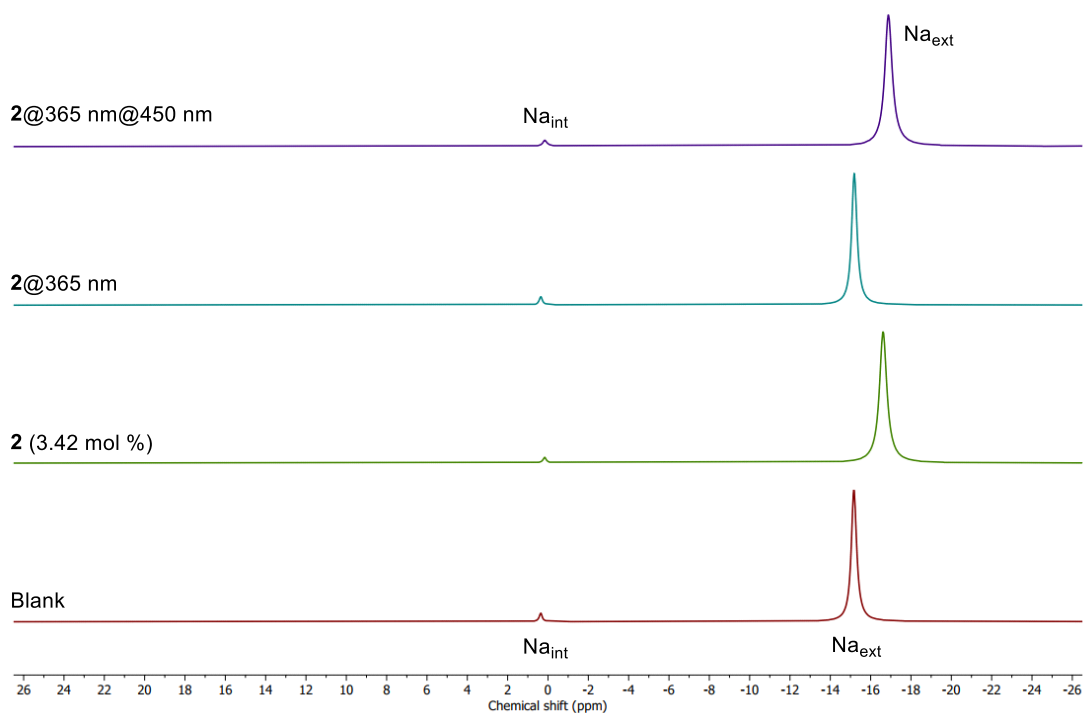
Fig. S46 Change in intravesicular and extravesicular ^{23}Na signal after photoirradiation of compound **2** with 365 nm and 450 nm of light.

VI. Single Crystal X-Ray Diffraction Study:

The single crystals of **2** were grown from dimethyl sulfoxide, allowing for the slow evaporation of the solvents over time. X-ray diffraction data on single crystals of **2** was collected on a Bruker D8 Venture Duo X-ray diffractometer equipped with a Microfocus X-ray source (operated at 50 W; 50 kV/1 mA) and graded multilayer optics for monochromatic Mo Kα radiation (λ = 0.71073 Å) with a focused X-ray beam and a Photon 100 CMOS chip based detector system at 296 K. The crystal was mounted on nylon Cryo Loops (Hampton Research) with Paraton-N (Hampton Research). The data integration and reduction were processed with SAINT software.1 A multi-scan absorption correction was applied to the collected reflections. The structure was solved by a direct method using SHELXTL3,4 and was refined on F2 with a full-matrix least squares technique using the SHELXL 5 program package. All of the hydrogen atoms were refined anisotropically. All of the hydrogen atoms were located in successive difference Fourier maps and treated as riding atoms using SHELXL default parameters. The structures were examined using the Adsym subroutine in PLATON to ensure that no additional symmetries could be applied to the models.

Table S1. Details of the crystal structure data of compound **2**.

| Identification code	Compound_2
CCDC No	2340801
Empirical formula	C14 H7 F6 N3 O3 S
Formula weight	411.29
Temperature	296(2) K
Wavelength	1.54178 Å
Crystal system	Monoclinic
Space group	$P2_1$
Unit cell dimensions	a = 8.549(2) Å α= 90°.
	b = 16.670(3) Å β= 91.58(3)°.
	c = 22.998(5) Å γ = 90°.
Volume	3276.2(12) Å^3
Z	8
Density (calculated)	1.668 Mg/m^3
Absorption coefficient	2.601 mm^{-1}
F(000)	1648
Crystal size	0.300 x 0.200 x 0.200 mm^3
Theta range for data collection	2.650 to 62.496°
Index ranges	-9<=h<=9, -18<=k<=19, -26<=l<=26
Reflections collected	35006
Independent reflections	10123 [R(int) = 0.1381]
Completeness to theta = 62.496°	99.7 %
Absorption correction	Semi-empirical from equivalents
Max. and min. transmission	0.66 and 0.42
Refinement method	Full-matrix least-squares on F^2
Data / restraints / parameters	10123 / 1303 / 975
Goodness-of-fit on F2	1.463
Final R indices [I>2sigma(I)]	R1 = 0.1367, wR2 = 0.3499
R indices (all data)	R1 = 0.1678, wR2 = 0.3750
Extinction coefficient	0.0015(6)
Largest diff. peak and hole	1.693 and -0.730 e.Å^{-3}
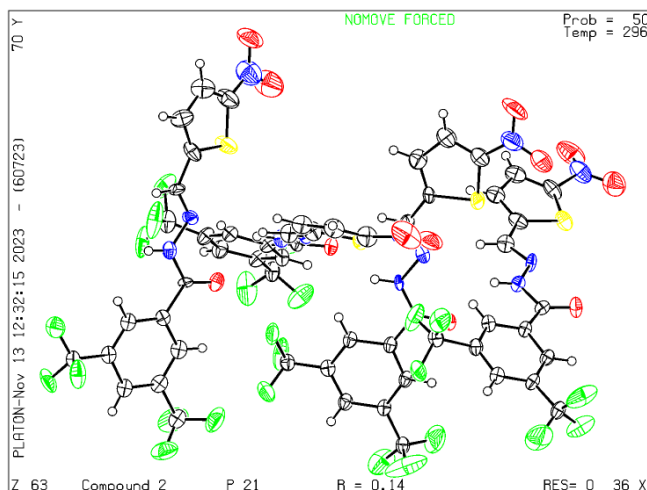
Fig. S47 ORTEP diagram of the crystal structure of compound **2**.

Table S2. Atomic coordinates (x 10^4) and equivalent isotropic displacement parameters ($Å^2$ x 10^3) for Compound_2. U(eq) is defined as one third of the trace of the orthogonalized U^{ij} tensor.

	x	y	z	U(eq)
C(1)	3030(20)	1399(12)	6307(9)	25(3)
C(2)	2840(20)	1893(13)	5821(10)	30(3)
C(3)	3190(20)	1578(13)	5279(10)	29(3)
C(4)	3690(20)	805(12)	5190(10)	27(3)
C(5)	3840(20)	311(12)	5697(9)	24(3)
C(6)	3550(20)	624(12)	6220(9)	25(3)
C(7)	3020(30)	2127(14)	4745(11)	36(4)
C(8)	4480(20)	-498(12)	5620(9)	22(3)
C(9)	2640(20)	1778(11)	6868(8)	19(4)
C(10)	2650(30)	1202(13)	8316(8)	30(5)
C(11)	2150(30)	1435(15)	8889(11)	45(6)
C(12)	2330(30)	1058(17)	9407(11)	47(6)
C(13)	1600(30)	1456(19)	9845(12)	52(7)
C(14)	870(40)	2113(19)	9657(12)	62(8)
N(1)	2820(20)	1281(11)	7360(8)	29(4)
N(2)	2370(20)	1638(11)	7871(7)	30(4)
N(3)	-310(40)	2580(20)	9978(13)	78(8)
O(1)	2227(18)	2476(9)	6897(7)	35(4)
O(2)	-320(30)	2460(16)	10527(9)	83(7)
O(3)	-970(40)	3116(17)	9777(12)	101(9)
F(1)	3510(30)	2879(10)	4869(8)	76(6)

S37

F(2)	1585(16)	2201(13)	4563(8)	72(5)
F(3)	3820(20)	1896(11)	4306(7)	71(5)
F(4)	6021(17)	-506(9)	5564(8)	60(4)
F(5)	3870(30)	-867(9)	5161(6)	67(5)
F(6)	4260(20)	-979(8)	6059(7)	55(4)
S(1)	945(12)	2261(4)	8934(3)	66(2)
C(15)	-830(20)	3769(13)	7253(9)	27(4)
C(16)	-2000(20)	4242(12)	6959(9)	26(4)
C(17)	-3290(20)	3876(13)	6747(10)	30(4)
C(18)	-3530(30)	3064(14)	6785(10)	36(4)
C(19)	-2420(30)	2578(14)	7082(10)	34(4)
C(20)	-1060(20)	2936(13)	7318(9)	27(4)
C(21)	-4540(30)	4379(13)	6435(11)	35(5)
C(22)	-2700(30)	1739(15)	7199(12)	43(5)
C(23)	570(20)	4196(12)	7490(9)	24(4)
C(24)	4210(20)	3594(14)	8038(10)	32(4)
C(25)	5630(20)	3928(14)	8281(10)	35(4)
C(26)	6980(30)	3518(16)	8511(10)	40(4)
C(27)	8230(30)	4075(16)	8657(11)	42(4)
C(28)	7780(30)	4858(17)	8550(11)	45(4)
N(4)	1814(19)	3715(11)	7678(8)	28(4)
N(5)	3104(18)	4079(9)	7900(7)	21(3)
N(6)	8710(30)	5525(17)	8730(9)	54(6)
O(4)	631(17)	4940(9)	7529(6)	33(3)
O(5)	9990(30)	5439(19)	8906(11)	97(9)
O(6)	8010(30)	6191(17)	8651(9)	82(8)
F(7)	-3954(19)	5017(10)	6174(8)	68(5)
F(8)	-5538(19)	4681(13)	6807(8)	84(6)
F(9)	-5350(20)	3996(10)	6027(9)	82(6)
F(10)	-3400(20)	1372(8)	6746(8)	70(5)
F(11)	-3665(19)	1633(11)	7645(8)	68(5)
F(12)	-1481(19)	1324(9)	7328(11)	82(6)
S(2)	5941(6)	4948(4)	8279(3)	38(1)
C(29)	2240(20)	6425(11)	6289(9)	26(3)
C(30)	2290(20)	6887(12)	5788(9)	28(3)
C(31)	1920(20)	6591(12)	5252(9)	24(3)
C(32)	1370(30)	5809(13)	5197(10)	30(3)

C(33)	1220(20)	5310(13)	5673(9)	28(3)
C(34)	1690(20)	5612(12)	6221(9)	27(3)
C(35)	1950(20)	7139(13)	4702(10)	30(4)
C(36)	610(20)	4497(13)	5609(9)	30(4)
C(37)	2680(20)	6783(12)	6865(9)	28(4)
C(38)	2880(20)	6201(13)	8318(10)	30(4)
C(39)	3450(30)	6487(13)	8860(9)	34(4)
C(40)	3410(30)	6110(16)	9395(10)	44(5)
C(41)	4040(40)	6555(18)	9869(12)	56(6)
C(42)	4510(40)	7293(17)	9685(11)	54(6)
N(7)	2644(19)	6304(10)	7332(7)	25(4)
N(8)	3072(19)	6643(10)	7872(7)	26(4)
N(9)	5110(40)	7840(17)	10076(11)	64(7)
O(7)	3078(18)	7497(8)	6871(7)	33(3)
O(8)	5190(30)	7756(15)	10593(9)	82(7)
O(9)	5410(40)	8513(17)	9855(10)	96(9)
F(13)	1510(40)	7843(12)	4822(10)	107(8)
F(14)	3280(30)	7146(18)	4530(11)	124(10)
F(15)	1010(20)	6862(12)	4291(8)	80(6)
F(16)	1160(20)	4108(10)	5163(7)	69(5)
F(17)	-893(17)	4488(9)	5563(9)	67(5)
F(18)	950(20)	4020(7)	6064(6)	52(4)
S(3)	4229(11)	7452(4)	8969(3)	59(2)
C(43)	6210(20)	8773(12)	7265(9)	24(3)
C(44)	7280(20)	9240(12)	6984(9)	27(3)
C(45)	8590(20)	8886(12)	6716(9)	26(3)
C(46)	8810(20)	8084(12)	6760(9)	28(3)
C(47)	7790(20)	7627(13)	7050(9)	29(3)
C(48)	6470(20)	7947(12)	7304(9)	28(3)
C(49)	9780(20)	9413(13)	6454(10)	31(4)
C(50)	8060(30)	6712(13)	7137(10)	33(4)
C(51)	4860(20)	9202(12)	7491(9)	25(4)
C(52)	1340(20)	8550(14)	8030(9)	33(4)
C(53)	-120(30)	8886(15)	8256(10)	36(4)
C(54)	-1280(30)	8426(15)	8491(10)	38(4)
C(55)	-2600(30)	8913(16)	8711(10)	43(4)
C(56)	-2150(30)	9710(15)	8601(10)	40(4)

N(10)	3690(20)	8718(11)	7685(8)	30(4)
N(11)	2392(19)	9053(9)	7905(8)	26(4)
N(12)	-3150(30)	10348(15)	8828(10)	53(6)
O(10)	4830(17)	9916(9)	7569(7)	36(4)
O(11)	-2530(30)	11038(14)	8781(10)	72(6)
O(12)	-4450(30)	10207(16)	8956(10)	83(7)
F(19)	9132(19)	10027(11)	6179(7)	70(5)
F(20)	10790(20)	9744(13)	6833(7)	86(7)
F(21)	10570(30)	9030(13)	6071(11)	98(7)
F(22)	9140(20)	6605(9)	7542(7)	61(4)
F(23)	8670(20)	6410(8)	6650(7)	62(5)
F(24)	6810(20)	6318(9)	7275(9)	73(5)
S(4)	-437(6)	9893(4)	8325(3)	39(1)

VII. Theoretical studies:

Computational details: Based on the Hill coefficient value of $n \sim 2$ obtained from dose-response studies of compounds **1a-1c** and **2**, geometry optimization of compound **2** and [(2_E)$_2$+NaCl] were performed.

Initially, the most probable conformers of [(2_E)$_2$+NaCl] were obtained by using the CONFLEX 8 software program,[S19] and subsequently, their geometry optimization was carried out by using the Gaussian 09 program package.[S20] The geometry optimized [(2_E)$_2$+NaCl] confirmed the formation of H-bonding interactions between the chloride anion and N-H$_a$, H$_a$-Cl$^-$(2.167 Å), hydrazone C-H$_b$, H$_b$-Cl$^-$ (2.984 Å) and aromatic C-H$_c$, H$_c$-Cl$^-$ (2.691 Å) group. Whereas sodium ion binds through the electrostatic interaction between sodium cation and CONH group C=O···Na$^+$ (2.283 Å), hydrazone nitrogen atom N ···Na$^+$ (2.643 Å) and sulfur atom S···Na$^+$ (3.870 Å). The binding energy of the geometrically optimized [(2_E)$_2$+NaCl] complex was calculated to be −28.2201941 kcal/mol.

To visualize the different conformers of the [(2_E)$_2$+NaCl] complex, several geometries of the complex were obtained by using the CONFLEX 8 software package using the MMFF94S force field.[S19] The calculation provided the 1306 possible conformers of the [(2_E)$_2$+NaCl] complex. The Boltzmann populations of the ten highest populated conformations are **Conf-I$_E$** with 19.62%, **Conf-II$_E$** with 15.09%, **Conf-III$_E$** with 13.96%, **Conf-IV$_E$** with 11.23%, **Conf-V$_E$** with 10.12%, **Conf-VI$_E$** with 8.41%, **Conf-VII$_E$** with 5.73%, **Conf-VIII$_E$** with 4.05%, **Conf-IX$_E$** with 1.61%, **Conf-X$_E$** with 1.22%.
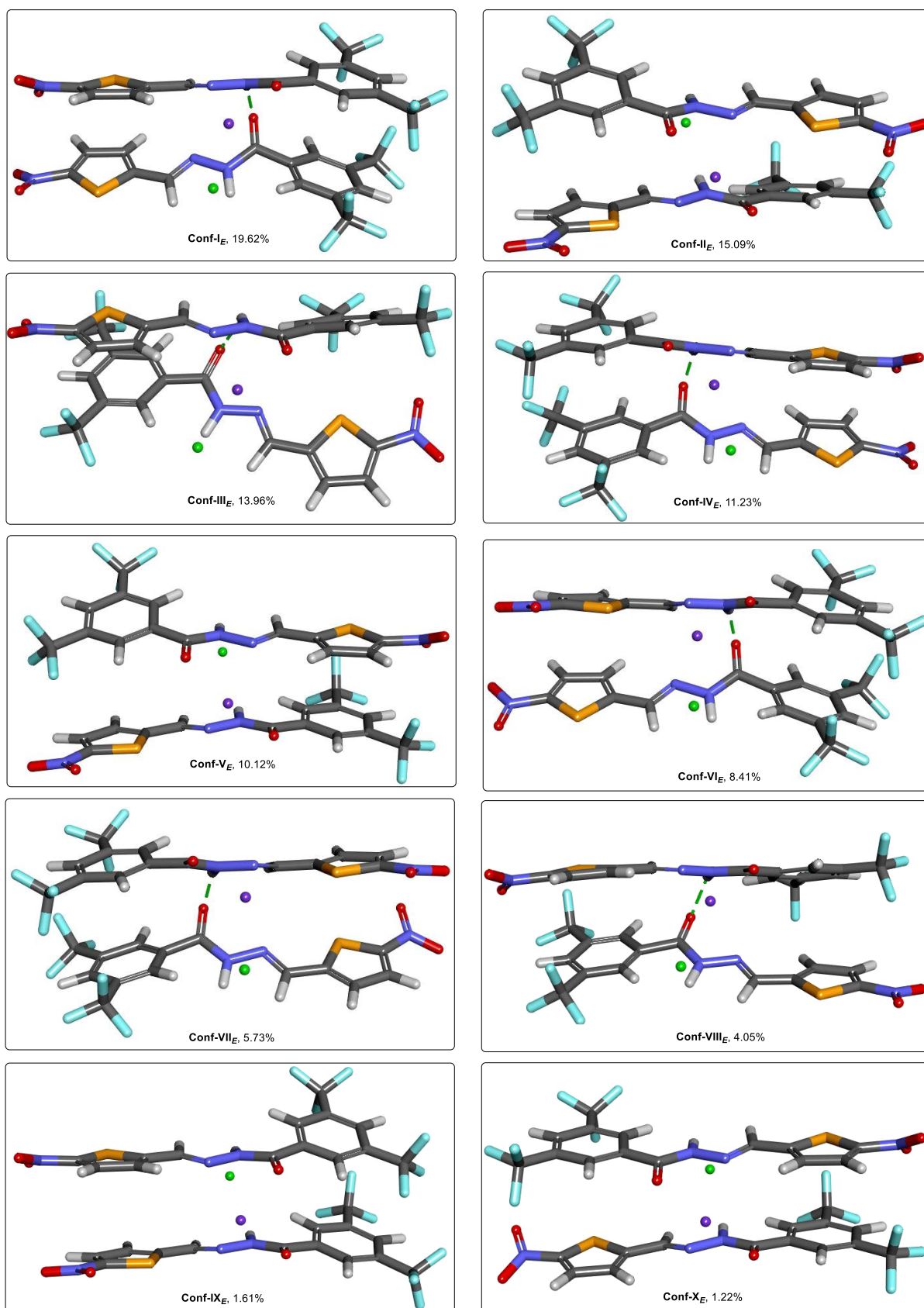
Fig. S48 CONFLEX 8 optimized structures of ten most probable conformations **Conf-I–Conf-X** of [(**2**$_E$)$_2$+NaCl]complex along with the Boltzmann distribution of populations.

The ten highest populated conformers of $[(2_E)_2+NaCl]$ complex were further geometry optimized by the Gaussian 09 program package[S20] using B3LYP functional and 6-311++G(d, p) basis set.[S21] The dimeric structure of compound 2_E was taken from its crystal structure and used for optimization by the Gaussian 09 program package using the same basis set. For both structures, 2_E and $[(2_E)_2+NaCl]$, the vibrational frequency calculation during the geometry optimization has not shown any imaginary frequencies, which indicates that all optimized structures are ground state minima.

The Gaussian 09 program[S20] was used to calculate the zero-point energy (ZPE) and basis set superposition error (BSSE) corrected bonding energy of $[(2_E)_2+NaCl]$, which was used for the calculation of binding energy (BE) using the following equations. Geometry-optimized compound 2_E and energetically more stable **Conf-II**$_E$ of $[(2_E)_2+NaCl]$ complex were used during the binding energy (BE) calculation.

$$BE = \left[HF_{[(2_E)_2+NaCl]} + ZPE_{[(2_E)_2+NaCl]} + BSSE_{[(2_E)_2+NaCl]} \right] - \left[HF_{2_E} + ZPE_{2_E} \right] - [HF_{NaCl}]$$

where, $HF_{[(2_E)_2+NaCl]}$ = electronic energy of $[(2_E)_2+NaCl]$ complex, $ZPE_{[(2_E)_2+NaCl]}$ = zero-point energy of $[(2_E)_2+NaCl]$ complex, $BSSE_{[(2_E)_2+NaCl]}$ = BSSE of $[(2_E)_2+NaCl]$ complex, HF_{2_E} = electronic energy of the receptor 2_E, ZPE_{2_E} = zero-point energy of the receptor 2_E, HF_{NaCl} = electronic energy of cation NaCl.

Table S3. The electronic energy (HF), zero-point energy (ZPE), basis set superposition error (BSSE) corrected energy (in Hartree unit) for all structures and complexes are calculated at the DFT B3LYP/6-311++G (d, p) level of theory.

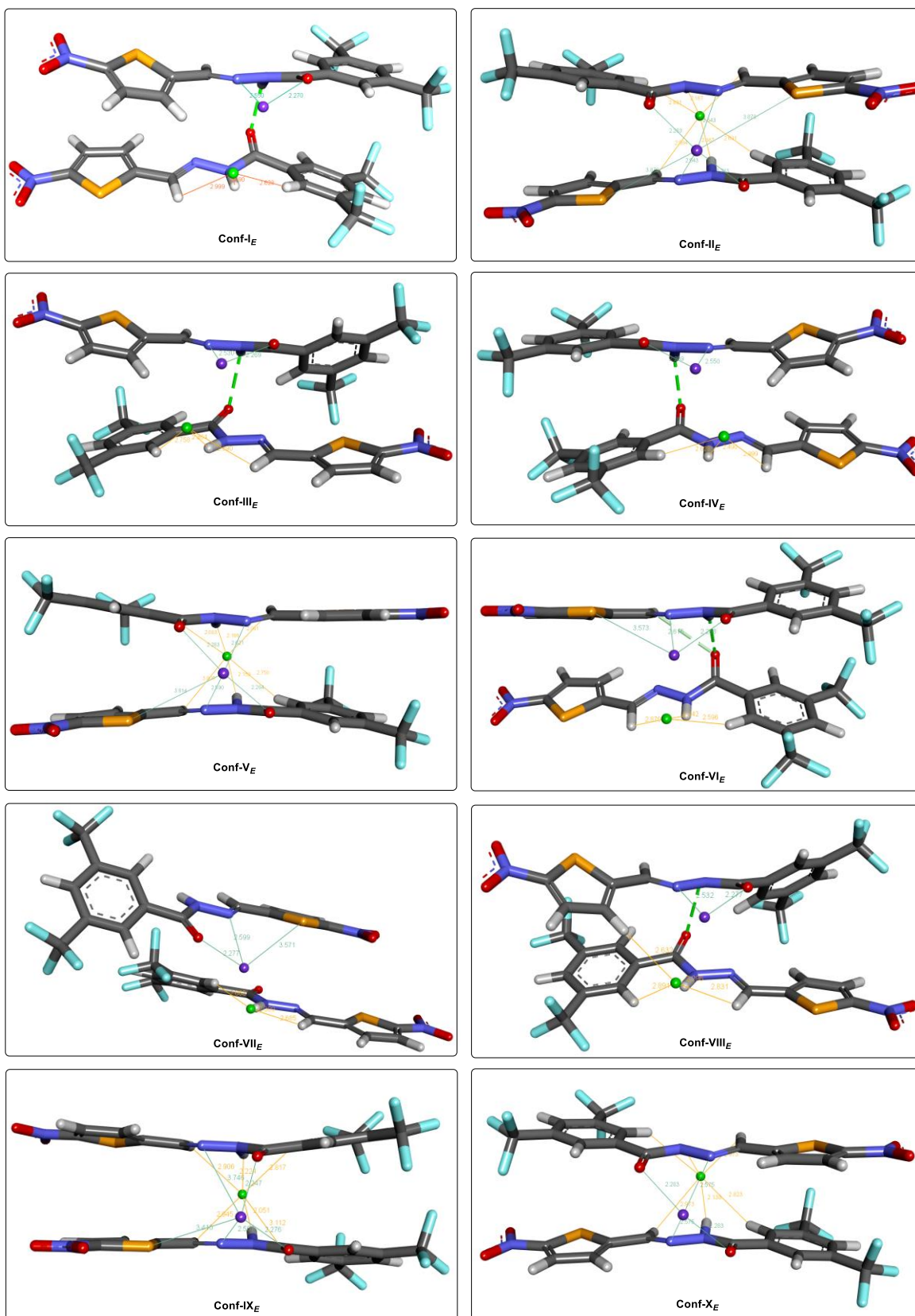| Parameters	Energy
$HF_{[(2_E)_2+NaCl]}$ (in Hartree)	−4473.1322011
$ZPE_{[(2_E)_2+NaCl]}$ (in Hartree)	0.4154831
$BSSE_{[(2_E)_2+NaCl]}$ (in Hartree)	0.010598394123
HF_{2_E} (in Hartree)	−3850.4732404
ZPE_{2_E} (in Hartree)	0.413104
HF_{NaCl} (in Hartree)	−622.601011
BE (in Hartree)	−0.044972206
BE (in kcal/mol)	−28.2201941

Fig. S49 Gaussian 09 optimized structures of ten most probable conformations **Conf-I$_E$−Conf-X$_E$** of [(**2$_E$**)$_2$+NaCl] complex.

Further, to understand the effect of hydrogen bonding in *Z*-conformer upon changing the coordinating oxygen to sulfur atom in chromophoric moiety, both **1a$_Z$** and **2$_Z$** were initially optimized using the CONFLEX 8 software package using the MMFF94S force field.[S19] The analysis provided that 17 no of possible structures for **1a$_Z$** and 19 no of possible structures for **2$_Z$**. The Boltzmann populations of the two highest populated structures for **1a$_Z$** are **Conf-II$_Z$** (51.82%) and **Conf-II$_Z$** (48.17%). Whereas, for **2$_Z$**, the Boltzmann populations of the two highest populated structures are **Conf-I$_Z$** (33.95%) and **Conf-II$_Z$** (32.12%).
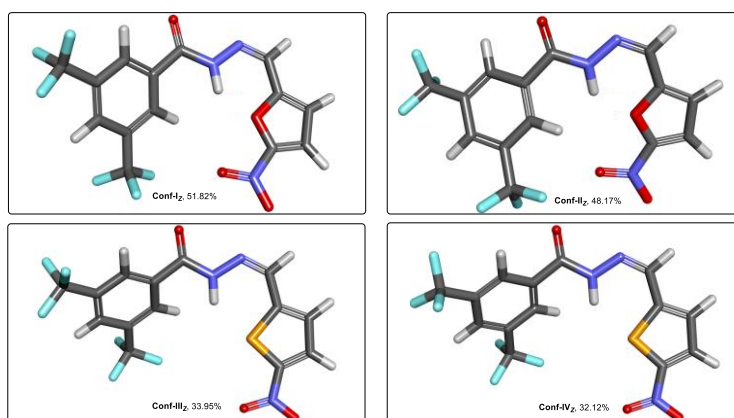
Fig. S50 CONFLEX 8 optimized structures of two most probable conformations, **Conf-I$_Z$** and **Conf-II$_Z$** of **1a$_Z$** and **2$_Z$**, along with their Boltzmann distribution of populations.

For both compounds **1a$_Z$** and **2$_Z$**, the highest populated **Conf- I$_Z$** and **Conf- II$_Z$** were subsequently used to get the optimized structure by using the Gaussian 09 program[S20] package using B3LYP functional and 6-311++G(d, p) basis set.[S21] Optimized data revealed for both **1a$_Z$** and **2$_Z$**, **Conf- II$_Z$** is energetically more stable than **Conf- I$_Z$**. Compound **1a$_Z$** formed an intramolecular H-bond with the N-H$_a$ proton with an H-bonding length of 2.014 Å, whereas **2$_Z$** formed an intramolecular H-bond with the N-H$_a$ proton with comparatively longer H-bonding length 2.414 Å.
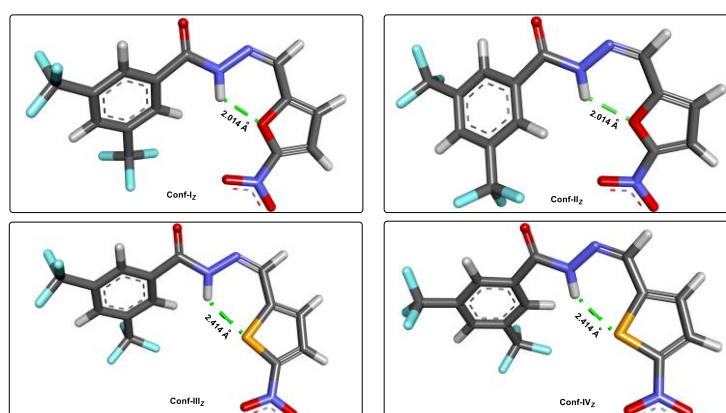

Fig. S51 Gaussian 09 optimized structures of two most probable conformations, **Conf-I$_Z$** and **Conf-II$_Z$** of **1a$_Z$** and **2$_Z$**.

Further, the H-bonding strength of individual $O\cdots H_a$ and $S\cdots H_a$ interaction present in more stable **conf-II$_Z$** of compound **1a$_Z$** and **2$_Z$** have been calculated qualitatively through natural bond orbital (NBO) analysis using NBO 6.0 software.[S22] The corresponding hydrogen bond interaction energies (E^2) are provided in Table S4.

Table S4. Comparison of H-bonding length and the NBO 2nd order perturbation energies (E^2) in **conf-II$_Z$** of compound **1a$_Z$** and **2$_Z$**.

	2$_Z$ ($S_{LP1}\cdots NH_a$)	**1a$_Z$** ($O_{LP1}\cdots NH_a$)
Bond length (Å)	2.41366	2.01361
E^2 (kcal.mol^{-1})	2.58	3.92

VIII. NMR Data:
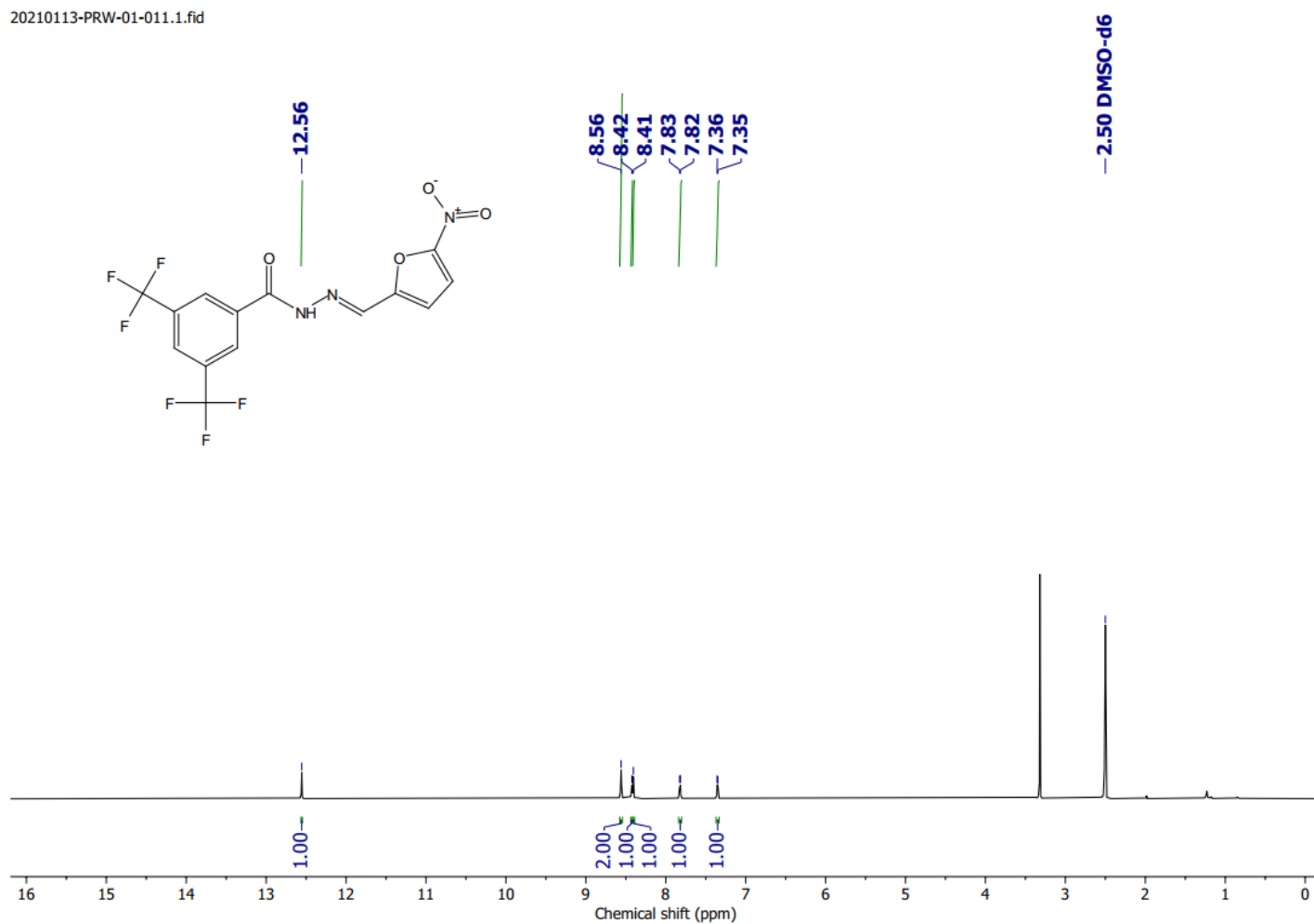
Fig. S52 ^{1}H NMR (400 MHz) spectrum of compound **1a** in DMSO-d_6.

−61.26
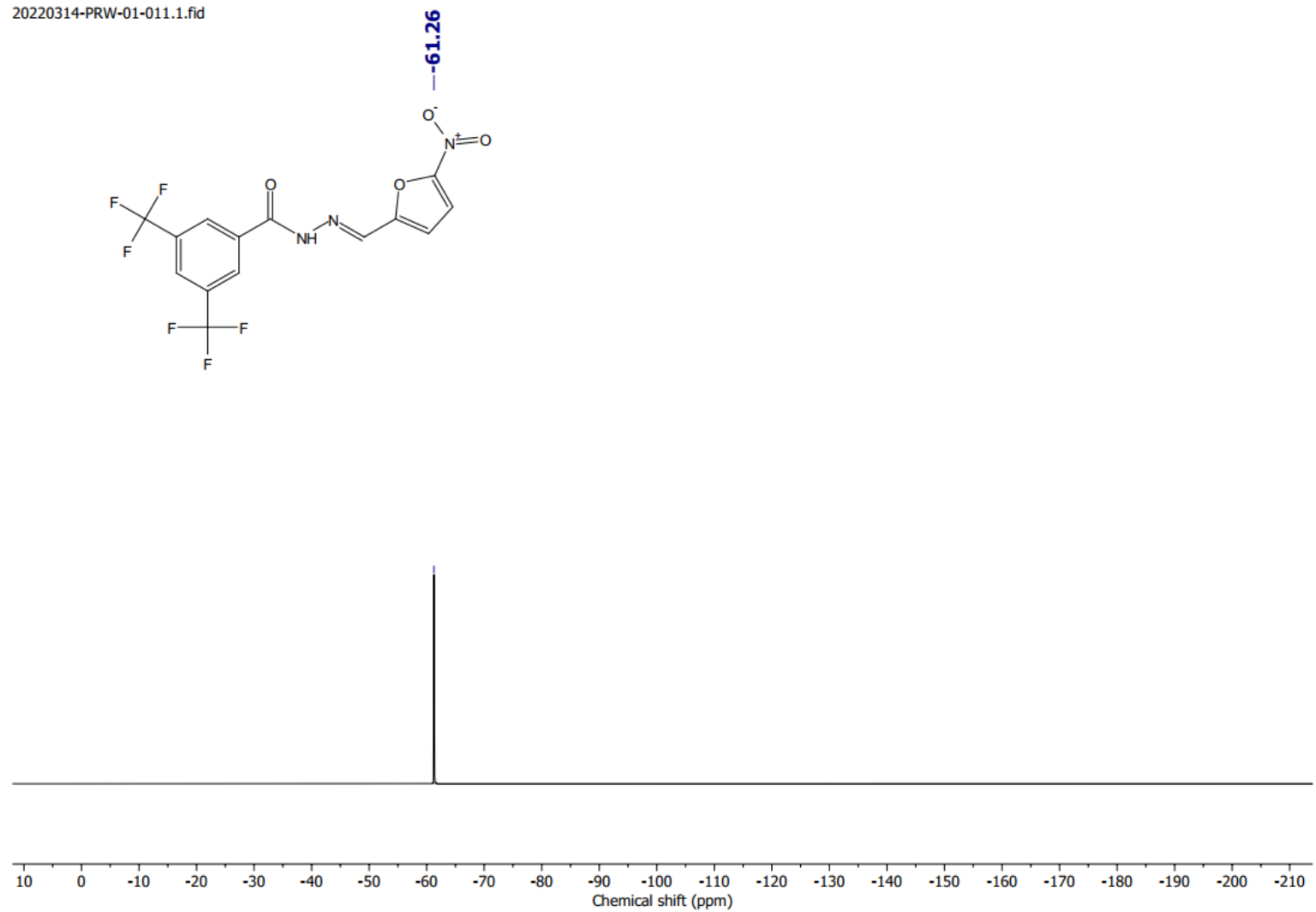
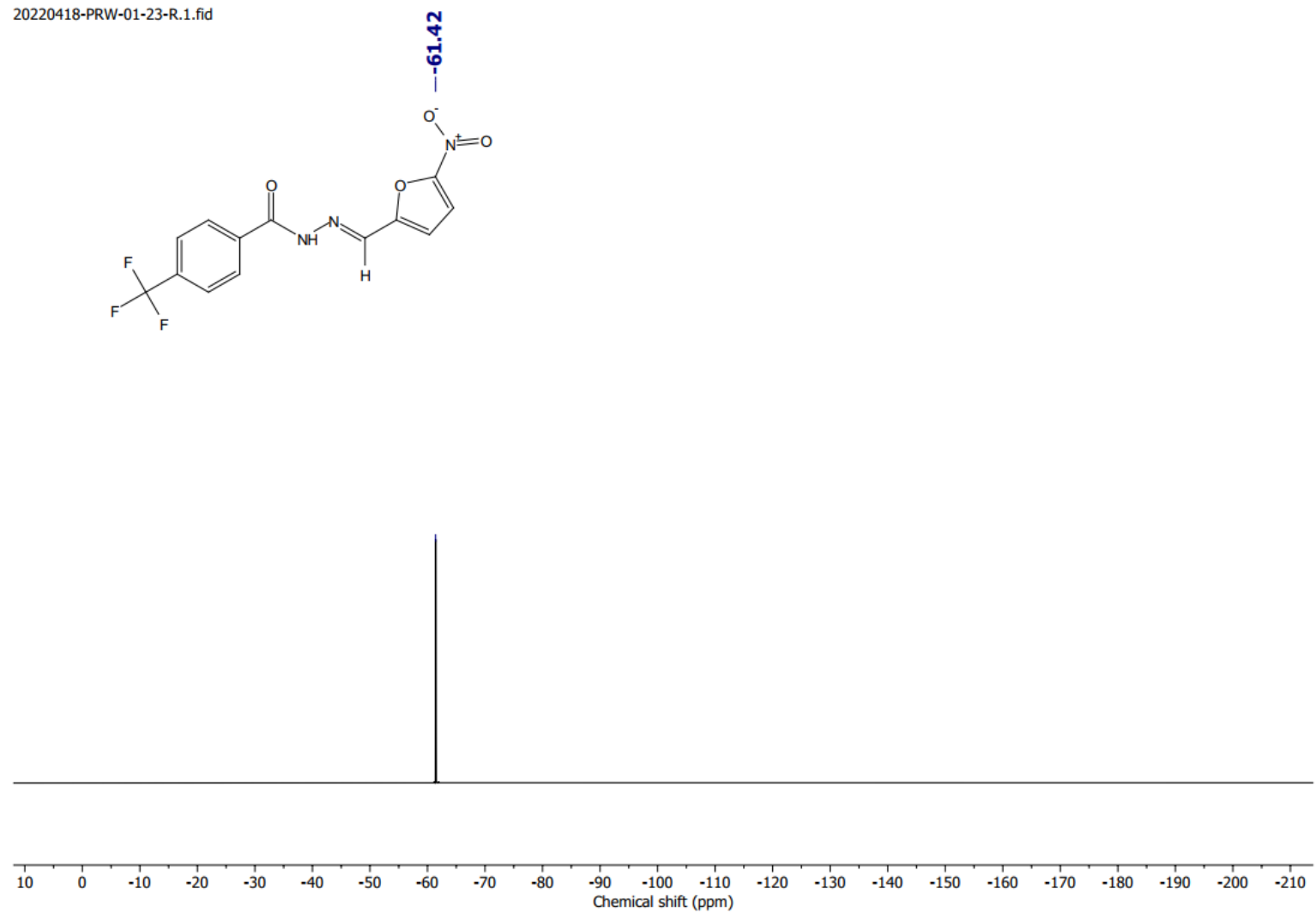**Fig. S53** ^{19}F NMR (377 MHz) spectrum of compound **1a** in DMSO-d_6.
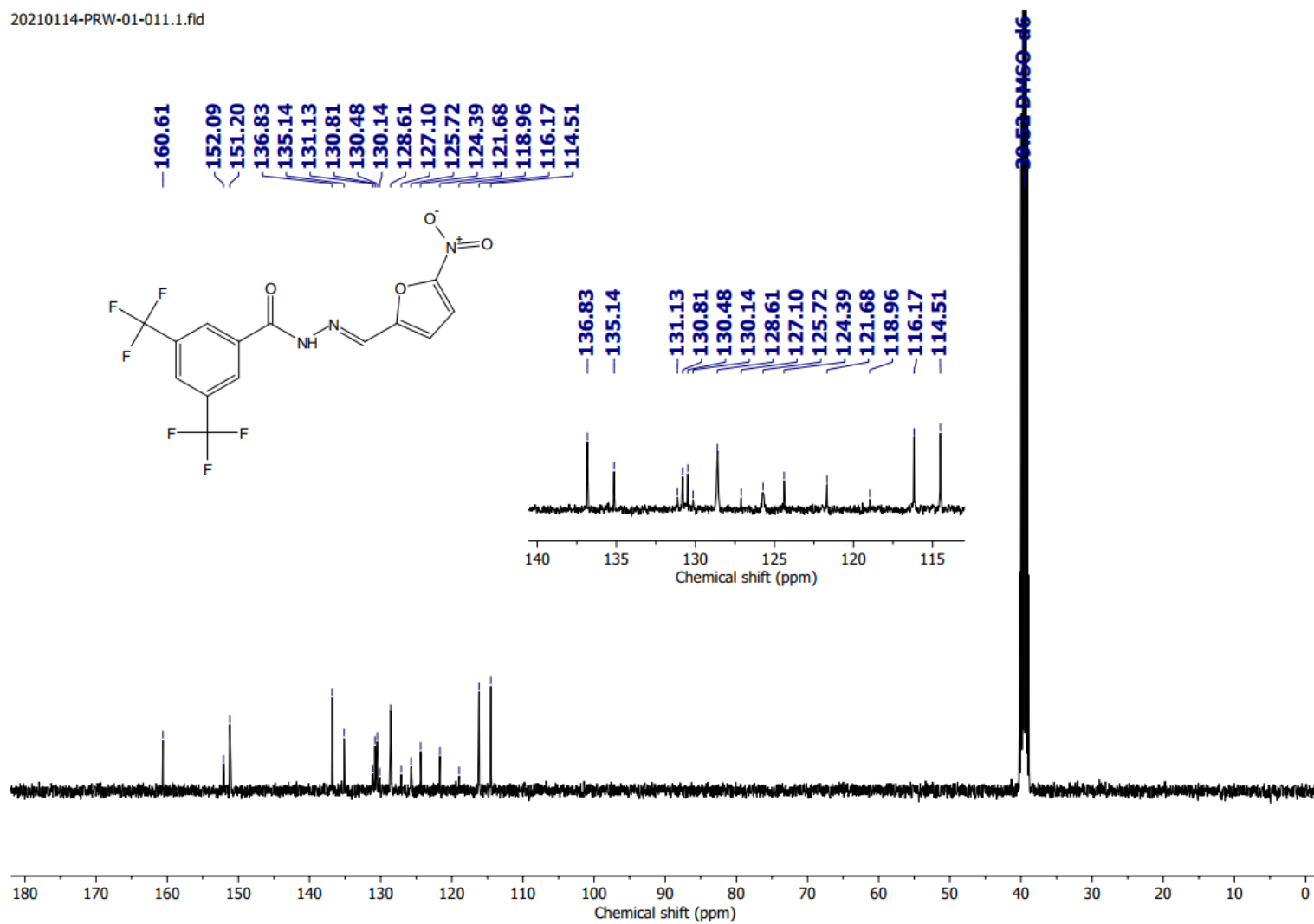
Fig. S54 ^{13}C NMR (101 MHz) spectrum of compound **1a** in DMSO-d_6.
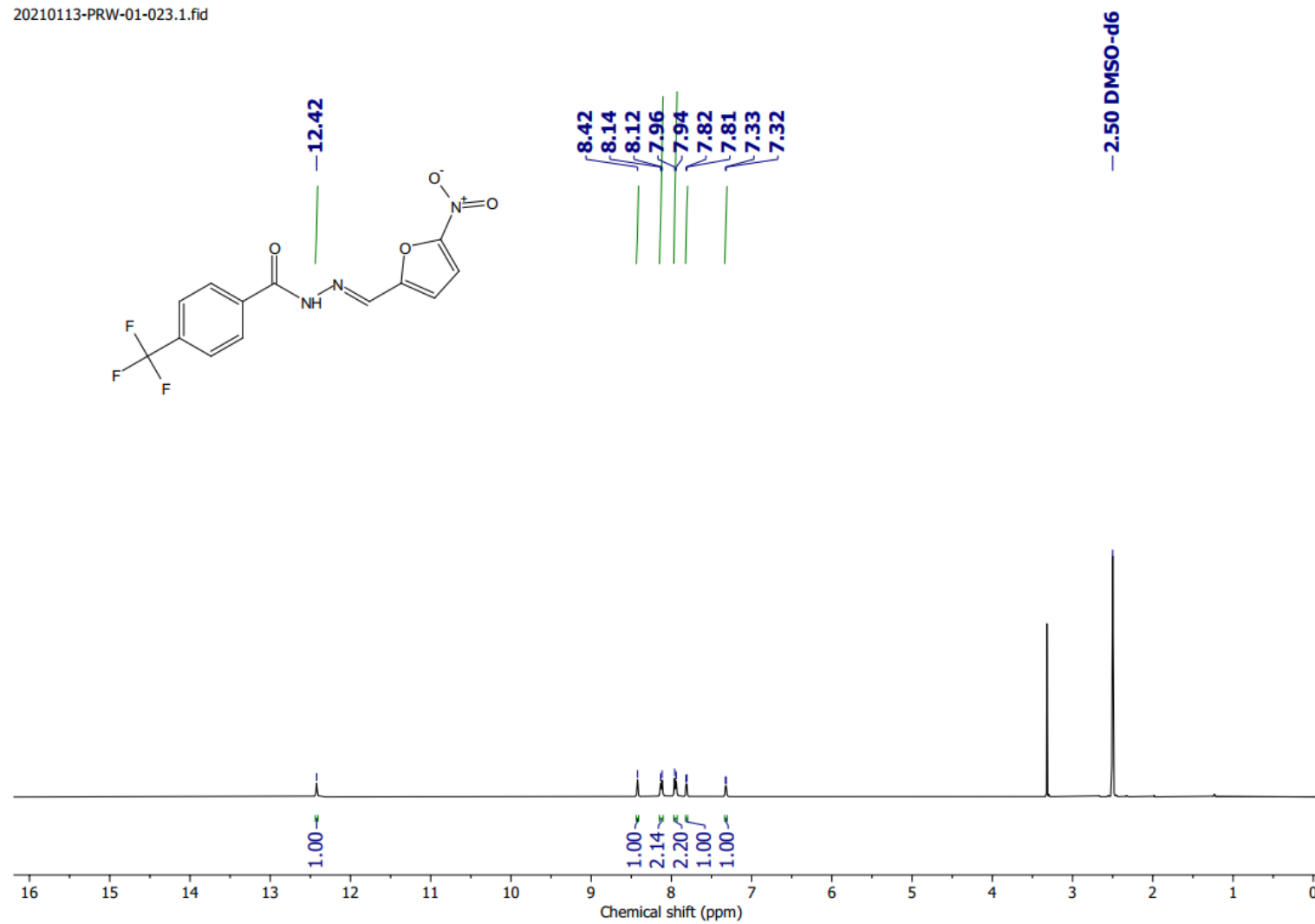
Fig. S55 ^{1}H NMR (400 MHz) spectrum of compound **1b** in DMSO-d_6.

-61.42

Fig. S56 ^{19}F NMR (377 MHz) spectrum of compound **1b** in DMSO-d_6.
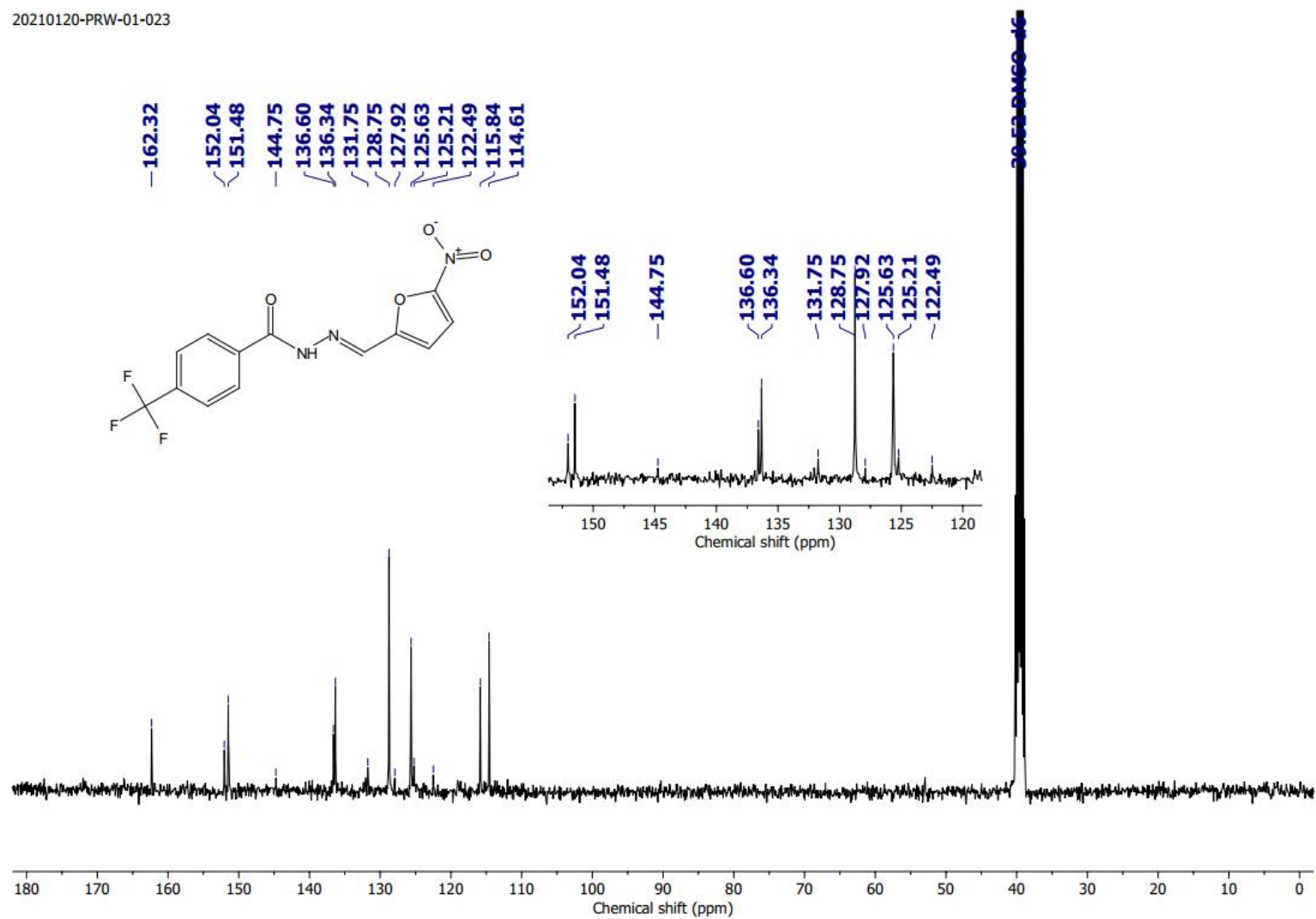
Fig. S57 ^{13}C NMR (101 MHz) spectrum of compound **1b** in DMSO-d_6.
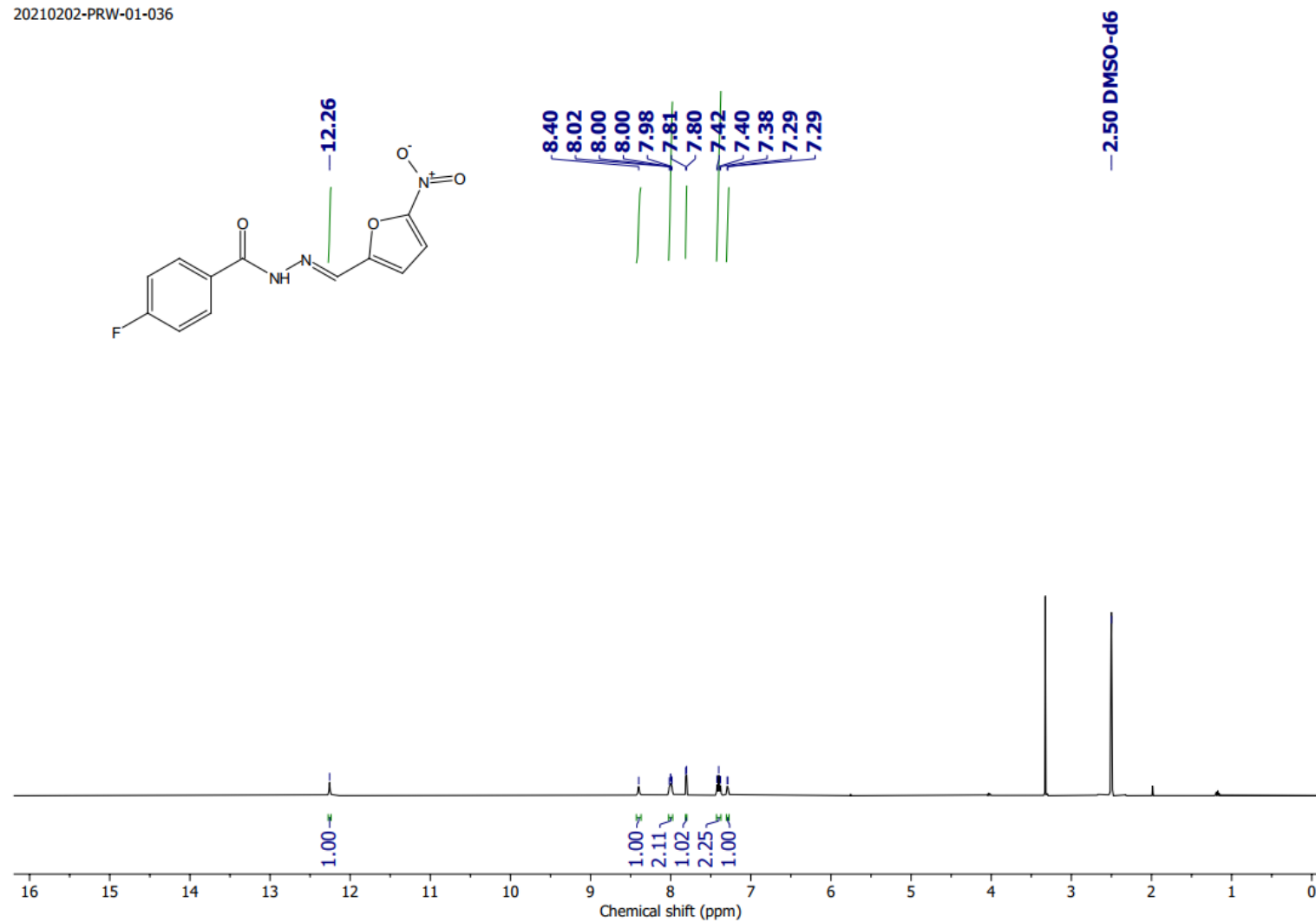
Fig. S58 ^{1}H NMR (400 MHz) spectrum of compound **1c** in DMSO-d_6.

--107.43

Chemical shift (ppm)
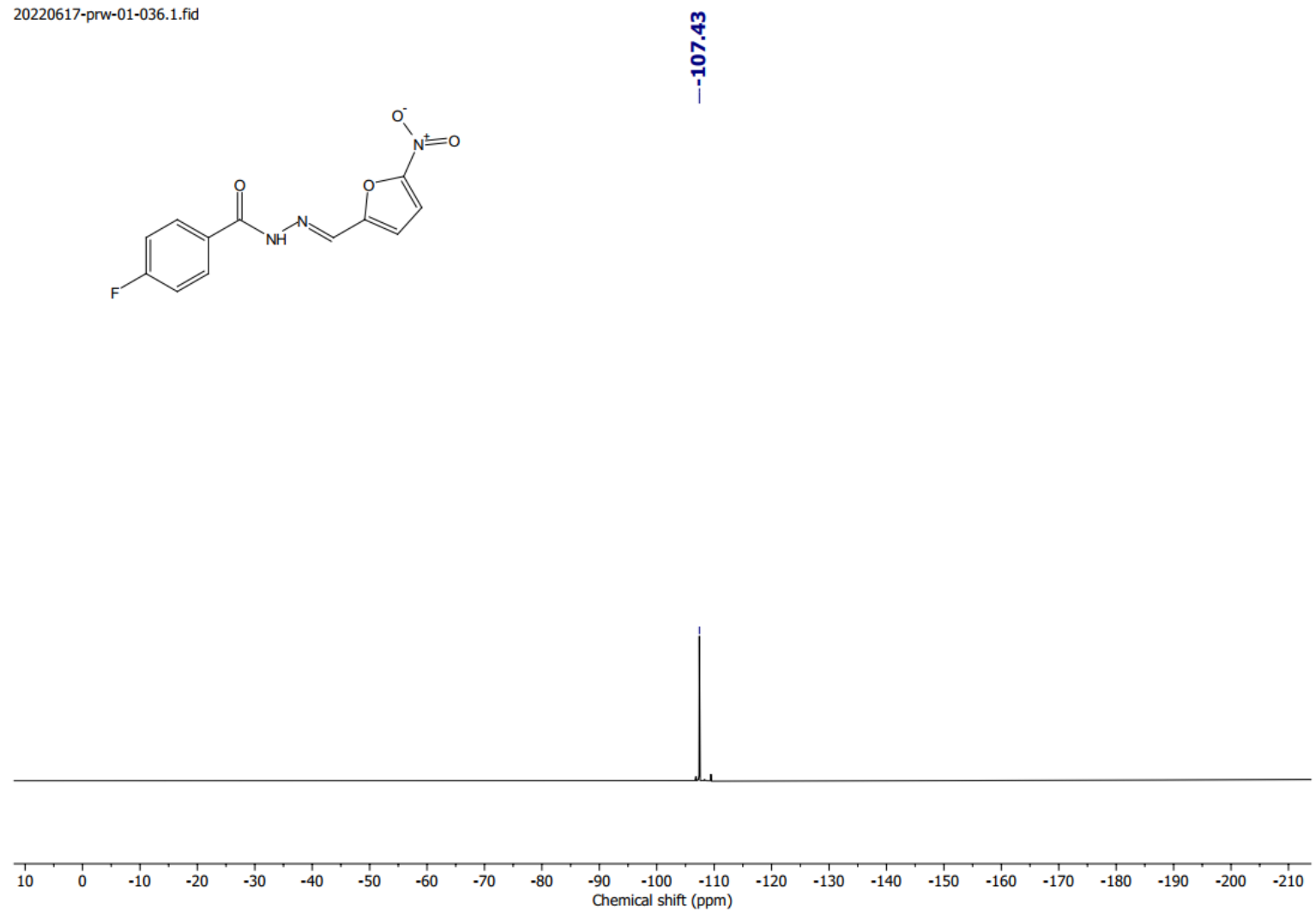
Fig. S59 ^{19}F NMR (377 MHz) spectrum of compound **1c** in DMSO-d_6.
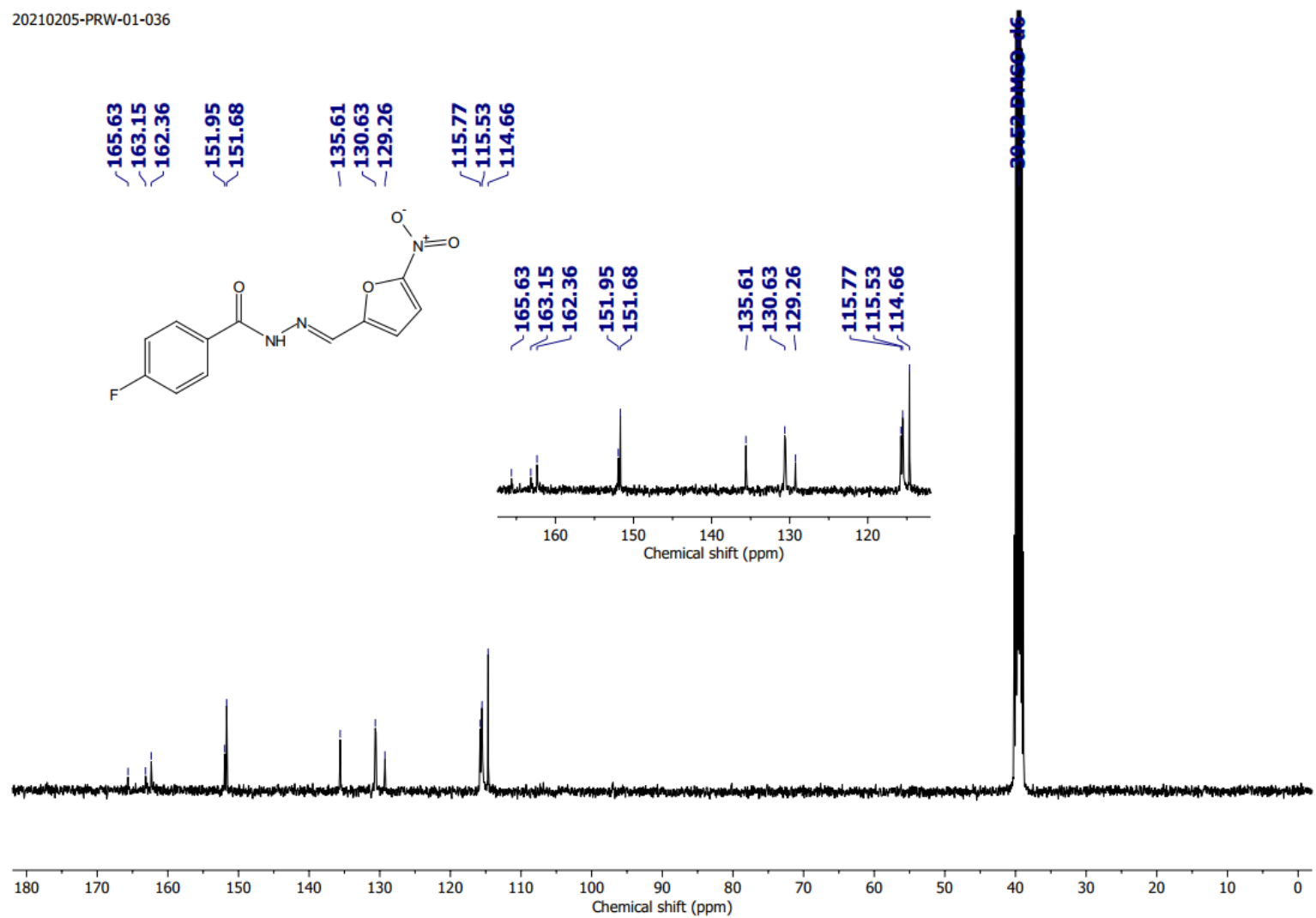
Fig. S60 ^{13}C NMR (101 MHz) spectrum of compound **1c** in DMSO-d_6.
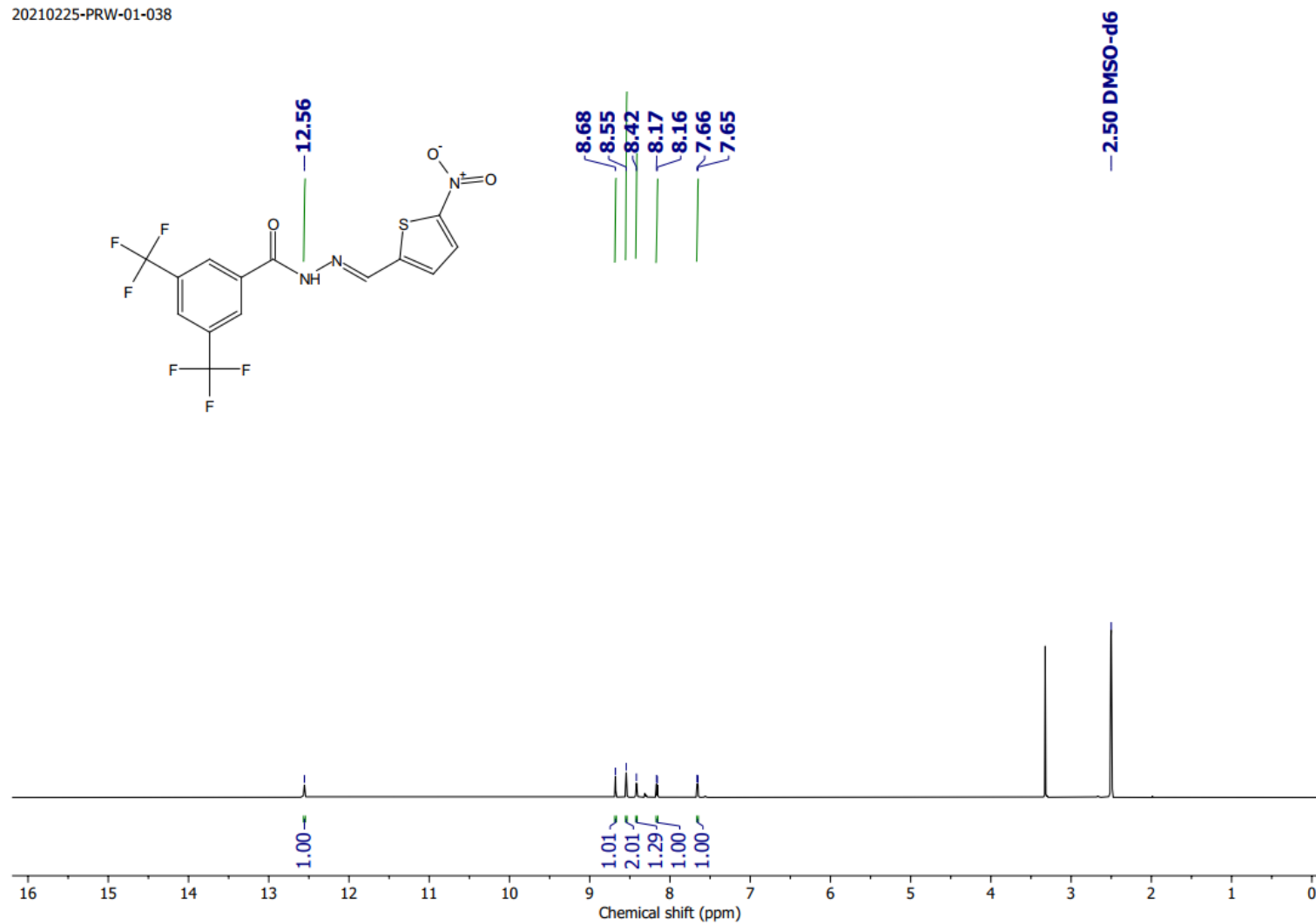
Fig. S61 ^{1}H NMR (400 MHz) spectrum of compound **2** in DMSO-d_6.

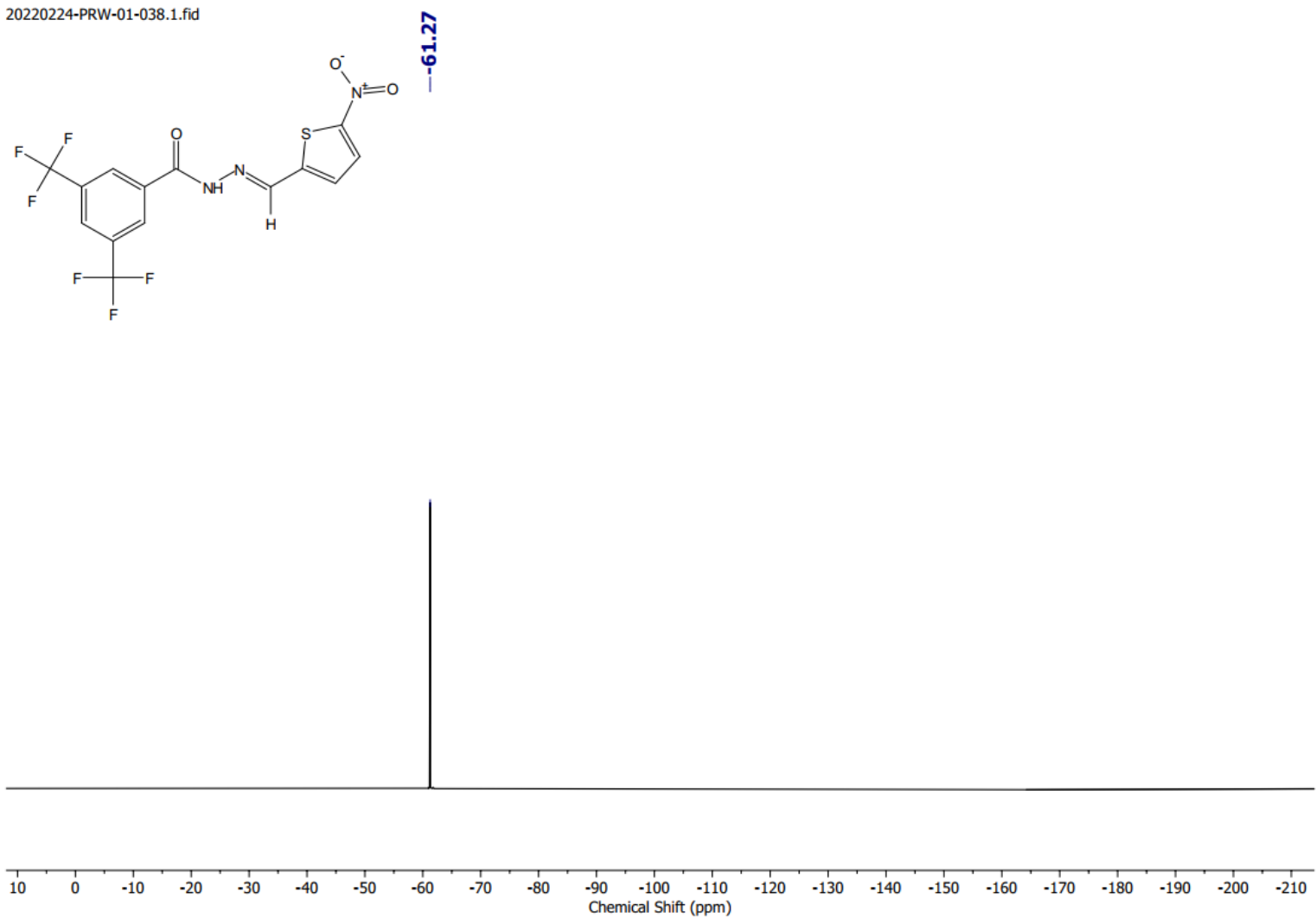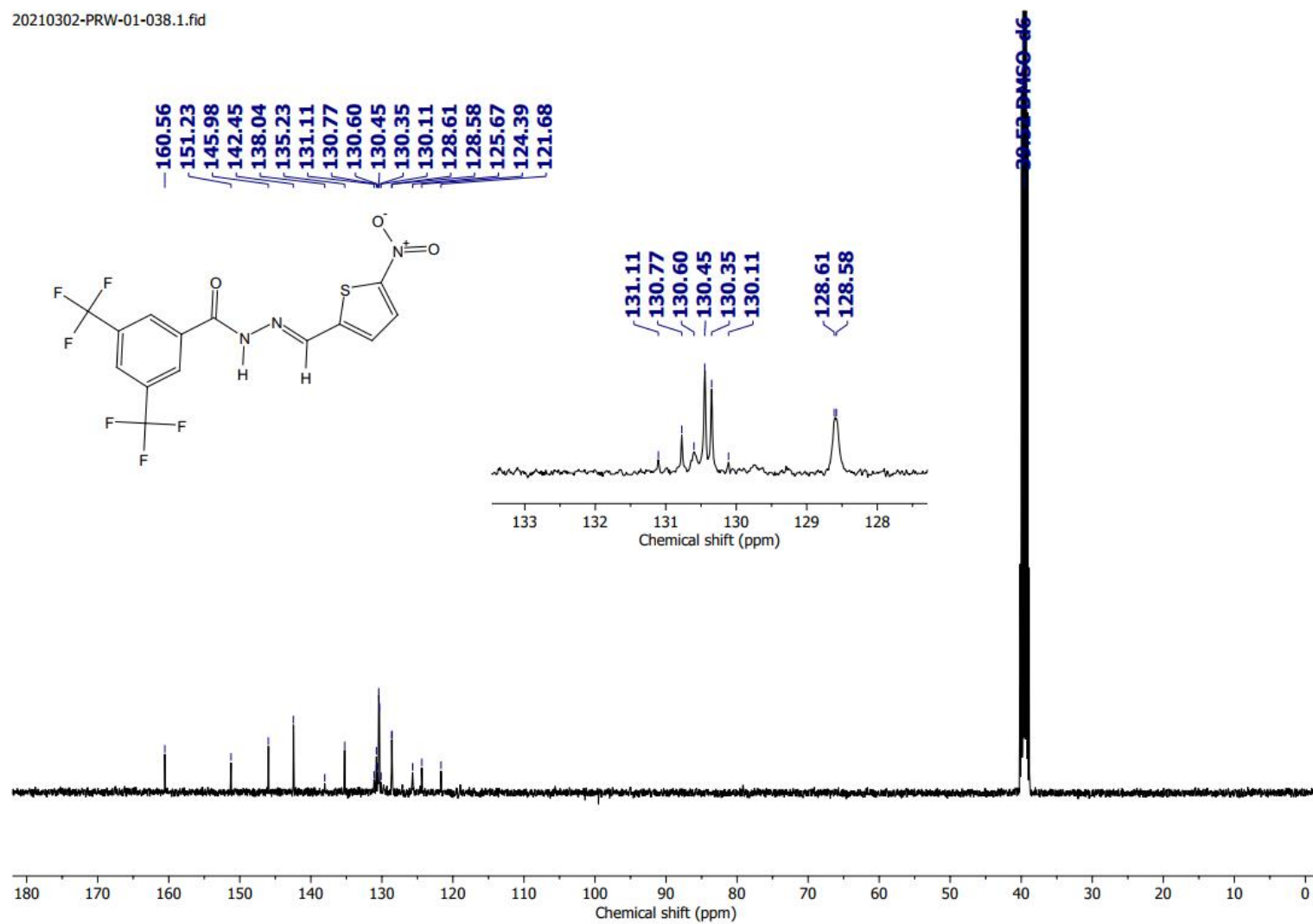**Fig. S62** ^{19}F NMR (377 MHz) spectrum of compound **2** in DMSO-d_6.

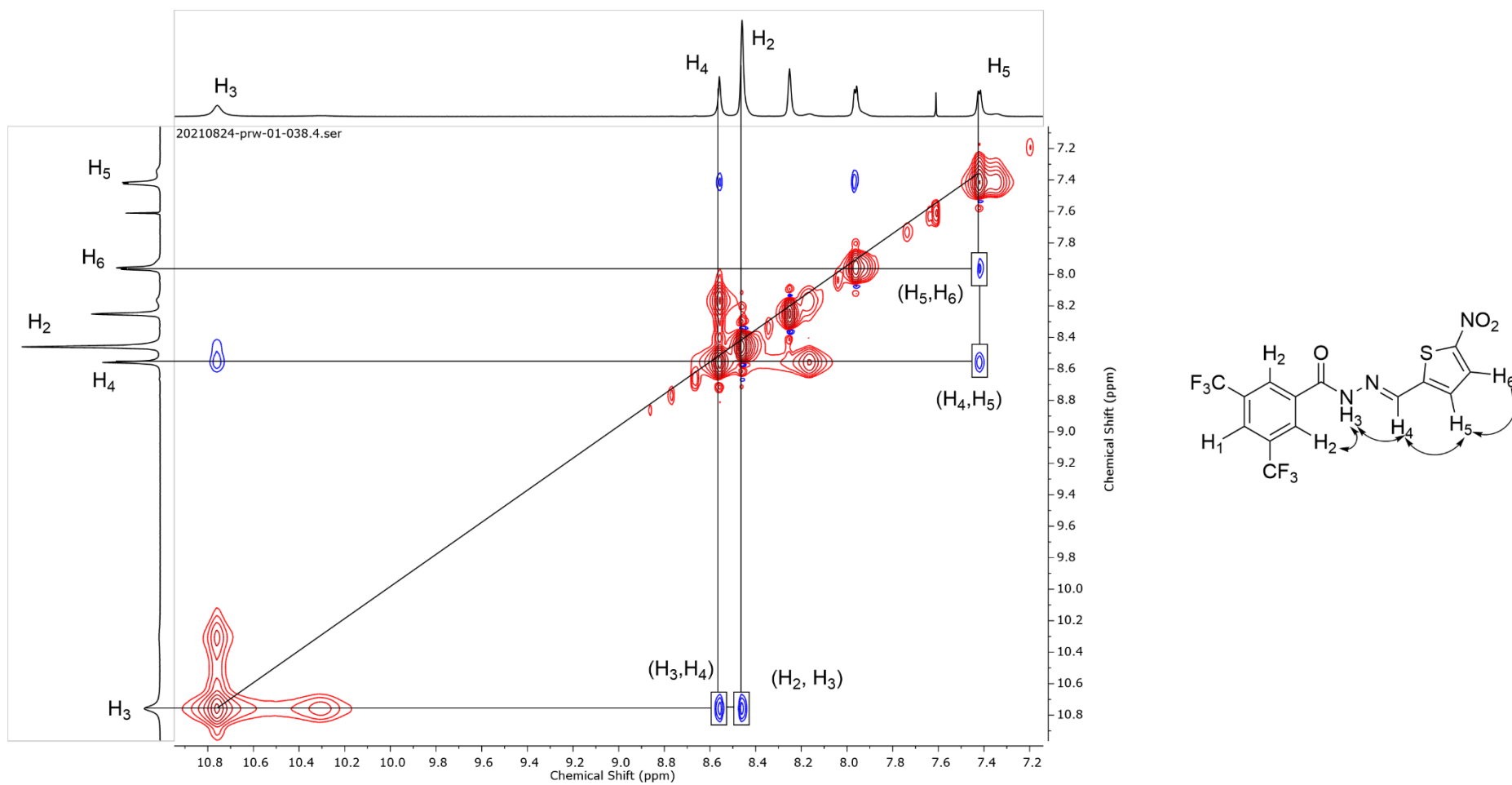**Fig. S63** ^{13}C NMR (101 MHz) spectrum of compound **2** in DMSO-d_6.

Fig. S64 ^{1}H-^{1}H NOESY NMR spectrum (400 MHz) of compound **2** in DMSO-d_6.

IX. References:

S1.   A. Mondal, S. N. Save, S. Sarkar, D. Mondal, J. Mondal, S. Sharma and P. Talukdar, *J. Am. Chem. Soc.,* 2023, **145**, 9737–9745.

S2.   S. Lin, J. Li, H. K. Bisoyi, A. Juan, J. Guo and Q. Li, *ChemPhotoChem,* 2019, **3**, 480–486.

S3.   M. Ahmad, S. Chattopadhayay, D. Mondal, T. Vijayakanth and P. Talukdar, *Org. Lett.,* 2021, **23**, 7319–7324.

S4.   P. Talukdar, G. Bollot, J. Mareda, N. Sakai and S. Matile, *J. Am. Chem. Soc.,* 2005, **127**, 6528–6529.

S5.   T. Saha, S. Dasari, D. Tewari, A. Prathap, K. M. Sureshan, A. K. Bera, A. Mukherjee and P. Talukdar, *J. Am. Chem. Soc.,* 2014, **136**, 14128–14135.

S6.   A. L. Sisson, M. R. Shah, S. Bhosale and S. Matile, *Chem. Soc. Rev.,* 2006, **35**, 1269–1286.

S7.   R. Sharma, A. Vijay, S. Chattopadhayay, A. Mukherje and P. Talukdar, *Chem. Commun.,* 2023, **59**, 3602–3605.

S8.   A. Roy, D. Saha, A. Mukherjee and P. Talukdar, *Org. Lett.,* 2016, **18**, 5864–5867.

S9.   S.V. Shinde and P. Talukdar, *Angew. Chem., Int. Ed.,* 2017, **56**, 4238–4242.

S10.   N. Madhavan and M. S. Gin, *ChemBioChem,* 2007, **8**, 1834–1840.

S11.   C. D. Cola, S. Licen, D. Comegna, E. Cafaro, G. Bifulco, I. Izzo, P. Tecilla and F. D. Riccardis, *Org. Biomol. Chem.,* 2009, **7**, 2851–2854.

S12.   N. Madhavan, E. C. Robert, and M. S. Gin, *Angew. Chem., Int. Ed.,* 2005, **44**, 7584–7587.

S13.   B. P. Benke, H. Behera and N. Madhavan, *Eur. J. Org. Chem.,* 2020, 6898–6902.

S14.   J. A. Malla, R. M. Umesh, A. Vijay, A. Mukherjee, M. Lahiri and P. Talukdar, *Chem. Sci.,* 2020, **11**, 2420–2428.

S15.   A. V. Jentzsch, D. Emery, J. Mareda, P. Metrangolo, G. Resnati and S. Matile, *Angew., Chem., Int. Ed.* 2011, **50**, 11675–11678.

S16.   P. Talukdar, N. Sakai, N. Sordé, D. Gerard, V. M. F. Cardona and S. Matile, *Bioorg. Med. Chem.,* 2004, **12**, 1325–1336.

S17.   N. Sordé and S. Matile, *J. Supramol. Chem.,* 2002, **2**, 191–199.

S18.   Q. He, G. M. Peters, V. M. Lynch and J. L. Sessler, *Angew. Chemie Int. Ed.*, 2017, **56**, 13396–13400.

S19.   H. Goto, S. Obata, N. Nakayama and K. Ohta, CONFLEX 8; CONFLEX Corporation: Tokyo, Japan, 2017.

S20.   M. J. Frisch, G. W. Trucks, H. B. Schlegel, G. E. Scuseria, M. A. Robb, J. R. Cheeseman, G. Scalmani, V. Barone, B. Mennucci, G. A. Petersson, H. Nakatsuji, M. Caricato, X. Li, H. P. Hratchian, A. F. Izmaylov, J. Bloino, G. Zheng, J. L. Sonnenberg, M. Hada, M. Ehara, K. Toyota, R. Fukuda, J. Hasegawa, M. Ishida, T. Nakajima, Y. Honda, O. Kitao, H. Nakai, T. Vreven, J. A. Montgomery, Jr., J. E. Peralta, F. Ogliaro, M. Bearpark, J. J. Heyd, E. Brothers, K. N. Kudin, V. N. Staroverov, T. Keith, R. Kobayashi, J. Normand, K. Raghavachari, A. Rendell, J. C. Burant, S. S. Iyengar, J. Tomasi, M. Cossi, N. Rega, J. M. Millam, M. Klene, J.

E. Knox, J. B. Cross, V. Bakken, C. Adamo, J. Jaramillo, R. Gomperts, R. E. Stratmann, O. Yazyev, A. J. Austin, R. Cammi, C. Pomelli, J. W. Ochterski, R. L. Martin, K. Morokuma, V. G. Zakrzewski, G. A. Voth, P. Salvador, J. J. S44 Dannenberg, S. Dapprich, A. D. Daniels, O. Farkas, J. B. Foresman, J. V. Ortiz, J. Cioslowski and D. J. Fox, *Gaussian 09,* Rev. D.01; Gaussian, Inc., Wallingford, CT, 2013.

S21. M. J. Frisch, J. A. Pople and J. S. Binkley, *J. Chem. Phys.,* 1984, **80**, 3265–3269.

S22. E. D. Glendening, C. R. Landis and F. Weinhold, *J. Comput. Chem.,* 2013, **34**, 1429–1437.